Review Article

Nano Research
2022, 15(10): 9410–9439

ISSN 1998-0124 CN 11-5974/O4
https://doi.org/10.1007/s12274-022-4695-6

# Advances in core–shell engineering of carbon-based composites for electromagnetic wave absorption

Lixue Gai, Honghong Zhao, Fengyuan Wang, Pan Wang, Yonglei Liu, Xijiang Han (✉), and Yunchen Du (✉)

*MIIT Key Laboratory of Critical Materials Technology for New Energy Conversion and Storage, School of Chemistry and Chemical Engineering, Harbin Institute of Technology, Harbin 150001, China*



**Received:** 21 May 2022 / **Revised:** 18 June 2022 / **Accepted:** 22 June 2022

## ABSTRACT

Electromagnetic (EM) absorption is paving the way to overcome the challenges related to conventional shielding strategy against EM pollution through sustainable energy dissipation. As characteristic functional media that can interact with electric or magnetic field branch, EM wave absorption materials (EWAMs) have received extensive attention and realized considerable development in the past two decades, where carbon-based composites are always considered as promising candidates for high-performance EMAWs due to their synergetic loss mechanism as well as diversified composition and microstructure design. Recent progress indicates that there is more and more interest in the fabrication of carbon-based composites with unique core–shell configuration. On one hand, core–shell configuration usually ensures good chemical homogeneity of final products and provides some positive protections for the components with susceptibility to corrosion, on the other hand, it creates enough heterogeneous interfaces between different EM components, which may bring enhanced polarization effect and intensify the consumption of EM energy. In this review, we firstly introduce EM wave absorption theory, and then highlight the advances of core–shell engineering in carbon-based composites in terms of built-in carbon cores and built-out carbon shells. Moreover, we also show some special core–shell carbon-based composites, including carbon/carbon composites, assembled composites, and decorated composites. After analyzing EM absorption performance of some representative composites, we further propose some challenges and perspectives on the development of core–shell carbon-based composites.

## KEYWORDS

carbon-based composites, core–shell configuration, synergetic effect, interfacial polarization, electromagnetic (EM) absorption performance

## 1 Introduction

After more than 150 years of gestation and development, electromagnetic (EM) technology has become one of the most important scientific and technological sources in current society, which helps us realize the dream of intelligent information and communication, and has been deeply penetrated into all aspects of our lives [1–5]. However, all kinds of electronic devices with an order of magnitude growth also breed some adverse side effects, i.e., EM interference and pollution, induced by the excessive radiation of EM waves [6–8]. The precaution on EM threats is evolving into a social issue of widespread concern [9–12]. Over the past few decades, EM absorption gradually receives more attention than conventional EM shielding, because it achieves the dissipation of incident EM waves through energy conversion rather than physical reflection, and thus the risk of secondary EM pollution can be significantly decreased [13–15]. What is more, EM absorption, in military field, also offers an effective strategy to reduce the radar cross section of mobile weapon equipment and the probability of information disclosure [16, 17].

It is well known that EM waves propagate in space through electric and magnetic fields with the same direction and perpendicular to each other, which determines that there will be two possible pathways to interrupt their propagation and accomplish EM absorption finally by interacting with either electric or magnetic field branch. Therefore, EM functional media with absorption characteristics, usually defined as EM wave absorption materials (EWAMs), can be divided into two categories, magnetic loss and dielectric loss types [13, 18]. Magnetic EWAMs dominate the early research of EM absorption due to their good performance, and some of them, e.g., ferroferric oxide and carbonyl iron, have been successfully developed as commercial EWAMs [19, 20]. However, their high density and filler loading cannot meet the application requirements of the oncoming generation of EM absorption technology, and especially, their intrinsic drawbacks of easy oxidation and corrosion even greatly restrain the long-term service under some harsh outdoor conditions, such as high-temperature exposure (dozens of degree), moisture, and salt spray [21, 22]. Among various candidates, carbon materials exhibit good chemical stability, which may protect magnetic materials from easy oxidation and corrosion to a great extent, and more importantly, they also show great potential due to their tailorable dielectric property, low density, diversified morphology, and abundant reserves [23, 24]. The advent of graphene drives the research of carbon materials as promising EWAMs more drastically [25–29]. It is unfortunate that a gap to practical application always exists in

Address correspondence to Yunchen Du, yunchendu@hit.edu.cn; Xijiang Han, hanxijiang@hit.edu.cn

single-component carbon materials as they easily suffer from insufficient loss capability and narrow EM response bandwidth, even seriously mismatched impedance with free space [30, 31].

In an effort to upgrade the performance of carbon materials, more and more groups have focused their research on the construction of carbon-based composites. A lot of successful examples have demonstrated that both magnetic (e.g., Fe, Co, Ni, and ferrites) and dielectric (e.g., conductive polymers, metal oxides/sulfides, and carbides) additives could effectively optimize EM characteristics, improve impedance matching, and enrich loss mechanisms [32–34]. Although physical mixing is the simplest method to construct EM functionalized carbon-based composites, such a composite approach is not conductive to full utilization of the synergy between different components due to serious compositional segregation. Recent progress indicates that it is of great significance to assemble different EM components with carbon materials into unique core–shell configuration, a concentric bilayer nanostructure composed of core (inner component) and continuously uniform shell (outer layer component) [3, 35, 36]. Along with the flourishment of nanotechnology, the morphologies of core–shell carbon-based composites have also extended from initial spherical particles to one-dimensional tubes/fibers, even to three-dimensional (3D) aerogels [37–40]. Apart from the intrinsic loss characteristics of carbon-based composites, the creation of core–shell configuration may endow these composites with some additional advantages. First, core–shell configuration favours the full contact between carbon materials and additive components, and the sufficient heterogeneous interfaces therein will significantly contribute to the energy consumption of incident EM waves through powerful polarization effect [41, 42]. Second, core–shell configuration may further stimulate the synergistic effect between core and shell, which can effectively optimize their impedance characteristics and broaden EM response bandwidth [3, 43]. Third, core–shell configuration provides us with an opportunity to conduct more detailed microstructural design in the cores and shells, respectively. Some state-of-the-art core–shell carbon-based composites with hollow cores, porous cores/shells, multiple shells, and tailorable voids between cores and shells, have been frequently reported in recent years, and it is widely accepted that the formation of these hierarchical microstructures could bring multiple reflections of incident EM waves and thus reinforce absorption performance [44–47]. Fourth, core–shell composites have good chemical homogeneity, and thus the compositional segregation in conventional composites can be eliminated effectively, which results in their stable EM functions rather than random performance highly dependent on some non-scientific parameters (e.g., mixing time, stirring rate, and separation method) [48]. Fifth, the core–shell composites usually have good dispersion, which facilitates their further processing in practical applications.

In the field of EM absorption, core–shell carbon-based composites are becoming a kind of very attractive EWAMs and show bright prospect in EM pollution precaution, as indicated by the publications with an order of magnitude growth worldwide. Therefore, it is very necessary to sort out the status in this research branch, summarize common findings, and explore hidden clues, which will be helpful for the researchers in the related field to make more breakthroughs. Herein, we not only summarize the mechanism of EM wave absorption, but also introduce the advances of core–shell carbon-based composites as high-performance EWAMs, which are divided into three categories: i.e. built-in carbon cores, built-out carbon shells, and special core–shell composites. Finally, we also discuss in-depth the challenges and opportunities faced by the current development of core–shell carbon-based composites, and further provide some perspectives in the future research.

## 2 EM wave absorption theory

### 2.1 Intrinsic loss mechanisms

#### 2.1.1 *Magnetic loss*

Magnetic loss usually appears in the process of magnetization and re-magnetization of magnetic materials, which is caused by a part of energy irreversibly transformed into thermal energy. Generally, magnetic materials can consume EM energy through three pathways: magnetic hysteresis loss, eddy current loss, and residual loss [49]. Magnetic hysteresis loss is the energy attenuation induced by irreversible displacement of domain wall to overcome the obstacles from stress and impurities during magnetization process, which is roughly proportional to the area of the corresponding hysteresis loop [50]. However, magnetic hysteresis loss is usually ruled out of total magnetic loss when EM absorption is discussed, because its contribution is almost negligible under weak field [51, 52].

According to Faraday's law of EM induction, as well as Joul–Lenz's law, when a magnetic conductor is applied in an alternate magnetic field, an induced electromotive force will be generated inside the magnetic conductor, and this induced electromotive force will further drive the formation of induced current (i.e., so-called eddy current) and finally produce a thermal effect [49, 53]. This is a conversion process from EM energy to heat energy in essence, and thus eddy current loss is positively contributed to EM absorption. However, if the eddy current is strong, there will be a shielding effect on the alternate magnetic field, which makes the interior of the magnetic conductor unable to be magnetized [54, 55]. This phenomenon is generally described as skin effect, and the consequent partial invalidation of magnetic conductor will weaken the total magnetic loss to a certain degree. It is worth noting that the undesirable skin effect can be effectively suppressed by decreasing the particle size and increasing the resistivity of magnetic conductors [56, 57]. In some cases, eddy current loss may dominate magnetic loss of EWAMs, and such a situation always gives constant $C_0$ ($C_0 = \mu_r''(\mu_r')^{-2}f^{-1}$) values independent on the frequency ($f$) of incident EM waves [52, 58], where $\mu_r'$ and $\mu_r''$ are real and imaginary parts of relative complex permeability of EWAMs, respectively.

As for residual loss, it can be further divided into three parts: domain wall resonance, natural resonance, and exchange resonance [50]. When ferromagnetic materials are subjected to an alternated magnetic field, their domain walls will vibrate near the equilibrium position, and domain wall resonance will be generated under the condition that the frequency of the applied alternated magnetic field is equal to the natural frequency of the domain wall vibration. However, domain wall resonance is seldom discussed in gigahertz EM absorption as it mainly occurs in the megahertz range [59, 60]. Natural resonance is a special form of ferromagnetic resonance, which refers to the situation that the maximum value of relative complex permeability will also appear due to the existence of magnetocrystalline anisotropy equivalent field even without a steady external magnetic field. In ferromagnetic materials, some electron spins contributing to magnetic response deviate from the original ordered arrangement direction because of the influence of thermal turbulence or other factors, and under the interaction of exchange and magnetic dipole moment, these locally deviated spins will precess and propagate to other ordered parts, resulting in so-called spin waves. Once the effect of exchange interaction is much greater than that

of dipole interaction, exchange resonance will be active and create multiple resonance peaks [50, 61]. Both natural resonance and exchange resonance are common in ferromagnetic EWAMs, and they can be easily identified by multiple maximum values in frequency-dependent $\mu_r'$ and $\mu_r''$ curves. The specific resonance frequency can be determined by the exchange resonance mode in terms of Eq. (1) [62, 63]

$$f = \gamma_0 \left( H_c + \frac{k}{D^2 M_s} \right) \quad (1)$$

where $\gamma_0$ is the gyromagnetic ratio ($3.0 \times 10^7$ $Oe^{-1}\cdot s^{-1}$), $k$ is exchange constant ($1.73 \times 10^{-5}$ erg/cm), $H_c$, $M_s$, and $D$ represent coercivity, saturation magnetization, and crystal size, respectively, and $\gamma_0 H_c$ and $\gamma_0 k/D^2 M_s$ correspond to natural resonance frequency and exchange resonance frequency, respectively. In general, natural resonance usually occurs in the frequency range of 0.10–10.0 GHz, whereas exchange resonance works in higher frequency region, especially with the decrease in the particle size of ferromagnetic EWAMs [51, 63].

#### 2.1.2 *Dielectric loss*

The classical dielectric theory holds that the consumption of electric energy in a dielectric medium is mainly dependent on conductivity loss and polarization loss [64–66]. Conductivity loss benefits from the heat effect of micro current induced by the directional movement of residual carriers under an alternating electric field, and the electron migrating during this process may be achieved in two different modes [67, 68]. One is the routine electron migrating along with conductive networks, and this model is always established in highly conductive scaffolds, such as carbon nanotubes (CNTs) and graphene. For example, Zhang et al. found that a controllable compression on three-dimensional graphene foams could bring a significant enhancement for their microwave absorption performance, because the compression caused a moderate shrinkage of three-dimensional networks and more physical contacts between conductive graphene sheets, thus increasing the circuit density and loss efficiency [69]. The other mode relates to electron hopping between different components, interfaces, and defects [64, 70]. In ternary $Mo_2C$/Co/C composites, the introduction of poorly conductive $Mo_2C$ nanoparticles resulted in higher conductivity and stronger dielectric loss, which was attributed to the facilitation of electron hopping in multicomponent composites [71]. Of note is that, in most cases, EWAMs are embedded into resin matrix, and thus either of these two modes requires sufficient filler loading to supply conductive networks and decrease the energy barrier of electron hopping [67]. If the filler loading is less than the critical value, electron migrating and hopping will be greatly suppressed, leading to feeble conductivity loss. However, this dilemma can be moderately alleviated by elevating temperature [72].

Polarization loss can be generally understood as the result when charged particles overcome thermal motion driven by electric field force [67, 68]. It has long been considered that there are four typical polarization relaxations responsible for energy loss, namely ionic polarization, electronic polarization, dipolar polarization, and interfacial polarization [48, 65]. Ionic polarization and electronic polarization are very fast relaxation processes that can complete in $10^{-15}$–$10^{-12}$ s, which suggests that their contribution in megahertz and gigahertz range will be negligible. Dipolar polarization actually refers to the orientation process of intrinsic dipoles. Under an external alternating electric field, the rotation of these intrinsic dipoles always lags behind the field change, which makes them have to extract energy from this field to complete the re-orientation as soon as possible [73]. However, some nonpolar matters can also conduct similar process through the generation of instanteous dipole moments under an alternating EM field, and in addition, some defect sites, including vacancies, heteroatoms, line defects, and planar defects, in EM functional materials may play as polarization centers generated from the bound charges or functional groups therein [67, 74]. The occurrence of dipolar polarization will result in frequency dispersion behaviors in the curves of both real parts ($\varepsilon_r'$) and imaginary parts ($\varepsilon_r''$) of relative complex permittivity [73]. Interfacial polarization widely exists at any heterogeneous interfaces, even at solid/air interfaces, because different dielectric properties of bilateral EM components induce the accumulation and uneven distribution of space charges [75, 76]. Shi et al. ever depicted such heterogeneous interfaces as a capacitor-like structure, and visualized interfacial polarization with an equivalent circuit model [77]. More recently, Che's group characterized the interfacial polarization with off-axis electron holography technique for the first time [78–80]. As observed in Figs. 1(a)–1(h), there was distinguishable charge density distribution between MoC nanoparticles and N-doped carbon (NC), where red referred to positively charged region and blue represented negatively charged region. These results clearly demonstrated the generation of charge polarization at MoC(−)/carbon(+) interfaces. It is interesting that interfacial polarization is not only effective in heterogeneous composites, but also active in some EWAMs composed of two allotropes. Our group designed sandwich-like composites through the self-assembly of amorphous carbon microspheres (ACMs) and reduced graphene oxide (rGO), and their different dielectric properties created considerable interfacial polarization to dissipate the energy of electric field, as supported by computer simulation technology (CST) stimulation results (Figs. 1(i)–1(k)) [81].

After in-depth investigation, Cole and Cole transformed Debye equation into the following expression [82, 83]

$$\left( \varepsilon_r' - \frac{\varepsilon_s + \varepsilon_\infty}{2} \right)^2 + (\varepsilon_r'')^2 = \left( \frac{\varepsilon_s - \varepsilon_\infty}{2} \right)^2 \quad (2)$$

where $\varepsilon_s$ and $\varepsilon_\infty$ are the static dielectric constant and dielectric constant at infinite frequency, respectively. Based on this equation, there will be a semicircle, known as Cole–Cole semicircle or Debye semicircle, in the curve of $\varepsilon_r''$ versus $\varepsilon_r'$ if one polarization relaxation process occurs [84, 85]. Although many studies often identify multiple semicircles in $\varepsilon_r''$ versus $\varepsilon_r'$ curves, it is still hard to assign these semicircles to a specific polarization relaxation process, and it is not reliable to conclude that more semicircles correspond to more powerful polarization loss. Cao's group pioneered the decomposition of dielectric loss of MWCNTs/silica composites into conductivity loss and polarization loss by fitting Debye equations, and they found that conductivity loss gradually decreased in X band, while polarization loss could present a reverse trend [64]. Xu et al. further demonstrated the methodology about the division of dielectric loss in a following study, which greatly facilitated the investigation on conductivity loss and polarization loss of different EWAMs [86].

### 2.2 Loss intensity and impedance matching

Relative complex permittivity ($\varepsilon_r = \varepsilon_r' - j\varepsilon_r''$) and complex permeability ($\mu_r = \mu_r' - j\mu_r''$) are very important parameters that can affect EM properties of EWAMs greatly, where $\varepsilon_r'$ and $\mu_r'$ represent their storage capabilities of electric and magnetic energy, and $\varepsilon_r''$ and $\mu_r''$ are associated with their loss capabilities of electric and magnetic energy [87–89]. The intensities of dielectric loss and magnetic loss are usually determined by dielectric dissipation factor ($\tan\delta_e = \varepsilon_r''/\varepsilon_r'$) and magnetic dissipation factor ($\tan\delta_m = \mu_r''/\mu_r'$), respectively [90]. However, in many cases, EWAMs have

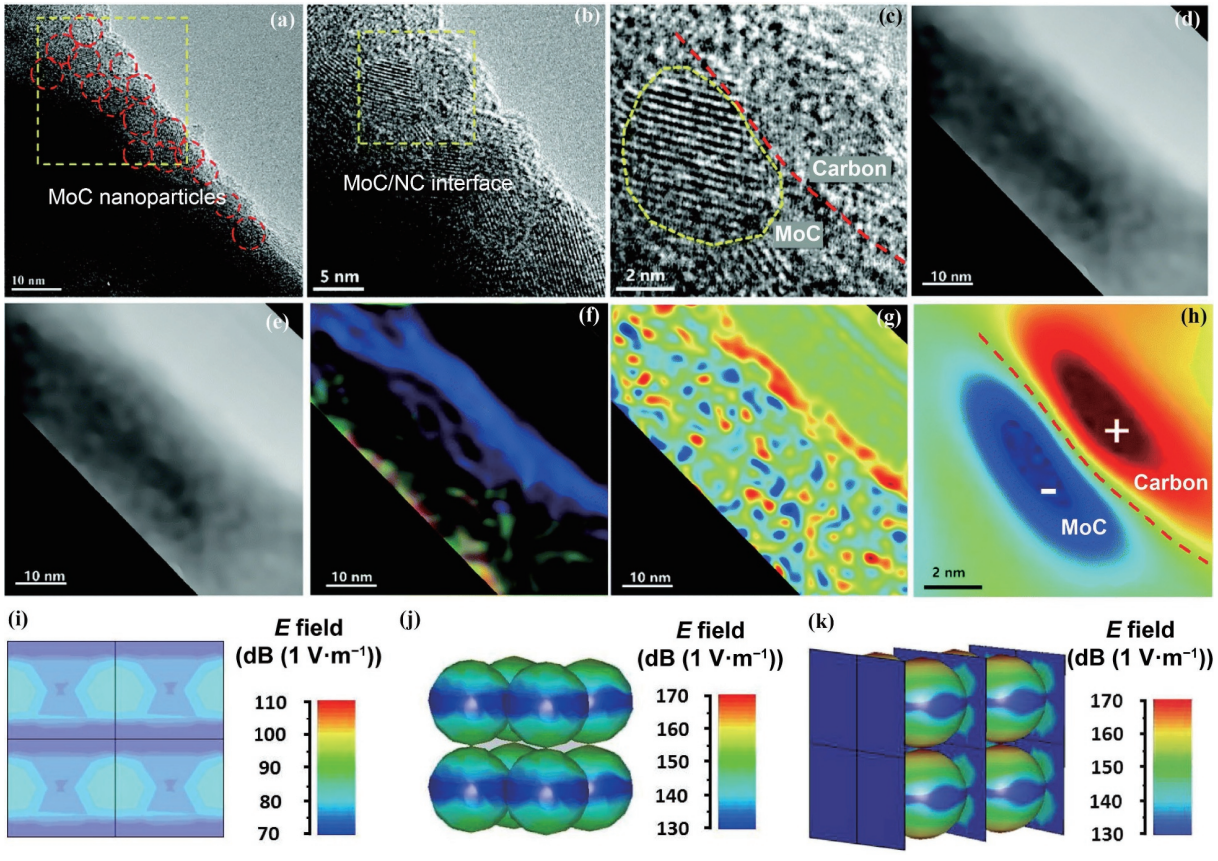


**Figure 1** (a)–(c) Transmission electron microscopy (TEM) images, (d) hologram, (e) reconstructed phase image, (f) electric-filed map, (g) charge density map, and (h) charge distribution on the MoC(−)/carbon(+) interface of MoC/NC composites. Reproduced with permission from Ref. [78], © Huang, W. et al. 2021. Simulated electric field distribution of (i) rGO, (j) ACMs, and (k) sandwich-like rGO/ACMs/rGO. Reproduced with permission from Ref. [81], © WILEY-VCH Verlag GmbH & Co. KGaA, Weinheim 2016.

compatible dielectric and magnetic characteristics, which make it difficult to evaluate the overall loss intensities of different EWAMs, especially when there is a trade-off relationship between dielectric loss and magnetic loss. Attenuation constant ($\alpha$), as calculated by Eq. (3), is originally employed to describe the amplitude attenuation of EM waves in transmission medium, while it has become a universal indicator to indicate the overall loss intensity of EWAMs in recent years [91–93].

$$\alpha = \frac{\sqrt{2}\pi f}{c}\sqrt{\mu_r''\varepsilon_r'' - \mu_r'\varepsilon_r' + \sqrt{\left(\mu_r''\varepsilon_r'' + \mu_r'\varepsilon_r'\right)^2}} \quad (3)$$

In theory, the more powerful loss EWAMs have, the stronger EM absorption should be. However, the actual performance of EWAMs is not always consistent with their loss capability. This is because there is another important concept, impedance matching, related to EM absorption performance [94, 95]. Impedance matching determines the transmission behavior of EM waves at the interface between free space and EWAMs, and most EM waves will be reflected back at the interfaces if impedance of EWAMs is mismatched with that of free space [37]. Stergiou and Litsardakis elucidated the conditions for zero reflection of incident EM waves from three aspects in detail [96], while all of them required very accurate prerequisites that, unless EWAMs had extremely low $\varepsilon_r$ and $\mu_r$, were nearly impossible to be realized in relatively broad frequency range. That is to say, only wave-transparent materials may have the chance to achieve approximate zero-reflection conditions. The values of $\varepsilon_r$ and $\mu_r$ in EWAMs are significantly larger than those of wave-transparent materials, and thus the front surface of EWAMs inevitably deviates from zero-reflection conditions, which is essentially induced by the gap between $\varepsilon_r$ and $\mu_r$ ($\varepsilon_r > \mu_r$ in most cases) [97]. Such a situation means that it is necessary to pay close attention to the gap between $\varepsilon_r$ and $\mu_r$ when EWAMs are designed, and otherwise, an overlarge gap will bring mismatched impedance and very poor absorption performance no matter how powerful intrinsic loss intensity they have [37]. Generally speaking, there are two ways that may improve impedance matching of EWAMs. One is to increase the contribution of magnetic loss, while this way requires high content of magnetic components [80, 98], which is not favourable for the formation of lightweight EWAMs. The other way is to reduce relative complex permittivity moderately. For carbon-based composites, this goal can be achieved through the decrease in the relative graphitization degree of carbon matrix and the filler loading of carbon-based composites [99, 100], and furthermore, the introduction of porous structure will also show a similar effect, because the presence of porous structure can pull down the effective permittivity according to Maxwell–Garnett's theory [101, 102]. Ma et al. proposed a delta-function method to deduce in terms of Eqs. (4)–(6) [103]

$$|\Delta| = \left|\sinh^2(Kfd) - M\right| \quad (4)$$

$$K = \frac{4\pi\sqrt{\mu_r\varepsilon_r}\sin\frac{\delta_E+\delta_M}{2}}{c\times\cos\delta_E\cos\delta_M} \quad (5)$$

$$M = \frac{4\mu_r'\cos\delta_E\varepsilon_r'\cos\delta_M}{\left(\mu_r'\cos\delta_E - \varepsilon_r'\cos\delta_M\right)^2 + \left[\tan\left(\frac{\delta_M}{2} - \frac{\delta_E}{2}\right)\right]^2\left(\mu_r'\cos\delta_E + \varepsilon_r'\cos\delta_M\right)^2} \quad (6)$$

and they concluded that the region with the modulus of delta close to zero would possess excellent impedance matching. In some

following studies, $|\Delta| \leq 0.4$ was usually considered as a threshold for acceptable impedance matching [104, 105]. One thing to note is that this delta-function method is established on the test model of EM absorption, where a back metal plate is always integrated with EWAMs [103]. As a result, this method is trouble in evaluating the impedance matching of low-loss EWAMs or wave-transparent materials, and assumes the very poor impedance matching of these materials. Another method is from the calculation on the normalized input impedance ($Z_{in}$) of EWAMs layer

$$Z_{in} = \sqrt{\frac{\mu_r}{\varepsilon_r}} \tanh\left[j\left(\frac{2\pi}{c}\right) fd\sqrt{\mu_r \varepsilon_r}\right] \quad (7)$$

where $c$ and $d$ are the velocity of incident EM waves and the thickness of EWAMs layer, respectively. It is widely accepted that there will be the optimum impedance matching when the modulus of $Z_{in}$ approaches to 1 or the modulus of $Z_{in} - 1$ approaches to 0 [106–108]. However, an error still exists due to the difference between real $Z_{in}$ and the modulus of $Z_{in}$, and thus this method usually cannot explain why the values of reflection loss (RL) do not reach infinity under the condition that the modulus of $Z_{in}$ equals to 1 or the modulus of $Z_{in} - 1$ equals to 0. As we all know, the wave impedance of free space is 377 Ω, and thus one can also obtain the intrinsic wave impedance of EWAMs according to Eq. (8) [109, 110]

$$\eta_{in} = \sqrt{\frac{\mu_0}{\varepsilon_0}} \times \sqrt{\frac{\mu_r}{\varepsilon_r}} \quad (8)$$

where $\varepsilon_0$ and $\mu_0$ are complex permittivity and complex permeability of free space, respectively. The difference in wave impedance between free space and EWAMs can be directly presented, and thus as far as we know, it will be an effective pathway to assess the impedance matching of EWAMs in the future.

### 2.3 EM test and performance evaluation

There are three common methods that can be employed to show the performance of EWAMs in previous studies, namely arch method, waveguide method, and coaxial method [111]. Arch method obtains EM absorption performance by comparing the difference in EM signals reflected from blank metal plate and the one with EWAMs layer. It is also easy to record angle-dependent absorption performance through the manipulation on the incident angle of EM waves during the test, and thus arch method is considered as one of the most effective methods to evaluate the actual performance of EWAMs [69, 112]. However, the test of arch method is always conducted on a resin film or moulded plate with large size, e.g., a size of 18 mm × 18 mm for 1–18 GHz test, which requires a large amount of EWAMs and consequently limits its popularization in some laboratories on theoretical research. In contrast, waveguide method and coaxial method are more widely used in research papers. Although their testing principles are different, both of them can ascertain RL characteristics calculated from normalized input impedance (please refer to Eq. (8)) with Eq. (9) [111, 113]

$$\text{RL (dB)} = 20\log\left|\frac{Z_{in} - 1}{Z_{in} + 1}\right| \quad (9)$$

Compared with coaxial method, waveguide method is not only effective for the calculation of EM absorption, but also works for the theoretical estimation on total EM shielding efficiency [114–116]. It has to be mentioned that the test frequency band of waveguide is relatively narrow, and most studies using waveguide method focus on their frequency range in 8.2–12.4 GHz (X band), while the test of coaxial method is easily completed in 1.0–18.0 GHz (L, S, C, X, and Ku bands) [117–123]. The results from these three methods are very susceptible, and thus stable operation and accurate calibration are extremely important before the test in order to avoid the emergence of some abnormal and unreliable data.

Minimum RL and wideband absorption are two highly concerned characteristics for EWAMs. Minimum RL usually corresponds to the largest absorption efficiency in the studied frequency range. It is worth noting that more and more studies attempt to deduce the matched thickness of EWAMs layer with the calculated minimum RL at a specific frequency point from Eqs. (7) and (9), and conclude that the consumption of incident EM waves complies with a quarter-wavelength model, because the so-called experimental thickness is always very pretty close to the theoretical thickness. In fact, Eqs. (7) and (9) applied to calculate minimum RL are established on the quarter-wavelength model [124–126], and thus the deduced thickness is inevitably consistent with the theoretical one. Therefore, such a comparison is not necessary in our opinion. Instead, the researchers in the related field should pay more attention to intrinsic loss and impedance matching of EWAMs. The extensive studies on EWAMs have brought us valuable experience in keeping the balance between intrinsic loss and impedance matching, and thus it is common that many EWAMs can have powerful absorption with minimum RL less than −50.0 dB [43, 127]. However, such a balance is still difficult to maintain in a wide frequency range, and the difference in absorption efficiency will be exponentially diminished once minimum RL exceeds −10.0 dB, and thus wideband absorption has become a hotter topic in EM absorption. The threshold for effective absorption is generally set at −10.0 dB, and effective absorption bandwidth (EAB), the frequency range with RL less than −10.0 dB, is defined as a popular indicator for wideband absorption [43, 104, 128]. It is worth noting that some EWAMs may possess considerable RL intensity and EAB in a specific frequency range, while their performance drastically degrades in other frequency ranges. Therefore, the performance evaluation of EWAMs should be comprehensively carried out in a broad frequency range rather than in an appointed range, and moreover, some other parameters, such as filler loading, absorber thickness, and even corrosion resistance, highly related to their practical applications, should also be concerned [97, 129].

## 3 Core–shell composites with built-in carbon cores

Although carbon materials exhibit great potential in the field of EM absorption, there are few reports on core–shell carbon-based EWAMs in early studies, because conventional carbon materials, such as graphite and carbon black, usually have disordered morphology and random particle size, which pose considerable obstacle to the rational design on core–shell carbon-based composites. Since the 1990s, the controllable synthesis of carbon materials has made great progress, and many novel carbon materials with tailorable size, including carbon spheres, CNTs, graphene, and 3D aerogel, are definitely reported and start to be applied in various research fields. There is no doubt that this situation also promotes the development of core–shell carbon-based EWAMs immensely, and thus we will discuss, in this section, the related composites with built-in carbon cores according to their morphologies.

### 3.1 Carbon spheres

Thanks to intrinsic dielectric loss, pure carbon spheres can generate moderate EM attenuation without the assistance of any

additives, and their performance is even superior to those of graphitic carbon materials because their amorphous nature endows them obvious advantages in impedance matching [18, 130]. For example, Wang et al. reported that solid carbon microspheres derived from biomass could exhibit good EM absorption performance in Ku band, whose minimum RL intensity and EAB were −37.2 dB and 5.7 GHz, respectively, with a route thickness of 2.0 mm [131]. It was unfortunate that when the frequency of incident EM waves was out of Ku band, the performance of these carbon microspheres would be drastically reduced. The introduction of magnetic shells on the surface of carbon spheres is considered as a well-directed strategy to enhance EM functions, not only for the expected profits from the formation of magnetic loss mechanism, but also for the additional interfacial synergy through the establishment of core–shell configuration. Wang et al. carried out the physical adsorption of $Fe^{3+}$ and $Co^{2+}$ on the surface of glucose-derived carbon microspheres, and then harvested core–shell carbon@FeCo microspheres via high-temperature carbothermal reduction [132]. However, the limited loading of FeCo alloy shells, as well as the graphitization of carbon microspheres during high-temperature treatment, did not bring significant improvements, and the minimum RL intensity and EAB were only −16.0 dB and 2.0 GHz (7.6–9.6 GHz), respectively. Li et al. induced *in situ* growth of needle $NiCo_2O_4$ on the surface of carbon microspheres densely, and the presence of $NiCo_2O_4$ made solid contribution to impedance matching and magnetic loss, which consolidated the absorption performance of the final composites in C and X bands to a certain degree [133]. More recently, Zhao et al. investigated the evaluation of Ni, Co, and NiCo shells under the conditions of hydrothermal reduction, and found that only when cobalt and nickel ions coexisted could a continuous metallic shell be formed on carbon microspheres [134]. This careful modulation on external metallic shells indeed produced effective improvement in EM absorption, and the EAB of C@NiCo was extended to 6.7 GHz with an absorber thickness of 2.1 mm and the total effective absorption almost covers C, X, and Ku bands by manipulating the thickness from 2.0 to 4.5 mm.

It is a consensus that there are strong forces between magnetic nanoparticles, including electron affinity, surface tension, van der Waals forces, and magnetic dipole interactions [135], and thus the construction of a continuous shell on carbon microspheres is not easy to realize and always requires a very precise control. In the past few years, binary dielectric composites have been extensively developed and displayed tremendous potential as lightweight and durable EWAMs [32, 136]. Several groups, in this context, show their interest in integrating the design concepts of binary dielectric composites and core–shell composites, and the typical additives for external shells includes metal oxides, metal sulphides, and conductive polymers [137–140]. Literature review indicated that these dielectric shells could promise similar enhancement in both minimum RL intensity and EAB to those magnetic counterparts, and especially for $MoS_2$, the resultant core–shell C@$MoS_2$ microspheres gave a minimum RL intensity of −52.6 dB and the best EAB of 6.2 GHz with a small absorber thickness (1.4–1.6 mm, Figs. 2(a)–2(d)) [140]. Such a good performance was attributed to the interfacial synergy between interior carbon spheres and external $MoS_2$ shells, as well as multiple refraction among $MoS_2$ layers and possible inhibition on skin effect.

Apart from the intrinsic loss and the synergy of different EM components, microstructure is playing as a very active role in the design of high-performance EWAMs, because it may intensify the multiple reflection of incident EM waves and promote the consumption of EM energy [141, 142]. As a result, hollow carbon spheres (HCSs) become much more popular scaffolds for core–shell carbon-based EWAMs in the latest studies [143–149]. The formation of hollow cavity is usually dependent on the space occupation of inorganic hard templates, which is finally etched through acidic or alkaline treatment. Yang et al. coated HCSs with $MnO_2$ nanosheets through the decomposition of $KMnO_4$ under acidic condition, and HCSs played as the nucleation sites for the growth of $MnO_2$ nanosheets (Fig. 2(e)) [149]. The external diameter and the shell thickness of HCSs were about 230 and 10 nm (Figs. 2(f)–2(h)), respectively, and $MnO_2$ nanosheets were found to be grown vertically on the surface of HCSs (Fig. 2(i)). After the optimization of $MnO_2$ loading, they found that when the mass ratio of $KMnO_4$ to HCSs reached 20:1, the resultant composite, HCS-Mn-2.0, could produce the best EM absorption characteristics, whose minimum RL intensity was −53.5 dB with an absorber thickness of only 1.5 mm and the corresponding EAB was 4.6 GHz (Fig. 2(j)). Both minimum RL intensity and EAB of HCS-Mn-2.0 were much better than those of the solid counterpart (CS-Mn-2.0, Figs. 2(j) and 2(k)), and they attributed this enhancement to the balance between impedance matching and dielectric loss, as well as multiple polarization relaxations induced by hollow cavity. Hu et al. manipulated the growth of $NiCo_2S_4$ nanosheets on HCSs with a hydrothermal reaction (Fig. 2(l)). Although $NiCo_2S_4$ nanosheets presented similar growth style to $MnO_2$ nanosheets, their narrower band gap was more favourable for electron transfer and thus endowed the final composites with stronger attenuation ability. The minimum RL intensity and EAB were −65.1 dB and 6.6 GHz, and the overall EAB was as broad as 14.4 GHz by integrating the absorber thickness from 1.0 to 5.0 mm (Fig. 2(m)). The EM enhancement mechanism was also related with good conductivity loss, diversified polarization modes, and multiple reflection of incident EM waves (Fig. 2(n)).

### 3.2 CNTs/carbon nanofibers (CNFs)/carbon nanocoils (CNCs)

In recent years, one-dimensional carbon materials have been widely utilized as the main component in high-performance EWAMs, because their ultrahigh anisotropy ratio is favourable for electron transfer and hopping, resulting in the formation of conductive networks and powerful dielectric loss [3, 150]. It is unfortunate that one-dimensional carbon materials easily suffer from mismatched impedance due to their relatively high graphitization degree, and thus the surface coating with heterogeneous EM components can improve impedance matching and reinforce interfacial synergy at the same time. As a typical kind of commercially available carbon materials, carbon fibers (CFs) are very attractive for the construction of core–shell carbon-based EWAMs, which benefits from the fact that their large diameter over several microns simplifies the coating process. For example, SiC nanowire arrays can be harvested on the surface of CFs by chemical vapor deposition (CVD) [151–153], and hierarchical $MoS_2$ nanosheets can also be generated on CFs through *in situ* hydrothermal growth [154]. Several groups even paved the pathway for the formation of uniform and continuous metal-organic frameworks (MOFs) layers, and also provided a universal platform to convert these important intermediates into various functional heterogeneous shells [155–157]. Of note is that the good conductivity and large diameter of CFs may induce skin effect even if there are heterogeneous shells on their surface [158, 159], and thus most CFs-based composites fail to promise highly impressive EM absorption performance, especially for their EABs that are generally less than 5.0 GHz.

As we mentioned above, the decrease of the size is an effective method to suppress skin effect, and thus CNTs and CNFs are more popular candidates for core–shell carbon-based EWAMs than CFs, and nevertheless, their much smaller diameter also

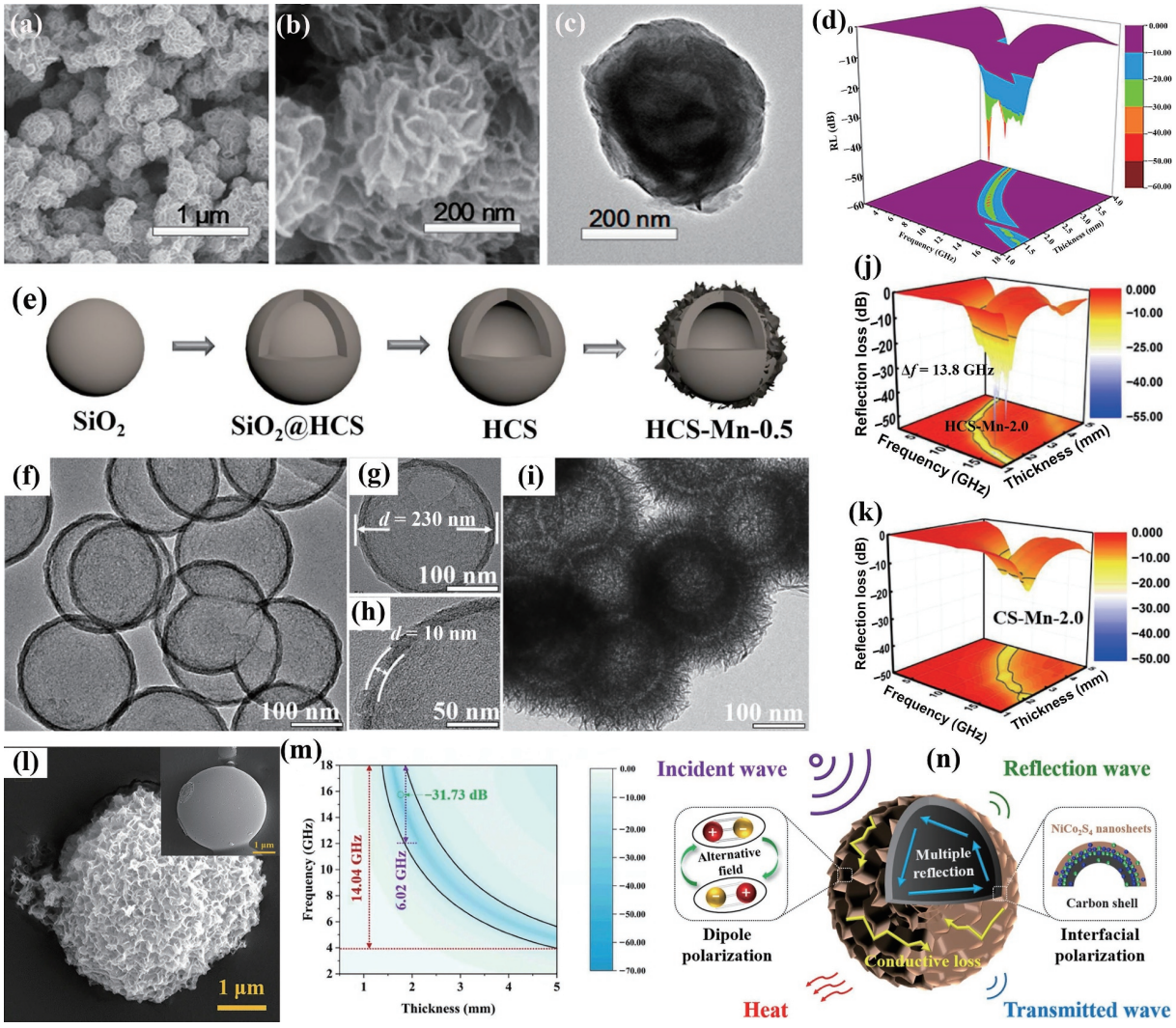


**Figure 2** (a) and (b) Scanning electron microscopy (SEM) images, (c) TEM image, and (d) RL map of solid CS@$MoS_2$. Reproduced with permission from Ref. [140], © Elsevier B.V. 2018. Schematic diagram for the preparation process of (e) HCS-Mn-2.0 and ((f)–(i)) its TEM images, and RL maps of (j) HCS-Mn-2.0 and (k) CS-Mn-2.0. Reproduced with permission from Ref. [149], © Elsevier B.V. 2019. SEM image of (l) C/$NiCo_2S_4$ (inset is SEM image of $SiO_2$@C spheres, scale bar: 1 μm), and (m) its RL map and (n) possible EM absorption mechanism. Reproduced with permission from Ref. [144], © Hu, P. T. et al. 2021.

poses a greater challenge for the construction of heterogeneous shells. Conductive polymers, such as polyaniline (PANI) and polypyrrole (PPy), always reside at the frontier of potential heterogeneous shells, because π–π stacking interaction between conductive polymers and graphitic carbon materials may induce the polymerization of organic monomers along with carbon surface [160–163]. In despite of that, it is still necessary to conduct the surface modification of these one-dimensional carbon nanomaterials [164, 165]. Cheng et al. treated CNTs with inductively coupled plasma and then oxygen was delivered to the surface of CNTs to produce oxygen radicals (Fig. 3(a)) [166]. This plasma pre-treatment significantly promoted the polymerization of aniline monomers on the surface of CNTs, and created uniform and dense core–shell CNTs@PANI composite (Fig. 3(b)). The EM absorption performance was found to be related with the radio-frequency power, and when the power was set at 50 W, the final composite would have the strongest RL intensity of −41.4 dB and the broadest EAB of 8.2 GHz (Fig. 3(c)). Wang et al. also obtained core–shell CNTs@PANI composites with PVP-modified CNTs as the nucleation sites (Figs. 3(d) and 3(e)). After an optimization on the loading of PANI, the final composite displayed minimum RL of −41.5 dB and EAB of 5.1 GHz with an absorber thickness of 2.0 mm (Fig. 3(f)). EM analysis revealed that electron migration in CNTs and electron hopping from CNTs to PANI layer resulted in good conductivity loss, and the coating of PANI layer not only created sufficient interfacial polarization, but also played as an impedance matching layer (Fig. 3(g)). Li et al. further induced the polymerization of aniline monomers on both external and internal surface of hollow prism-shaped carbon tubes, and they found this composite could produce broad EAB (9.5–14.5 GHz) in middle frequency range [167].

The extensive utilization of conductive polymers as external shells of core–shell carbon-based composites is benefitted from their continuous polymerization along the surface of CNTs/CNFs to a large extent. In contrast, it is not easy to create uniform shells with inorganic nanoparticles on the surface of CNTs/CNFs, because the agglomeration of inorganic nanoparticles usually leads to random cracks and incomplete coating [169, 170]. Only a few CNTs/CNFs-related composites with uniform inorganic shells, e.g., CNTs@Si, CNFs@FeCo, and CNFs@SiOC, have been successfully fabricated through CVD technique [171–173]. Although these core–shell composites may produce better EM absorption performance than their homologous composites, they do not exhibit any superiorities to those conductive polymers related composites, and thus there is no much attention on this kind of composites. Different from inorganic nanoparticles, some two-dimensional materials composed of ultra-thin nanosheets are usually anchored on the surface of carbon materials vertically,

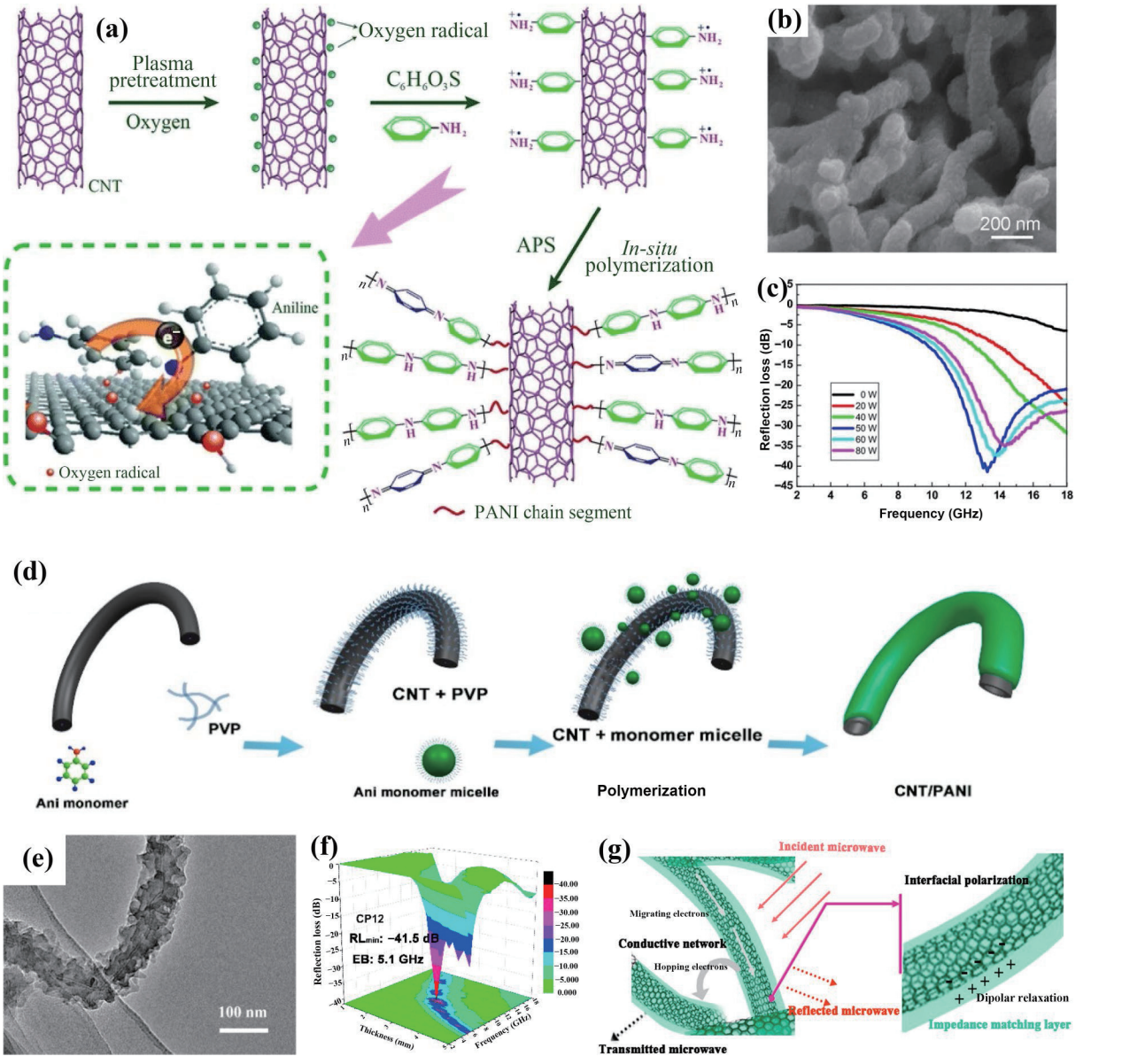


**Figure 3** (a) Formation mechanism of CNTs/PANI composite with plasma treatment, (b) SEM image, and (c) power-dependence RL curves of CNTs@PANI composite. Reproduced with permission from Ref. [166], © Springer-Verlag Berlin Heidelberg 2015. (d) Schematic diagram for the formation of CNTs@PANI composite through PVP modification, and (e) the corresponding TEM image, (f) RL map, and (g) possible EM absorption mechanism. Reproduced with permission from Ref. [168], © Elsevier Ltd. 2020.

which not only ensures the complete coating of CNTs, but also provides an opportunity to regulate the thickness of heterogeneous shells [174–177]. Xu et al. prepared core–shell CNFs@$MnO_2$ through ozone pre-treatment and hydrothermal reaction (Figs. 4(a) and 4(b)) [178]. The content of $MnO_2$ nanosheets could be tailored from 29.3 wt.% to 67.2 wt.%, and the optimal composite gave minimum RL of −35.0 dB and EAB of 5.0 GHz with an absorber thickness of only 1.8 mm (Fig. 4(c)). The alleviation on interface impedance gap, as well as multiple loss mechanisms, including intrinsic eddy current and conductivity loss, intensive reflection and scattering between nanosheets, defect-induced dipolar polarization, and interfacial polarization, is together responsible for good EM absorption.

CNCs are a kind of very unique one-dimensional carbon materials with characteristic chirality. Ro et al. ever revealed the dependence of the propagation behavior of incident EM waves on chiral parameters and found that cotton effect would occur at maximum power absorption [179]. Tang et al. reported that CNCs could produce EAB close to 4.0 GHz with an absorber thickness of 2.0 mm and the corresponding minimum RL was about −18 dB, superior to those of primitive CNTs and CNFs [180]. However, the chirality of CNCs makes it more difficult to construct uniform external shells. Qin's group pioneered the synthesis of core–shell composites based on CNCs through atomic layer deposition (ALD) [40]. As observed, when $Al_2O_3$ and $Fe_3O_4$ layers were coated on CNCs successively, the resultant composites would display much better performance than pure CNCs (Figs. 4(d)–4(h)). The fine manipulation on ALD cycles of $Al_2O_3$ and $Fe_2O_3$, as well as the number of supercycles, could result in periodical arrangement of $Al_2O_3$ and $Fe_3O_4$ layers on CNCs, which reinforced minimum RL (−40.4 dB) and EAB (5.7 GHz) effectively (Fig. 4(i)). It is very interesting that this advanced technique also provides a solution to the dilemma of CNTs/CNFs in supporting inorganic nanoparticles [181]. Zhao et al. even designed gradient multilayer nanofilms on CNCs (Figs. 4(j) and 4(k)) and raised minimum RL intensity up to −58.5 dB in the absence of any magnetic components. Multiple polarization loss and EM reflection were considered as the primary mechanisms for energy consumption (Fig. 4(l)) [182].

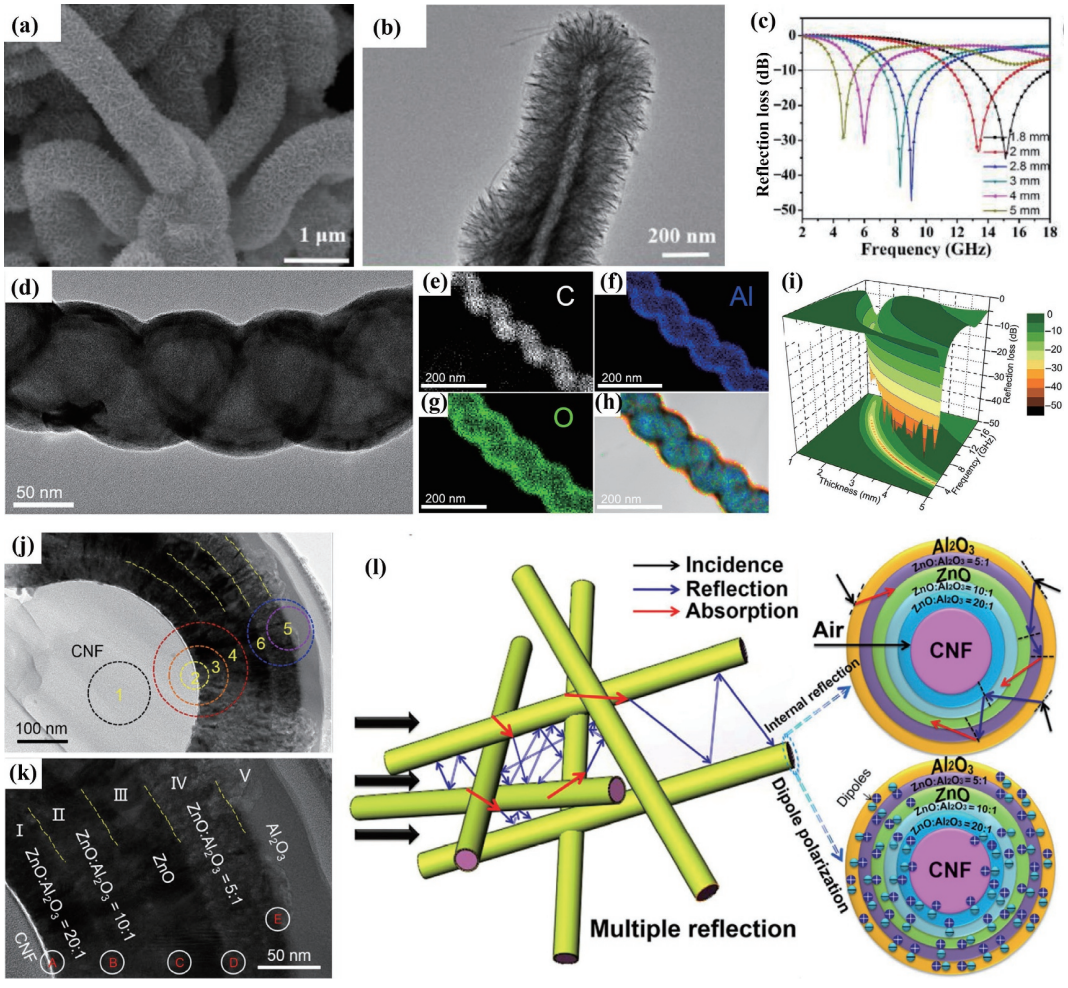


**Figure 4** (a) SEM image, (b) TEM image, and (c) RL curves of CNTs@$MnO_2$ composite. Reproduced with permission from Ref. [178], © Xu, X. F. et al. 2019. (d) TEM image, (e)–(h) elemental mapping images, and (i) RL map of CNCs@$Al_2O_3$@$Fe_3O_4$ from ALD technique. Reproduced with permission from Ref. [40], © American Chemical Society 2012. (j) and (k) TEM images of the cross section of CNCs with gradient multilayer nanofilms, and (l) the possible EM absorption mechanism therein. Reproduced with permission from Ref. [182], © Tsinghua University Press and Springer-Verlag GmbH Berlin Heidelberg 2017.

### 3.3 Graphene

The discovery of graphene is like a shot in the arm for the researchers in the field of EM absorption, because its intrinsic characteristics, including large carrier mobility, good thermal conductivity, high mechanical strength, and low coefficient of thermal expansion, provide tremendous potential to develop various high-performance EWAMs [25, 26]. In addition, the theoretical single-layer structure of graphene also offers an opportunity to fully utilize interfacial interaction in the related composites. Although hundreds of graphene-based composites have been reported in the past decade, most of them just decorated graphene or rGO nanosheets with different EM components in order to regulate EM property and improve impedance matching [27, 183, 184]. This situation suggests that the construction of graphene-based composites with core–shell configuration is still desirable to strengthen the profits from interfacial synergy, while the large size of graphene or rGO nanosheets remains a big challenge in creating uniform and complete shells. The first successful example was achieved by growing PANI nanorods vertically on the surface of graphene nanosheets [185]. The formation of PANI shells generated multiple polarization relaxations, and the charge transfer between graphene and PANI nanorods was revealed by theoretical simulation. As a result, the composite exhibited minimum RL of −45.1 dB and EAB of 6.2 GHz with an absorber thickness of 2.5 mm. Zhang et al. found that there would be covalent C=N bond between PANI nanorods and graphene nanosheets, and the optimization on the dosage of doping agent ($HClO_4$) could make the composite maintain its good performance (minimum RL: −38.6 dB, EAB: 5.8 GHz) in C and X bands as the absorber thickness was increased to 3.7 mm [186]. In addition to good EM performance, Wang et al. also demonstrated the excellent corrosion resistance of core–shell GO@sulfonated PANI composite, whose protection capability on Q235 steel could reach as high as 97.43% after immersion in corrosive medium for 168 h [187].

Similar to PANI nanorods, some inorganic nanorods and nanosheets can be also planted on graphene nanosheets densely [188–191]. For example, Chen's group induced the growth of $Fe_3O_4$ nanorods (length: 600 nm, diameter: 100 nm) on rGO nanosheets, and they found that neither rGO nanosheets nor $Fe_3O_4$ nanorods could produce RL intensity less than −10 dB in the frequency range of 2.0–18.0 GHz, while the composite pulled down RL intensity to −61.5 dB drastically (Figs. 5(a)–5(c)) [190]. In a following study, they further manipulated the vertical growth of γ-$Fe_2O_3$ with similar EM absorption performance, and they concluded that interfacial polarization and dipolar polarization, as well as geometrical effect and dielectric resonance induced by interfacial dual double layer model, generated considerable contribution [188]. Although one-dimensional nanorods can be successfully applied to be the external shells of graphene, it is very difficult for common nanoparticles to create such dense shells, because high surface energy will cause their serious agglomeration once the loading on graphene exceeds a critical value. It is very

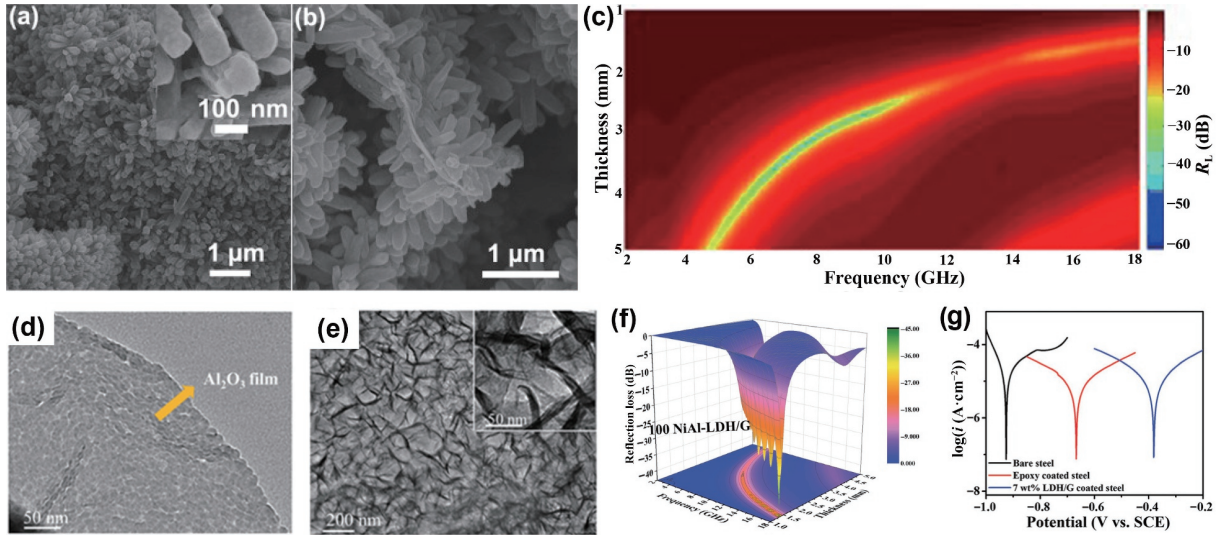


**Figure 5** (a) and (b) SEM images and (c) RL map of graphene@$Fe_3O_4$ nanorods. Reproduced with permission from Ref. [190], © Wiley-VCH Verlag GmbH & Co. KGaA, Weinheim 2014. TEM images of (d) $Al_2O_3$-deposited graphene and (e) graphene@NiAL-LDH, and (f) RL map of graphene@NiAL-LDH. (g) Corrosion potential curves of bare steel, epoxy coated steel, and graphene@NiAl coated steel. Reproduced with permission from Ref. [39], © Xu, X. F. et al. 2021.

interesting that Wang et al. broke through this bottleneck with ALD technique, where $Fe_3O_4$ and Ni shells composed of ultrafine nanoparticles were fabricated smoothly [76]. Thanks to the sufficient interfacial synergy, the resultant $Fe_3O_4$/graphene could dissipate EM energy effectively in the frequency range of 3.4–18.0 GHz by accumulating the absorber thickness from 1.2 to 5.0 mm. They also converted $Al_2O_3$ layers on graphene into NiAl-layered double hydroxide (NiAl-LDH) by a hydrothermal reaction (Figs. 5(d) and 5(e)) [39]. The final product from 100 deposition cycles of $Al_2O_3$ not only displayed good EM performance, but also presented better corrosion resistance than conventional resin protecting layer (Figs. 5(f) and 5(g)).

### 3.4 Three-dimensional carbon aerogel/foam

In 2015, Zhang et al. reported ultra-broadband EM response (60.5 GHz) of graphene foam with extremely low density of 14 mg/cm$^3$, and they proposed that induced current generated in the three-dimensional conductive network was primarily responsible for the energy consumption of incident EM waves [69]. This finding arouses extensive interest in the research of three-dimensional carbon aerogel/foam for the fabrication of lightweight and highly efficient EWAMs [183, 192, 193]. Actually, the open skeleton structure not only provides auxiliary pathway for energy consumption through multiple reflection of EM waves, but also endows final product with some additional functions, e.g., self-cleaning, thermal insulation, fire retardance, infrared stealth, and moisture capture [194–198]. Current research progress shows that the introduction of various heterogeneous EM components is still a mainstream direction to regulate EM property and reinforce EM absorption of three-dimensional carbon aerogel/foam [199–203]. However, a very similar phenomenon to graphene-based composites is that most examples for performance enhancement are established on the surface decoration of three-dimensional carbon aerogel/foam rather than the construction of a complete heterogeneous shell. This is because the complicated internal structure of three-dimensional carbon aerogel/foam from common methods, such as hard-template strategy, biomass transformation, and GO self-assembly, usually cannot ensure the uniform and continuous growth of heterogeneous components along with the skeleton [204–208].

Instead of these three-dimensional carbon aerogel/foam, more and more groups favour the utilization of some hydrophilic sponges commercially available, such as polyurethane and melamine, as the precursors of carbon scaffolds in core–shell composites. One option is to convert these sponges into carbon frameworks after thermal treatment, and then CVD technique is applied to create heterogeneous shells [209–211]. For example, Ye et al. coated melamine-derived carbon foam with SiC nanowires and built up a unique double network structure [211]. EM measurement revealed that the growth of SiC nanowires improved impedance matching significantly, but induced intensive interior multiple reflection, and meanwhile, the enough contact between carbon scaffold and SiC nanowires also brought obvious enhancement in interfacial polarization. The final composite displayed its minimum RL of −36.1 dB and EAB of 4.52 GHz with an absorber thickness of 2.60 mm. The other option is to adsorb inorganic salts or organic small molecules in some sponges, and then these inorganic salts or organic small molecules could be converted into heterogeneous shells during high-temperature pyrolysis and the employed sponge could be turned into three-dimensional carbon scaffold synchronously [194, 212–214]. Wei et al. soaked melamine foam into $Ni^{2+}$/$Co^{2+}$ solution and conducted the growth of NiCo hydroxides through hydrothermal reaction, and finally obtained continuous NiCo nanoarrays on three-dimensional carbon foam [213]. After the optimization on the loading of NiCo nanoarrays, the EAB of final composite could reach as broad as 7.16 GHz with an absorber thickness of 2.2 mm, and the corresponding RL was beyond −40.0 dB. Gu et al. absorbed $Co^{2+}$ on melamine foam and then manipulated the growth of ZIF-67 shells by the introduction of 2-methylimidazole [194]. High-temperature pyrolysis realized the conversion of ZIF-67/melamine into three-dimensional carbon foam coated by Co/C heterogeneous shells. Besides those predictable magnetic loss and polarization loss, the unique microstructure was found to be favorable for electron migration and hopping, as well as multiple reflection of incident EM waves, which accounted for good EM absorption performance (RL: −59.8 dB, EAB: 5.64 GHz) of final composite. Very recently, Meng's group pioneered the synthesis of macroscopic core–shell carbon-based composites through coaxial electrospinning-freeze frying technique (Fig. 6(a)) [215]. The interior cores of the composites (Carbon@RGO/$Fe_3O_4$) were three-dimensional carbon aerogel derived from chitosan, and their external shells were composed of graphene nanosheets attached with $Fe_3O_4$ nanoparticles (Figs. 6(b) and 6(c)). This novel structure provided sequential attenuation for incident EM waves, and surface current density suggested that a well-matched impedance was created in the composites, while volume loss intensity

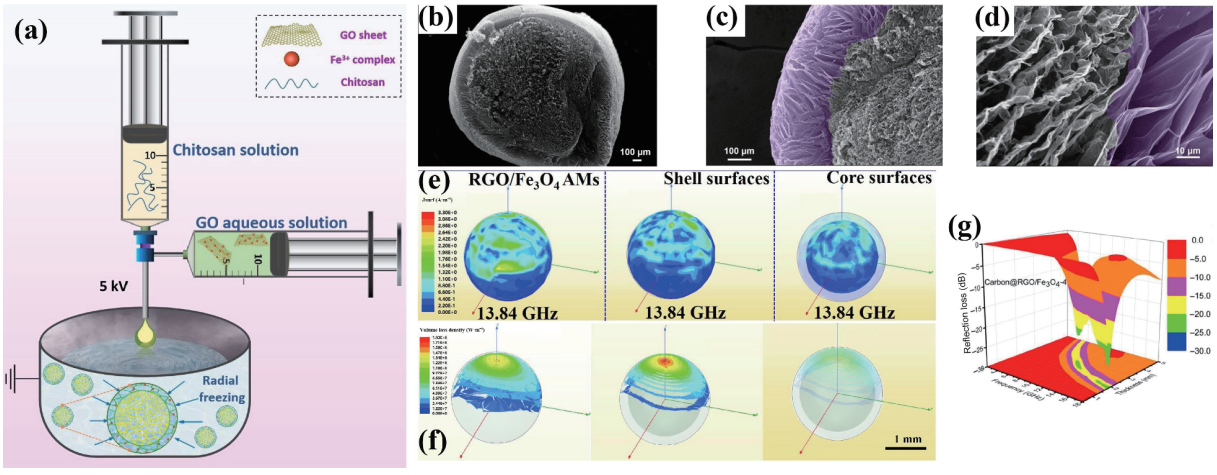


**Figure 6** (a) Schematic illustration of preparing the Carbon@RGO/$Fe_3O_4$ composites. SEM images of (b) the cross-section view and ((c) and (d)) partial enlarged cross section of the as-prepared Carbon@RGO/$Fe_3O_4$. (e) The surface current density and (f) volume loss density of Carbon@RGO/$Fe_3O_4$, external RGO/$Fe_3O_4$ shell, and chitosan-derived interior core at 13.84 GHz. (g) Three-dimensional representation of RL values at different thickness of Carbon@RGO/$Fe_3O_4$. Reproduced with permission from Ref. [215], © Elsevier B.V. 2022.

confirmed a great resonant cavity rooted by chitosan-derived carbon aerogel (Figs. 6(d)–6(f)). The regulation on the thickness of external graphene shells could lead to an extension of EAB to 7.52 GHz (Fig. 6(g)).

## 4 Core–shell composites with built-out carbon shells

The foregoing section has clarified the progress of core–shell composites with built-in carbon cores according to their different morphologies. Apart from serving as internal cores, carbon materials are more often utilized as the external shells of carbon-based composites, because their good chemical stability not only suppresses the agglomeration of internal cores effectively, but also protects them from corrosion under some harsh conditions. What is more, the dielectric property of carbon materials can be rationally manipulated by their crystallinity and microstructure, and thus it will be easier to regulate EM functions of core–shell composites as carbon shells are controllably built up.

### 4.1 Nanoparticles embedding

Che et al. reported for the first time that crystalline Fe in CNTs could produce strong anisotropy field due to the confinement effect and contribute to magnetic loss greatly [216]. This exiting discovery drives intensive interest in the embedment of magnetic nanoparticles into some as-prepared carbon materials. In early studies, CNTs were taken as one of the most popular hosts due to their proper void and good dielectric property [217, 218]. For example, Zhao et al. filled CNTs with Fe and Co nanoparticles via a wet-chemical method, and they found that Fe-filled CNTs could exhibit smaller RL than Co-filled CNTs (−31.7 vs. −21.8 dB), while the corresponding EAB was less than that of Co-filled CNTs (2.9 vs. 3.4 GHz) [219, 220]. Zhu's group compared the performance of Co-filled CNTs and Fe-filled CNTs from wet-chemical method and CVD technique, respectively [221, 222]. The results indicated CVD technique could increase the loading of Fe nanoparticles and even produce Fe nanowires inside CNTs, and thus Fe-filled CNTs from CVD technique extended EAB from 2.9 to 4.2 GHz successfully [219, 221]. Although the embedment of Fe and Co nanoparticles indeed improved EM absorption performance of CNTs to some extent, the agglomeration of nanoparticles on the external surface of CNTs easily occurred due to their strong interaction [223]. As a result, some dielectric components, such as Ag nanowires, $Er_2O_3$ nanoparticles, $Sm_2O_3$ nanoparticles, and Sn nanoparticles, were also applied to be the fillers inside CNTs [224–228]. It is unfortunate that the limited loading of these fillers and the high crystallinity of CNTs cannot create desirable impedance matching, and thus such composites usually suffer from narrow EAB less than 4.0 GHz.

Ordered mesoporous carbon with cylindrical channels can also be selected as the hosts to confine some heterogeneous EM components [229–232]. Wang et al. ever confined γ-$Fe_2O_3$, $Fe_3O_4$, and Fe nanoparticles within ordered mesoporous carbon by a combined process of impregnation, pre-hydrolysis, and reduction, and investigated their EM performance in detail [233]. Although all of them could generate magnetic loss and multiple polarization relaxations, γ-$Fe_2O_3$ and $Fe_3O_4$ nanoparticles made a larger contribution to impedance matching than Fe nanoparticles, resulting in better EM absorption in X band. In addition, some dielectric components, e.g., $Al_2O_3$, $TiO_2$, and $Ni_2O_3$, also displayed significant promotion on EM absorption of ordered mesoporous carbon, where the composite of $Al_2O_3$/mesoporous carbon even produced EAB as broad as 7.4 GHz with an absorber thickness of 3.0 mm [232, 234, 235]. However, ordered mesoporous carbon faces the same matter as CNTs, i.e., the agglomeration of heterogeneous components on the external surface may pull down the EM performance of the corresponding composites [236–238]. In order to avoid external deposition and agglomeration of heterogeneous components, hollow mesoporous carbon microspheres are utilized as the hosts to accommodate additional EM components in the latest research [100, 239, 240]. For example, Cheng et al. induced the nucleation and growth of $Fe_3O_4$ nanocrystals inside hollow mesoporous carbon microspheres, and the resultant composite promised strong RL of −60.2 dB and broad EAB of 5.7 GHz with an absorber thickness of 2.3 mm [240]. Ning et al. conducted a "ship-in-bottle" growth of $MoS_2$ nanosheets inside hollow carbon microspheres ($MoS_2$@HCS, Figs. 7(a)–7(e)). Although the formation of $MoS_2$ nanosheets did not bring essentially enhanced EM absorption, the required absorber thickness for similar absorption was much decreased in the frequency range of 2.0–40.0 GHz, because the impedance matching was significantly improved and more loss mechanisms were created (Figs. 7(f) and 7(g)).

### 4.2 Arc discharge

Since arc discharge was successfully applied for the synthesis of $LaC_2$ nanoparticles coated with thin graphite layer in 1993, it has attracted extensive attention in the construction of core–shell

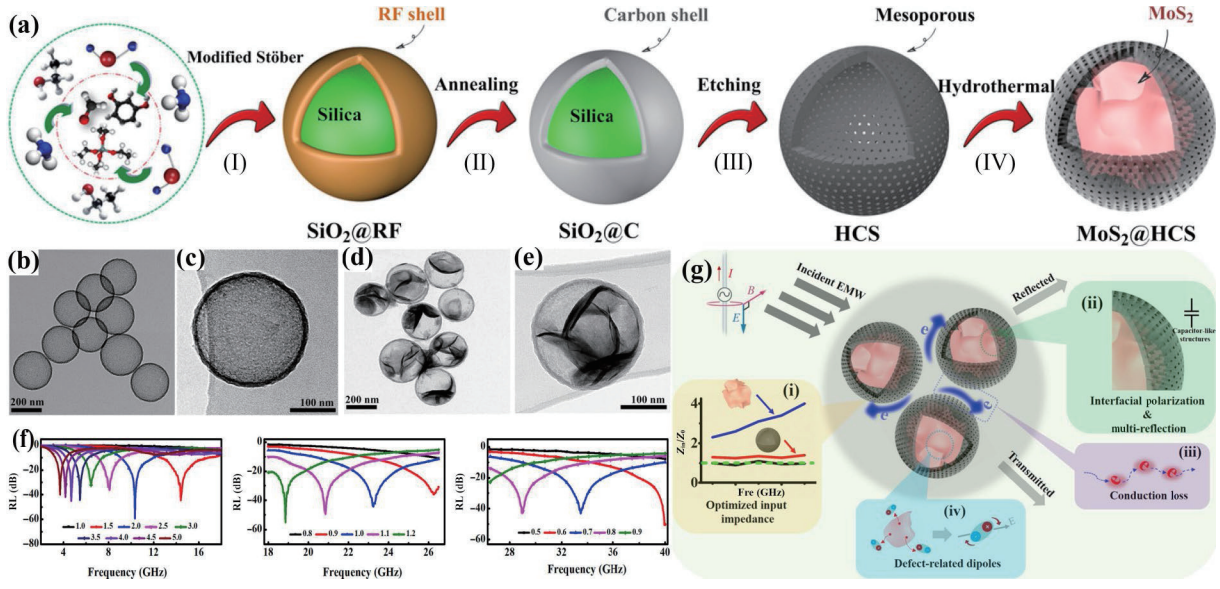


**Figure 7** (a) Schematic illustration of the synthesis process of $MoS_2$@HCS. TEM images of ((b) and (c)) hollow carbon microspheres and ((d) and (e)) $MoS_2$@HCS. (f) RL curves of $MoS_2$@HCS in the frequency range of 2.0–40.0 GHz with different absorber thicknesses and (g) the corresponding EM absorption mechanism. Reproduced with permission from Ref. [100], © American Chemical Society 2020.

carbon-based composites [241]. When magnetic metal (Fe, Co, and Ni) and graphite ingots are served as the anode in arc chamber, core–shell metal@C nanoparticles can be harvested after the ignition of arc discharge [242]. Zhang et al. ever compared the EM properties of Fe@C, Co@C, and Ni@C nanoparticles from arc discharge, and they found that Co@C could produce the strongest dielectric and magnetic loss among them under the same condition [243–245]. Although such composites may also benefit from interfacial polarization generated at the interfaces, their EM absorption performance is not as good as expected, especially for their relatively narrow EAB (less than 4.0 GHz), which is possibly attributed to the fact that dielectric and magnetic properties have not reached a desirable matching state yet. As a result, many strategies have been adopted to improve EM absorption of core–shell carbon-based composites prepared by arc discharge. Wu et al. tailored the average size of Ni@C nanocapsules from 25 to 53 nm by manipulating the arc-discharge currents from 40 to 100 A, and kept the independence of the thickness of carbon shells [246]. The results indicated that the change of particle size did not produce visible impact on magnetic loss, while small size could lead to the decrease of dielectric loss in low-frequency range and the increase of dielectric loss in high-frequency range. In this context, there was a positive complementary behaviour between magnetic loss and dielectric loss, and EAB of the optimum sample was significantly extended to 5.3 GHz with an absorber thickness of 2.0 mm. Wang et al. thickened carbon shells from 2 to 9 nm by increasing the ethanol concentration from 7 to 35 ppm [247]. It was unfortunate that the thickening of carbon shells consolidated dielectric loss but weakened magnetic loss, and thus the relationship between dielectric loss and magnetic loss was further deteriorated, which did not bring any enhancement in EM absorption. As we know, carbon shells in these composites are mainly responsible for dielectric loss therein, and dielectric loss of carbon materials is highly dependent on their relative graphitization degree [248, 249]. Liu et al. decreased the relative graphitization degree of carbon shells through an arc plasma method [250]. The introduction of plasma reactor created more defect sites in carbon shells, which reduced dielectric loss moderately and increased the matching degree of characteristic impedance, and the final composite could exhibit EAB as broad as 8.0 GHz with the absorber thickness of 2.0 mm. By considering the difficulty in the combination of arc discharge and plasma, more and more groups preferred to introduce defect sites through heteroatom substitutions [69, 251]. Zhang's group systematically investigated the heteroatom substitution (e.g., S, N, and O) in carbon shells by arc discharge and uncovered the correlation between improved EM properties and the atomic-scale microstructure [251–253]. Both experimental and theoretical results indicated that heteroatom substitution broke the atomic-scale symmetry and induced the separation of space charge at heteroatom-substituted sites, which increased the dipole polarization relaxation and ultimately updated the EM wave absorption. They even realized O-S co-substitutions in Fe@C nanocapsules, and confirmed its advantages in EM absorption as compared with S-substituted Fe@C nanocapsules.

Generally speaking, when different magnetic atoms are located in a specific lattice, i.e., the alloying process, their different atomic properties will induce electron transfer and enhance spin polarizability, and these behaviours are considered to be favourable for EM absorption [104, 254, 255]. Such a situation further arouses the interest in core–shell alloy@C composites, and the related research is extensively developed because the formation of various alloys can be easily achieved by changing anode ingots of arc discharge. In early studies, NiFe@C, CoNi@C, and FeCo@C are common candidates for high-performance EWAMs [256–259], and they indeed established their superiority to those single-metal core–shell composites. Han et al. demonstrated that FeCo@C composites could promise broad EAB of 8.0 GHz with an absorber thickness of 2.0 mm [260]. Lei et al. found that when superalloy $FeNi_3$ was employed as the magnetic core, the final product not only displayed good EM absorption performance with strong RL intensity of −47.3 dB and broad EAB of 7.0 GHz, but also exhibited good anti-oxidation characteristics even up to 719 K [261]. Of note is that the enhancement effect in alloy cores can be also observed when some non-magnetic atoms are introduced [262, 263]. Core–shell $FeSn_2$/Sn@C nanocomposites were harvested when FeSn alloy was chosen as the anode ingot [264], and the absorption performance could be regulated by the atomic ratio of Fe/Sn, where the optimum composite, $Fe_{24}Sn_{76}$@C, could extend EAB to 9.0 GHz with an absorber thickness of 2.0 mm. The similar EM absorption performance also observed in core–shell FeNiMo@C nanocapsules, whose broadest EAB from 9.0 to 18.0 GHz, covering the whole Ku-band and almost the whole X-band, was achieved with 2.0 mm absorber thickness, and

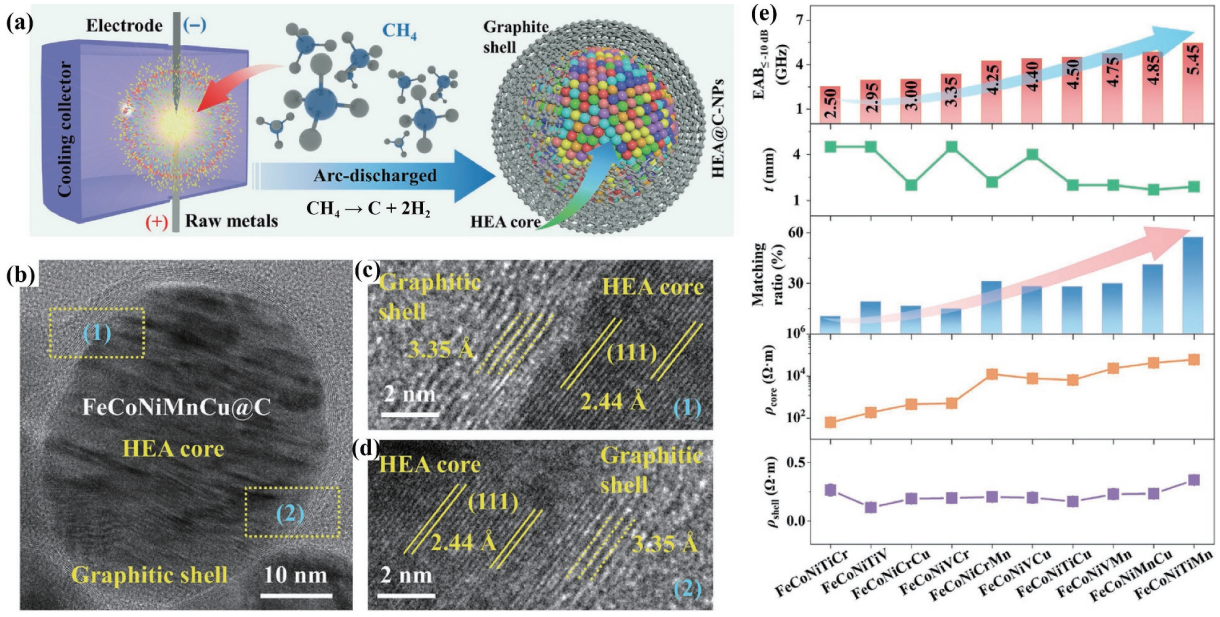


**Figure 8** (a) Schematic illustration of the synthesis process of HEA@graphite nanocapsules. (b)–(d) TEM images of core–shell structural FeCoNiMnCu@C nanocapsules. (e) Summarization of EAB with the corresponding absorber thickness, the impedance matching ratio of HEA@C-NPs, and the resistivity of graphitic shells or HEA cores, respectively. Reproduced with permission from Ref. [266], © Wiley-VCH GmbH 2021.

the corresponding RL was close to −64.0 dB at 13.2 GHz [265]. Possibly, the synergy among different atoms in alloy cores brings better EM compatibility in wide frequency range, thus contributing to the extension of EAB. Following this direction, Li et al. prepared high-entropy-alloy (HEA)@graphite nanocapsules through arc discharge (Fig. 8(a)) and investigated their EM absorption performance [266]. Although five kinds of metal atoms (FeCoNiTiMn) were involved in the ingot, the final product still maintained core–shell configuration with the cores of ca. 25 nm and the shells of ca. 2.7 nm (Figs. 8(b)–8(d)). EM measurements detected the influence of different atoms on EM absorption (Fig. 8(e)), while FeCoNiTiMn@C did not produce comparable EAB to FeNiMo@C (5.45 vs. 9.0 GHz) temporarily, because the specific effect of each atom was still not addressed comprehensively. Once the chemical composition can be accurately designed, there will be a great opportunity to generate excellent EM performance. On the other hand, the bloom of pure dielectric loss EWAMs in recent years also drives the research of non-magnetic core–shell composites from arc discharge [267–270]. When non-magnetic metal ingots are applied as anodes in arc chamber, the final products are usually composed of carbide cores and carbon shells. These composites can produce strong RL (< −40 dB) with a small absorber thickness, while the corresponding EAB is only about 4.0 GHz in most cases, remaining another challenge in this field.

### 4.3 Surface coating

Although arc discharge can produce core–shell carbon-based composites with good EM absorption performance, the requirements of special instrument and high energy input limit the popularization of this technique to a large extent. On the other hand, the final products from arc discharge are composed of small nanoparticles (20–50 nm), and the interaction among magnetic cores may be weakened once these nanoparticles are dispersed into resin matrix during practical application except under the condition of high filler loading [246, 264, 266]. The utilization of magnetic assemblies is considered to be an effective strategy to ensure magnetic interaction and even break through the Snoek's limitation on ferrites in gigahertz range [19, 271], while arc discharge is incapable of creating carbon shells on such magnetic assemblies. A widely validated strategy is to coat some metal oxides with polymers, including phenolic resin (PR), conductive polymers, polydopamine (PDA), and polysaccharide, and then transform intermediate precursors into core–shell carbon-based composites with magnetic ferrites or metals as the cores through high-temperature pyrolysis [36, 37, 272, 273]. Our group reported EM properties of core–shell $Fe_3O_4$@C microspheres from this way for the first time [37], and we found that the synergy between magnetic loss and dielectric loss could be effectively regulated by the thickness of carbon shells. When the thickness reached ca. 40 nm, the final composite produced good EM absorption in the frequency range of 4.0–18.0 GHz by manipulating the absorber thickness from 1.5 to 5.0 mm. Later, we further demonstrated the synthesis of core–shell Co@C microspheres with a similar method except the utilization of $H_2$ during heat transformation [274]. It was found that the presence of carbon shells not only maintained the dispersion of Co cores, but also suppressed the skin effect. As a result, carbon shells consolidated dielectric loss and magnetic loss simultaneously, and the minimum RL and EAB of Co@C microspheres were −40.0 dB and 4.0 GHz, respectively, with an absorber thickness of 1.5 mm. In the following studies, the internal magnetic cores have been widely extended to various magnetic ferrites, metals, and alloys [275–278]. Guan et al. even harvested core–shell CoFe/$CoFe_2O_4$@C composites through controllable reduction of $CoFe_2O_4$@C microspheres, and the formation of CoFe alloy induced a remarkable increase of magnetic loss, leading to very strong RL (−71.7 dB) in low-frequency range [279].

Similar to those core–shell carbon-based composites from other strategies, the construction of carbon shells is not only limited on the surface of magnetic particles, and many dielectric components can also be selected as the internal cores. The common dielectric cores include ZnO, MnO, $BaTiO_3$, and SiC [280–283]. For example, Xu et al. coated $MnO_2$ nanotubes with PPy layers and obtained core–shell MnO@C nanorods after high-temperature pyrolysis, and they observed a significant enhancement of electric field at the interfaces between MnO particles and carbon shells [282]. The final composite could display minimum RL of −62.8 dB and EAB of 5.4 GHz with an absorber thickness of 2.4 mm. Our group fabricated core–shell $BaTiO_3$@C microspheres through a space-confined strategy, and experimentally testified that EM enhancement indeed benefitted from the core–shell

configuration to a great extent, and the best composite could even produce RL value as low as −88.9 dB [280]. More importantly, the resultant $BaTiO_3$@C microspheres performed better oxidant and corrosion resistance than metal-based EWAMs. The EM absorption of SiC could also be sufficiently reinforced by depositing carbon shells, broadening EAB over 6.3 GHz, and decreasing RL intensity less than −50 dB [281, 284]. Although these results suggest that such non-magnetic core–shell composites can be taken as highly promising candidates for conventional magnetic EWAMs and they are less susceptible to application environment, their performance in S and C bands are often criticized unless the absorber thickness is accumulated over 5.0 mm [281, 284]. More recently, Lv et al. designed core–shell SnS/$SnO_2$@C and Sn/SnS/$SnO_2$@C composites as EWAMs and broke through low-frequency absorption limitation of dielectric materials successfully with the assistance of external electric field [285, 286]. Their works open a new avenue toward the practical applications of dielectric EWAMs in the future.

Besides the chemical composition of internal cores, many groups also pay considerable attention to their morphology and microstructure. Although some $Fe_3O_4$ assemblies with different morphologies, such as nanosheets, nanospindles, and nanorings, have been employed to construct core–shell composites, they did not bring remarkable improvements as compared with those common microspheres [287–289]. In contrast, microstructure usually plays a more progressive role in the enhancement of EM absorption performance. Yolk–shell and hollow microstructures are two typical architectures for carbon-based composites from the strategy of surface coating. The former is generally created by the differential shrinkage between internal cores and external shells during high-temperature pyrolysis, as well as the removal of some mediated templates [44, 283, 290–296]. For example, Li et al. coated $(Co_{0.9}Fe_{0.1})Fe_2O_4$ microspheres with PR layer and then pyrolyzed the precursor in the presence of $H_2$ (Fig. 9(a)) [44]. The reduction of $(Co_{0.9}Fe_{0.1})Fe_2O_4$ microspheres into $Co_3Fe_7$ particles induced a drastic volume shrinkage, thus resulting in the formation of yolk–shell microstructure (Figs. 9(a)–9(c)). This unique architecture improved impedance matching, strengthened polarization relaxations, and intensified interior reflection of EM waves, which broadened the EAB of final $Co_3Fe_7$@C microspheres effectively (8.4 GHz with an absorber thickness of 1.5 mm, Fig. 9(d)). As for hollow microstructure in core–shell composites, it can be created through the pre-cavitation of internal cores [297–300]. Our group ever etched Prussian blue analogue (PBA) microcube with $NH_3{\cdot}H_2O$ and then coated hollow PBA microbox with PR layer (Fig. 9(e)) [301]. The hollow NiCo@C microbox could be yielded after high-temperature pyrolysis (Fig. 9(f)), and they exhibited good EM absorption performance in a wide frequency range (3.9–18.0 GHz) by integrating the absorber thickness from 1.0 to 5.0 mm (Fig. 9(g)). When a heterogeneous layer is coated on the surface of ZIFs, the pyrolysis will prefer to start at the interfaces, which may also lead to the formation of hollow microstructure through the out-diffusion of carbon-containing species [68]. With this method, Xu et al. further obtained dual-shell Co@C composite, whose EAB almost reached 6.0 GHz with an absorber thickness of 2.4 mm [299]. Of note is that Meng et al. employed $Fe_3O_4$ aerogel as the internal core of carbon-based composites, and the profitable microstructure indeed upgraded the performance as compared with previous homologous composites [38].

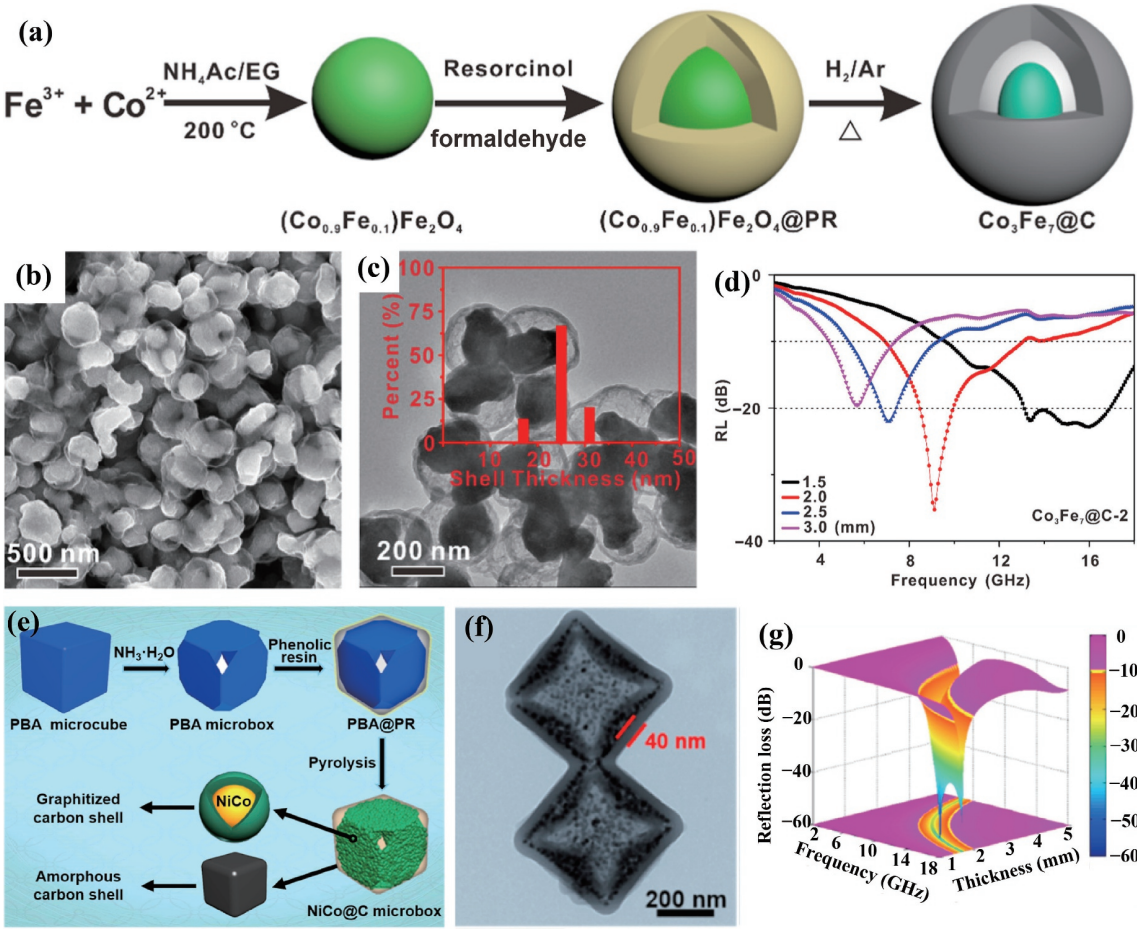


**Figure 9** (a) Schematic illustration of the synthesis process of $Co_3Fe_7$@C microspheres. (b) SEM image, (c) TEM image, and (d) RL curves of $Co_3Fe_7$@C microspheres. Reproduced with permission from Ref. [44], © American Chemical Society 2018. (e) Schematic illustration of the synthesis process of NiCo@C microbox. (f) TEM image and (g) RL map of NiCo@C microbox. Reproduced with permission from Ref. [301], © Elsevier Ltd. 20201.

### 4.4 Spontaneous formation

In addition to the methods mentioned above, there are also some successful examples that can produce core–shell carbon-based composites or their precursor through a spontaneous pathway. The thermal decomposition of organometallic compounds, such as ferrocene and cobaltocene, is validated to be effective for the growth of metal-filled CNTs [302]. It is different from the mode of embedding nanoparticles into CNTs, and thus the deposition and agglomeration of nanoparticles on the external surface of CNTs can be eliminated, and instead, metal nanowires may be generated inside CNTs [302, 303]. Lv et al. prepared FeCo@CNTs, FeNi@CNTs, and FeCoNi@CNTs in this way, and they found that RL intensity in S, C, and X bands was in the order of FeCoNi@CNTs < FeNi@CNTs < FeCo@CNTs, while this order would be FeNi@CNTs < FeCo@CNTs < FeCoNi@CNTs in Ku band [304]. The strongest RL of FeCoNi@CNTs was −28.2 dB at 15.2 GHz with an absorber thickness of 2.0 mm, and the broadest EAB could be identified as 8.0 GHz in FeCo@CNTs. Su et al. further converted FeNi@CNTs into $Ni_{17}S_{18}/Fe_7S_8$@CNTs through the introduction of dimethyl sulfide, and this transformation enhanced RL characteristics in Ku band, where minimum RL and EAB were −29.6 dB and 5.6 GHz, respectively, with an absorber thickness of 2.0 mm [305]. By considering the disadvantage of CVD technique in mass production, Zhu et al. ever attempted to find a simple method, where they employed the mixture of ferrocene and activated carbon as the precursor of Fe@CNTs [306]. Although CNTs filled with Fe nanowires could be generated, the serious external agglomeration was also observed, and the RL characteristics of final product were drastically decreased. Inspired by some interesting findings in previous studies, we harvested pea-like $Fe/Fe_3C$ nanoparticles embedded in N-doped CNTs ($Fe/Fe_3C$@NCNTs) through a direct pyrolysis of $FeCl_3$/melamine mixture [307]. The final product could display very uniform one-dimensional morphology, and $Fe/Fe_3C$ nanoparticles were discontinuously dispersed inside CNTs (Figs. 10(a) and 10(b)). The diameter and EM properties of $Fe/Fe_3C$@CNTs could be easily regulated by the pyrolysis temperature, and the composite from 600 °C promised powerful absorption in the frequency range of 3.2–18.0 GHz by accumulating the thickness of 1.0–5.0 mm (Fig. 10(c)). This strategy was extensively extended in the following studies, where $Ni(NO_3)_2$/melamine, $Co(NO_3)_2$/melamine, and Fe-MOF/melamine were all confirmed to be robust precursor to produce high-performance CNTs-based composites with embedded magnetic particles [308–311].

It is well known that glucose may be moderately carbonized under hydrothermal condition, and thus some groups realized the preparation of some core–shell precursor through one-pot hydrothermal reaction. For example, Sun et al. prepared core–shell $FeNi_3$@C nanowires through hydrothermal reduction of $Ni^{2+}$ and $Fe^{3+}$ in the presence of glucose, and the minimum RL and EAB of the resultant composite were −43.3 dB and 5.0 GHz, respectively, with an absorber thickness of 2.0 mm [312]. Wu et al. also reported the formation of rice-like γ-$Fe_2O_3$ nanorods as EWAMs through the hydrothermal treatment of the solution containing $Fe^{3+}$, urea, and glucose [313]. More recently, our group triggered the polymerization of pyrrole monomer in phosphomolybdic acid ($H_3PMo_{12}O_{40}{\cdot}nH_2O$, $PMo_{12}$) solution at room temperature, and then transformed the intermediate $PMo_{12}$/PPy nanospheres into pomegranate-like $Mo_2C$@C nanospheres under high-temperature inert atmosphere (Fig. 10(d)) [314]. The pyrolysis temperature was found to be a key factor to affect EM absorption properties of $Mo_2C$@C nanospheres. When the temperature was set at 700 °C, $Mo_2C$@C nanospheres could exhibit strong RL intensity of −48.0 dB at 12.5 GHz with a thickness of 1.9 mm and the integrated EAB was as broad as 14.5 GHz by accumulating the thickness from 1.5 to 5.0 mm (Fig. 10(e)). The good performance of $Mo_2C$@C nanospheres was ascribed to their multiple loss mechanisms, including conductivity loss, interfacial polarization, dipole polarization, and multiple reflections (Fig. 10(f)). This study provided a new selection to design core–shell carbon-based composites.

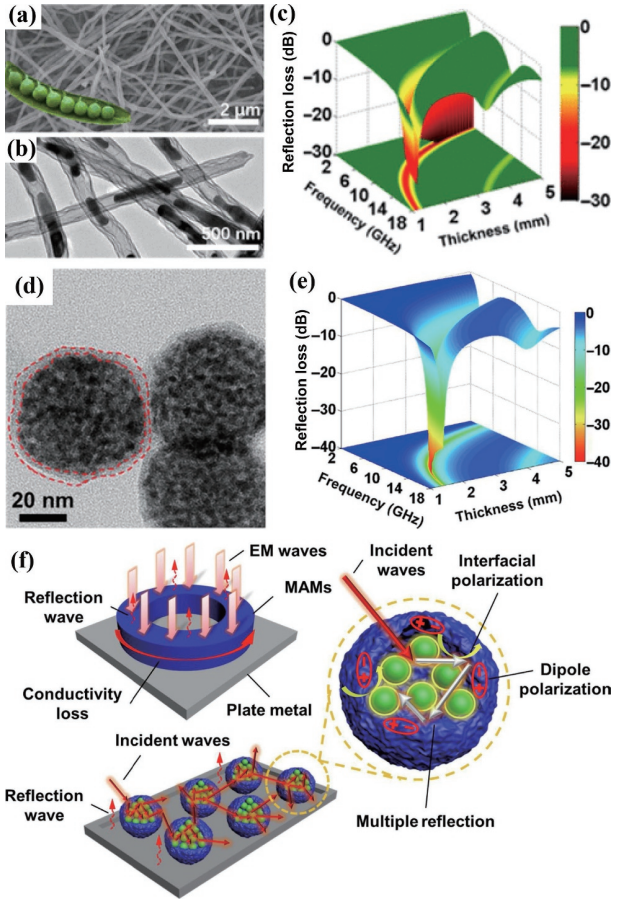


**Figure 10** (a) SEM image, (b) TEM image, and (c) RL map of $Fe/Fe_3C$@NCNTs. Reproduced with permission from Ref. [307], © American Chemical Society 2019. (d) TEM image, (e) RL map, and (f) EM absorption mechanisms of $Mo_2C$@C nanospheres. Reproduced with permission from Ref. [314], © Elsevier B.V. 2019.

## 5 Special core–shell carbon-based composites

With the in-depth research on EWAMs, the construction of core–shell carbon-based composites is not limited by simple built-in carbon cores or built-out carbon shells, and more elaborate designs have been applied to various novel carbon-based composites. In this section, three kinds of special core–shell carbon-based composites, including core–shell carbon@carbon composites, carbon-based composites with assembled core–shell units, and decorated core–shell carbon-based composites, will be the focus of the discussion.

### 5.1 Core–shell carbon@carbon composites

As we introduced above, the construction of core–shell carbon-based composites is usually carried out between carbon materials and other EM components. However, in fact, the positive EM synergy can also be performed at the interfaces of two different carbon components when they have distinguishable relative graphitization degree [75, 81, 92], which stimulates the

development of core–shell carbon@carbon composites. Liu et al. ever planted helical CNFs on CFs densely through CVD method, and they found quite different EM properties after the growth of helical CNFs, and the resultant composite could display the minimum RL of −32.0 dB at 9.0 GHz and EAB of 9.8 GHz with an absorber thickness of 2.5 mm [315]. Singh et al. further developed the growth of CNTs forest on CFs, and the composite gave acceptable EM absorption performance (minimum RL: −42.0 dB) in X band even under an extremely low filler loading (0.35 wt.%), because the hierarchical microstructure of CFs@CNTs facilitated electron hopping through conductive networks [316]. Zhang et al. wrapped CNFs with rGO nanosheets, and the defect dipoles and interfacial dipoles were confirmed to be helpful for EM attenuation [317]. More recently, our group directed an *in situ* growth of ZIF-8 nanocrystals on the surface of CNTs and then converted the intermediate into CNTs@porous carbon nanoparticles (PCNs) composites with a unique core–shell structure (Figs. 11(a) and 11(b)) [318]. The great difference between amorphous carbon nanoparticles and graphitic CNTs induced considerable interfacial polarization, so that the final composite could show very strong RL of −71.5 dB with the absorber thickness of only 1.1 mm, whose performance was actually superior to those of many conventional carbon/carbon composites (Fig. 11(c)).

The enhancement of EM absorption can also be witnessed when there is a void between carbon cores and carbon shells (i.e., the formation of yolk–shell microstructure) even in the case that they have same relative graphitization degree. This phenomenon is usually attributed to the intensified energy consumption induced by multiple reflection behaviours of incident EM waves [43, 319, 320]. Our group ever innovatively fabricated yolk–shell C@C microspheres through a "coating-coating-etching" route, and revealed that the yolk–shell microstructure in these microspheres was indeed helpful to improve impedance matching and strengthen dielectric loss [321]. As a result, the final C@C microspheres exhibited much better performance than solid carbon microspheres, including both smaller RL (−39.4 vs. −14.2 dB) and broader EAB (5.4 vs. 2.6 GHz). In the following studies, some groups further proposed that multi-shell carbon microspheres could generate higher conductivity loss and polarization loss than single-shell (i.e., yolk–shell) carbon microspheres due to more complex interior microstructure and more abundant heterogeneous interfaces [46, 322]. For example, Wang et al. tailored the shell number of hollow carbon microspheres through repeated deposition of $SiO_2$/PR (Figs. 11(d) and 11(e)) [322]. The final three-shell hollow carbon microspheres (THCS) could give a very small RL value of −48.5 dB at 11.3 GHz and broad EAB of 5.6 GHz with the absorber thickness of 2.8 and 2.5 mm, respectively (Fig. 11(f)), and the authors also confirmed that this enhancement was from multiple reflection and interfacial polarization (Fig. 11(g)). It is believed that if the microstructure design can combine the manipulation on the relative graphitization degree of carbon shells, there will be a bigger breakthrough in EM absorption, while such a design concept is still inaccessible in current carbon@carbon composites.

### 5.2 Assembled core–shell composites

The periodic arrangement of EM units may regulate their synergy to some extent and bring desirable EM absorption enhancements [323]. Such a phenomenon also encourages the researchers in the related field to design carbon composites through the assembly of core–shell units. Yuan et al. fabricated novel three dimensionally ordered arrays of core–shell microspheres comprising $Fe_3O_4$ cores and ordered mesoporous carbon (OMC) shells through a confined interface coating strategy (Figs. 12(a)–12(c)) [324]. When the size of core–shell microspheres was about 1,200 nm, the minimum RL of up to −57.0 dB at 8 GHz and large EAB of 6.4 GHz (7.3–13.7 GHz) could be harvested with an absorber thickness of 3.0 mm (Fig. 12(d)), which were obviously better than those from dispersed $Fe_3O_4$@C microspheres [37]. In some following studies, this strategy was further extended for the synthesis of Co/$Co_3O_4$@OMC and ZnO@OMC micropsheres [325, 326], where ZnO@OMC microspheres even produced EAB as broad as 9.1 GHz with an absorber thickness of 2.0 mm. Although these three-dimensional arrays of core–shell carbon-based microspheres indeed display their advantages in EM absorption, the complicated procedures seriously restrain their further practical application as EWAMs.

In the past few years, MOFs have emerged as a kind of very popular precursors for carbon-based EWAMs, because their periodic arrangements of metal nodes and organic ligands provide a good prerequisite for the uniform distribution of different components in final composites [93, 97, 327–329]. Although high-temperature pyrolysis of MOFs usually induces the formation of small core–shell nanoparticles in carbon matrix, the final composites will not show dominant feature (a concentric bilayer

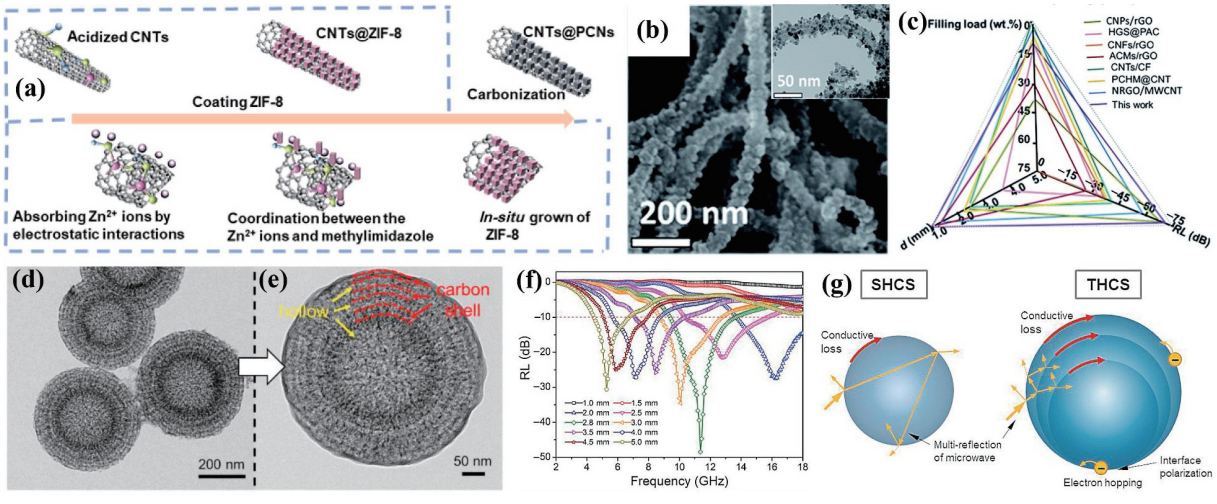


**Figure 11** (a) Schematic illustration of the synthesis process and (b) SEM image of CNTs@PCNs, and inset in (b) is the corresponding TEM image. (c) The comparison in RL characteristics of CNTs@PCNs and other carbon/carbon composites. Reproduced with permission from Ref. [318], © The Royal Society of Chemistry 2021. (d) and (e) TEM images and (f) RL curves of three-shell hollow carbon microspheres (THCS), and (g) EM absorption mechanism in single-shell hollow carbon microspheres (SHCS) and THCS. Reproduced with permission from Ref. [322], © Elsevier Ltd. 2021.

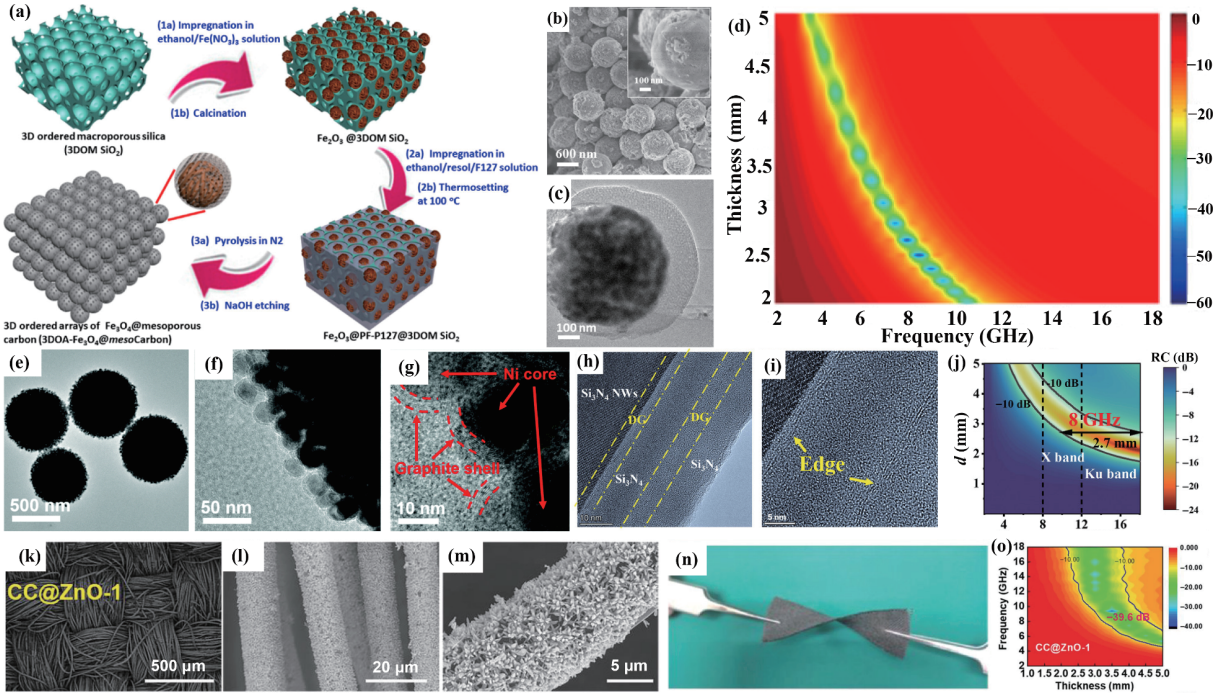


**Figure 12** (a) Schematic illustration of the synthesis process, (b) SEM image, (c) TEM image, and (d) RL map of three-dimensional $Fe_3O_4$@OMC microspheres. Reproduced with permission from Ref. [324], © American Chemical Society 2015. (e)–(g) TEM images of hierarchical Ni@C microspheres. Reproduced with permission from Ref. [99], © The Royal Society of Chemistry 2019. (h) and (i) TEM images and (j) RL map of $Si_3N_4$@DG@$Si_3N_4$ (DG: defect-engineered graphene). Reproduced with permission from Ref. [106], © Wiley-VCH GmbH 2022. (k)–(m) SEM images, (n) flexibility picture, and (o) RL map of CC@ZnO. Reproduced with permission from Ref. [336], © Wiley-VCH Verlag GmbH & Co. KGaA, Weinheim 2019.

nanostructure) of core–shell configuration on the whole, and thus we do not pay too much attention to MOFs-derived carbon-based composites. However, different from conventional MOFs transformation, when Ni-BTC (BTC = benzene-1,3,5-tricarboxylate) was utilized as the precursor, the resultant Ni nanoparticles would not be randomly dispersed in carbon framework any more, but uniformly coated by a thin carbon shell, and then these core–shell Ni@C units were further assembled into hierarchical microspheres (Figs. 12(e)–12(g)) [99]. This hierarchically core–shell configuration endowed Ni/C composites with both strong RL value (−73.2 dB) and broad EM response (14.2 GHz with the integrated thickness of 1.0–5.0 mm). If hollow cavity was created in these Ni-BTC microspheres before high-temperature pyrolysis, the final produce could present a moderate upgradation in EM absorption due to the microstructure contribution [330, 331].

In order to simplify the assembly of core–shell units, more and more groups attempt to build core–shell configuration on some substrates with pre-assembled units [106, 332]. For example, Liang et al. employed $Si_3N_4$ membrane with cross-linked $Si_3N_4$ nanowires as the substrate, and then conducted the growth of graphene and $Si_3N_4$ layers successively through CVD deposition (Figs. 12(h) and 12(i)) [106]. The alternant core–shell configuration and the assembly of multi-layered nanowires were together responsible for good EM absorption performance (EAB: 8.0 GHz, Fig. 12(j)), and more importantly, the final membrane also showed excellent corrosion and oxidant resistance, whose RL characteristics could be well preserved after alkaline, acidic, and high-temperature oxidation treatment. Under this context, commercially available carbon cloth (CC) emerged as a popular substrate, because it not only contains CFs with a regular arrangement, but also provides a good platform for flexible EWAMs. To date, some arrays of typical EM constituents, such as $MnO_2$, $CoS_2$, ZnO, and ZnS, have been successfully planted on the surface of CC [333–336]. Wang et al. manipulated the morphology of vertical ZnO arrays on CC surface with anion effect (Figs. 12(k)–12(m)), and they found that single-like ZnO rods could produce high concentration of polarized charge and three-dimensional intertwined CFs provided ballistic electron transportation [336]. Moreover, the sufficient interfaces, multiple scattering, and good impedance matching together contributed to excellent EM absorption of flexible CC@ZnO (Fig. 12(n)), whose minimum RL and EAB could reach up to −39.6 dB and 10.6 GHz, respectively (Fig. 12(o)).

### 5.3 Decorated core–shell composites

With the in-depth understanding on EM properties of various functional materials, there is increasing interest in the design of multicomponent EWAMs which may make some desirable breakthroughs in RL intensity and response bandwidth with the synergy among multiple EM components [129, 337–339]. This tendency also stimulates the related researchers to further modify and optimize core–shell carbon-based EWAMs through a decoration strategy. Shi et al. decorated core–shell Fe@$SiO_2$@C microspheres with Ni nanoparticles, and they found that in addition to the contribution from core–shell configuration, there was a significant magnetic coupling between neighbouring microspheres, as well as Fe core and Ni nanoparticles, which contributed to magnetic loss and overall EM absorption greatly [340]. The final quaternary composites displayed intense RL value of −45.5 dB and attractive EAB of 8.2 GHz with an absorber thickness of 2.0 mm. Compared with the decoration of nanoparticles, the creation of multiple coating layers in carbon-based composites is a commonly used method to achieve better EM absorption characteristics, where some dielectric components, e.g., $MnO_2$, $MoS_2$, and PPy, are considered to be promising candidates for the additional shells [338, 341–349]. For example, You et al. induced the growth of α-$MnO_2$ shell on the surface of core–shell γ-$Fe_2O_3$@C nanospindles [349]. By manipulating the thickness of α-$MnO_2$ shells, as well as the void between γ-$Fe_2O_3$ core and carbon shells, the final γ-$Fe_2O_3$@C@α-$MnO_2$ could generate EAB as broad as 9.2 GHz with an absorber thickness of

2.0 mm, almost four times wider than unmodified γ-$Fe_2O_3$@C spindles (2.26 GHz). Xu et al. conducted the polymerization of pyrrole monomers on the surface of core–shell SiC@C fibers, and the formation of PPy shells extended EAB from 7.16 to 8.40 GHz [347]. The multiple interface phases and good conductive networks were taken as the two main reasons for the enhancement of EM absorption performance. Similarly, it is also of great significance to build multiple core–shell composites based on CFs [350, 351]. For example, Wang et al. constructed two additional shells on CFs through the self-assembled of MXene nanosheets and subsequent anchoring of $MoS_2$ nanosheets, and they found that the coated intermediate dielectric MXene sheath enhanced the conductivity loss and $MoS_2$ at the outermost layer improved the whole impedance matching of the final composites [352]. With these positive modifications, the optimal RL value of CFs (−7.78 dB) would be drastically reduced to −61.51 dB with an absorber thickness of 3.5 mm, and meanwhile, the EAB of CF@MXene@$MoS_2$ could be easily regulated in Ku or X band by manipulating the thickness. More recently, Huang et al. modified $Fe_3O_4$ microspheres with PDA layer, $TiO_2$ layer, and $MoS_2$ layer in succession, and then converted the intermediate composites into Fe@C@$TiO_2$@$MoS_2$ with ternary core–shell configurations (Fig. 13(a)) [353]. The shrinkage of $Fe_3O_4$ cores during thermal hydrogen reduction accounted for the formation of a void between Fe cores and carbon shells, and the deposition of $TiO_2$ and $MoS_2$ resulted in densely dispersed nanoparticles and vertically grown nanosheets, respectively (Figs. 13(b)–13(e)). This multiple core–shell composite showed excellent EM absorption performance, whose minimum RL intensity was −54.2 dB at 11.6 GHz (*d*: 2.5 mm) and the broadest EAB reached 9.6 GHz (8.4–18.0 GHz, *d*: 2.6 mm, Figs. 13(f) and 13(g)). The enhanced EM absorption was attributed to the integrated contribution from significantly consolidated interfacial polarization from heterogeneous interfaces (Fe-C, C-$TiO_2$, and $TiO_2$-$MoS_2$), improved conductivity loss behaviors from intermediate carbon layer, magnetic-dielectric synergism effect, as well as intensified reflection behaviors of incident EM waves (Figs. 13(h) and 13(i)).

Apart from the deposition of heterogeneous magnetic nanoparticles and dielectric shells, *in situ* growth of CNTs on core–shell carbon-based composites is being considered as another effective strategy to strengthen their performance [354–356]. On the one hand, the spatial stretching of CNTs is quite favourable for the formation of conductive networks, and on the other hand, the mode of *in situ* growth can avoid the poor dispersion of CNTs. Our group employed waxberry-like Ni@C microspheres as the platform for the growth of CNTs, where Ni nanoparticles on the surface of microspheres acted as the catalyst and melamine was utilized as carbon source (Figs. 13(j)–13(l)) [354]. The emergence of CNTs enhanced dielectric loss of Ni@C microspheres significantly, and the final composite not only extended EAB from 4.8 to 5.2 GHz (Fig. 13(m)), but also decreased the filler loading from 40 wt.% to 30 wt.%. Xu et al. further found that the growth of CNTs on core–shell $Mo_2N$@CoFe@C fibers offered sufficient heterogeneous interfaces and triggered powerful interfacial polarization, and thus facilitated conductivity loss through unique electronic migration and hopping paths [356]. In addition, CoFe nanoparticles at the end of CNTs were greatly helpful to build multi-scale magnetic coupling network and reinforce magnetic response capability. The final $Mo_2N$@CoFe@C/CNTs composite almost induced the extension of EAB as 3.6 time (from 1.4 to 5.0 GHz).

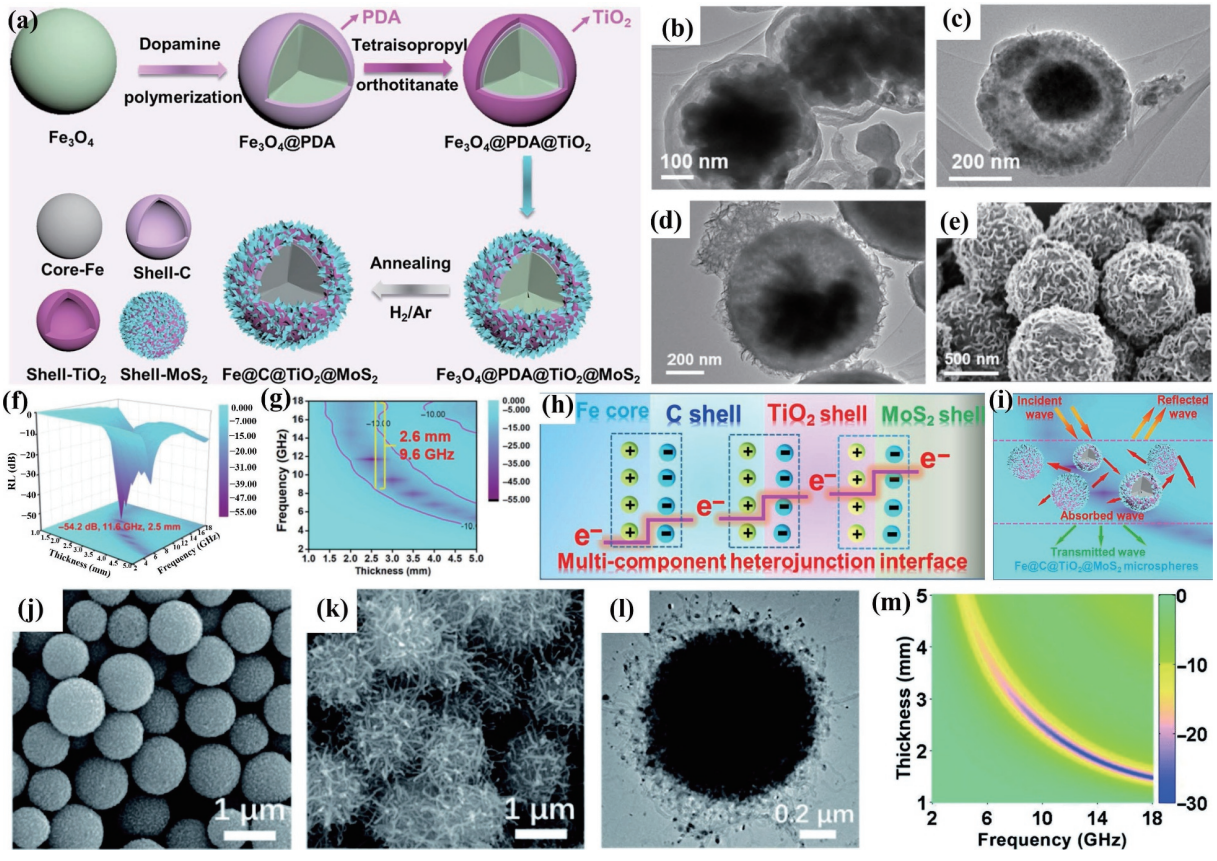


**Figure 13** (a) Schematic illustration of the synthesis process of ternary core–shell Fe@C@$TiO_2$@$MoS_2$. TEM images of (b) Fe@C, (c) Fe@C@$TiO_2$, and (d) Fe@C@$TiO_2$@$MoS_2$, and SEM image of (e) Fe@C@$TiO_2$@$MoS_2$. ((f) and (g)) RL maps and ((h) and (i)) absorption mechanisms of Fe@C@$TiO_2$@$MoS_2$ composite. Reproduced with permission from Ref. [353], © Elsevier B.V. 2021. SEM images of (j) waxberry-like Ni@C microspheres and (k) Ni@C/CNTs, and (l) TEM image and (m) RL map of Ni@C/CNTs. Reproduced with permission from Ref. [354], © The Royal Society of Chemistry 2021.

## 6 Conclusions and perspectives

In this review, we introduce recent advances of core–shell carbon-based composites toward EM absorption comprehensively. It is undoubted that the creation of core–shell configuration can make a solid supplement to intrinsic loss of carbon-based composites to a large extent and develop the positive synergy between different EM functional components effectively. In view of different chemical compositions and synthesis methods, there are numerous core–shell carbon-based composites that have been designed and fabricated as high-performance EWAMs, and we divide them into three categories, i.e., built-in carbon cores, built-out carbon shells, and special core–shell composites, to facilitate readers' understanding. Table 1 summarizes EM absorption performance in 2.0–18.0 GHz of some excellent EWAMs selected from the aforementioned categories. As observed, carbon-based composites with built-out carbon shells can establish some advantages in EM absorption as compared with those counterparts with built-in carbon cores. For example, FeNiMo@C has both strong RL and broad EAB in each frequency range. However, of note is that carbon-based composites with built-in carbon cores usually require smaller filler loading, because the built-in carbon cores are graphitic carbon materials, which can provide sufficient dielectric loss capability. In contrast, built-out carbon shells are composed of amorphous carbon materials, and thus they can improve impedance matching and reduce the back reflection of incident EM waves. These findings mean that one can choose the built-up mode of core–shell carbon-based composites according to the requirements of practical application. Carbon/carbon composites and assembled composites maintain the advantage of low filler loading, and some of them, such as CNTs@PCNs, even produce considerable RL intensity with a very small absorber thickness, while its EAB still needs to be further broadened. When multiple shells are rationally constructed, there will be significant improvement in EAB (e.g., Fe@C@$TiO_2$@$MoS_2$). It is unfortunate that this improvement is also at the expense of filler loading, implying that the expected synergy among different shells will be dependent on their thicknesses.

Although these core–shell carbon-based composites have made considerable achievements in EM absorption, there still remain some challenges in both performance and application. First, EM absorption in low-frequency range needs to be improved urgently.

**Table 1** Recent progress in core–shell carbon-based EM wave absorption material

| Category | Absorbers | C-band 4–8 GHz | | | X-band 8–12 GHz | | | Ku-band 12–18 GHz | | | Filled ratio (wt.%) | References |
|---|---|---|---|---|---|---|---|---|---|---|---|---|
| | | Thickness (mm) | $RL_{min}$ (dB) | EAB (GHz) (RL < −10 dB) | Thickness (mm) | $RL_{min}$ (dB) | EAB (GHz) (RL < −10 dB) | Thickness (mm) | $RL_{min}$ (dB) | EAB (GHz) (RL < −10 dB) | | |
| Core–shell composites with built-in carbon cores | C@Co | 4.0 | −54.2 | 2.1 (5.0–7.1) | 2.3 | −58.3 | 4.5 (10.0–15.5) | 2.1 | −33.5 | 6.0 (12.0–18.0) | 10 | [134] |
| | HCP@PANI | — | — | — | 2.5 | −64.0 | 5.0 (9.5–14.5) | 2.2 | −20.0 | 4.0 (12.0–16.0) | 30 | [167] |
| | CNF@$MnO_x$ | 4.0 | −32.0 | 2.0 (5.0–7.0) | 2.8 | −47.2 | 3.1 (7.9–11.0) | 1.8 | −36.0 | 5.0 (13.0–18.0) | 25 | [178] |
| | G@PANI | 4.0 | −20.0 | 4.1 (5.9–10.0) | 3.0 | −34.9 | 6.0 (7.0–13.9) | 1.5 | −45.1 | 8.0 (10.0–18.0) | 20 | [185] |
| | BAN/3dCF[a] | 4.0 | −45.0 | 2.5 (4.5–7.0) | 2.8 | −56.8 | 3.6 (7.5–11.1) | 2.0 | −50.0 | 6.1 (11.9–18.0) | 18 | [213] |
| | $FeNi_3$@C | 4.5 | −27.5 | 4.0 (5.9–9.9) | 3.5 | −34.0 | 4.9 (8.1–13.0) | 3.0 | −47.2 | 5.0 (9.0–16.0) | 60 | [261] |
| | $Fe_3O_4$@MCHS | 3.5 | −22.0 | 0.5 (7.5–8.0) | 2.9 | −40.0 | 4.9 (10.1–15.0) | 2.3 | −62.5 | 5.7 (12.3–18.0) | 20 | [240] |
| | $MoS_2$@HCS | 3.5 | −45.0 | 1.1 (4.9–6.0) | 2.0 | −60.0 | 3.0 (9.0–12.0) | 1.5 | −50.0 | 5.0 (3.0–18.0) | 60 | [100] |
| Core–shell composites with built-out carbon shells | FeNiMo@C | 3.0 | −32.0 | 6.3 (4.7–11.0) | 2.5 | −45.0 | 7.0 (6.0–13.0) | 1.9 | −64.0 | 8.0 (10.0–18.0) | 40 | [265] |
| | SiC@C | 4.0 | −21.0 | 2.0 (6.0–8.0) | 2.8 | −50.0 | 6.0 (8.2–16.2) | 2.5 | −19.0 | 6.5 (10.5–17.0) | 50 | [281] |
| | MnO@C | 5.0 | −14.0 | 2.1 (5.9–8.0) | 3.0 | −19.0 | 5.0 (8.0–13.0) | 2.4 | −62.8 | 5.4 (10.8–16.2) | 60 | [282] |
| | ZnO@C | 4.0 | −33.0 | 2.5 (5.5–8.0) | 2.5 | −41.0 | 5.0 (9.0–14.0) | 2.0 | −50.5 | 5.7 (12.3–18.0) | 60 | [283] |
| | Fe@void@C | 3.0 | −49.0 | 2.0 (5.5–7.5) | 2.5 | −30.0 | 4.0 (7.5–11.5) | 1.6 | −66.5 | 5.0 (13.0–18.0) | 60 | [291] |
| | H-$Fe_3O_4$@C | 4.0 | −24.0 | 3.0 (6.0–8.5) | 2.5 | −39.0 | 3.0 (10.0–13.0) | 1.9 | −58.4 | 6.0 (12.0–18.0) | 30 | [293] |
| | NiCo@C | 5.0 | −32.0 | 1.4 (4.0–5.4) | 2.5 | −32.0 | 4.5 (9.0–13.5) | 2.1 | −68.4 | 5.0 (11.0–16.0) | 40 | [301] |
| | CNTs@PCNs | 2.5 | −22.7 | 1.4 (5.6–6.8) | 1.5 | −28.8 | 2.0 (9.9–11.9) | 1.1 | −71.5 | 3.5 (14.5–18.0) | 10 | [318] |
| | THCS | 5.0 | −33.0 | 2.0 (4.5–6.5) | 2.8 | −48.5 | 4.2 (9.3–13.5) | 2.0 | −29.0 | 5.0 (13.0–18.0) | 20 | [322] |
| Special core–shell carbon-based composites | Ni@C | 4.0 | −15.4 | 2.8 (5.1–7.9) | 2.2 | −73.2 | 4.0 (10.8–14.8) | 1.8 | −26.0 | 4.8 (13.2–18.0) | 50 | [99] |
| | CC@$MnO_2$ | 4.5 | −53.2 | 1.1 (4.9–6.0) | 2.5 | −44.0 | 3.5 (9.5–13.0) | 2.0 | −43.0 | 5.8 (12.2–18.0) | 25 | [334] |
| | CC@NPC/$CoS_2$ | 3.5 | −17.5 | 1.5 (7.0–8.5) | 2.8 | −59.6 | 7.2 (8.5–15.7) | 2.0 | −38.0 | 6.1 (11.9–18.0) | 30 | [335] |
| | $Fe_3O_4$@NC/$MoS_2$ | 4.1 | −68.9 | 2.0 (5.0–7.0) | 2.6 | −45.0 | 3.4 (8.1–11.5) | 2.0 | −30.0 | 5.3(11.3–16.6) | 50 | [343] |
| | Fe@C@$TiO_2$@$MoS_2$ | 4.0 | −31.0 | 3.5 (5.6–9.0) | 2.5 | −54.2 | 9.6 (8.4–18.0) | 2.0 | −23.0 | 7.0 (11.0–18.0) | 60 | [353] |

[a]Bimetallic nanoarray composed of nickel/cobalt embedded three-dimensional carbon foam.

Most composites, to date, can produce good EM absorption performance in middle- and high-frequency ranges (8.0–18.0 GHz) even if a small absorber thickness is applied, while their performance will not be maintained in low-frequency range (2.0–8.0 GHz) unless the absorber thickness is accumulated up to 4.0 mm. This situation is caused by the fact that their dielectric loss and magnetic loss cannot meet the loss requirement of low-frequency EM waves, and thus rational regulation on their EM properties is still highly desired by composition optimization and microstructure design. Only when this problem is solved, it is possible to really harvest EWAMs with broadband response in the whole frequency range of 2.0–18.0 GHz. Second, environmental tolerance should also be paid much attention except for EM absorption performance, because it is highly related to the usability and lifetime of EWAMs in practical application. It is well known that EWAMs usually service in outdoor environment, which may involve acidity/alkalinity, large humidity, high-temperature exposure (dozens of degrees), and concentrated salt mist, and thus good environmental tolerance will ensure the durable application of EWAMs under some rigorous outdoor conditions. Magnetic metals or ferrites are typically popular candidates for high-performance EWAMs, while the susceptibility to corrosion and oxidation limits their application in many cases. From this aspect, the construction of stable dielectric composites, such as carbon/carbon composites, may be an attractive direction for the development of EWAMs. Third, the quantitative analysis on the contribution of different loss modes is highly desirable. Although magnetic coupling and interfacial polarization in EWAMs can be observed directly with the help of electron holography, it is still incapable of evaluating the contribution from a specific loss mode, and thus the absorption mechanism of EWAMs in most studies can only be roughly inferred by comparing the change of EM parameters (i.e., $\varepsilon_r$ and $\mu_r$). This context suggests that the development of a new technique or method to quantitatively illustrate EM absorption mechanism will be greatly helpful for the design of high-performance EWAMs. Fourth, the concept of machine learning is expected to play a crucial role in EM absorption. Current EWAMs are usually designed and constructed based on the experience of researchers, and thus it is difficult to summarize the macro change law of EM absorption only based on the results of several research teams. If we can build a huge database that contains information about the composition, microstructure, and performance of EWAMs, the prediction on ideal EWAMs may be deduced by the computer after comprehensive analysis and calculation, which will drastically shorten the time and save the cost for the explore of high-performance EWAMs.

## Acknowledgements

This work was financially supported by the National Natural Science Foundation of China (No. 21676065).

## References

[1] Andrews, M. R.; Mitra, P. P.; Decarvalho, R. Tripling the capacity of wireless communications using electromagnetic polarization. *Nature* **2001**, *409*, 316–318.

[2] Huang, C. W.; Zappone, A.; Alexandropoulos, G. C.; Debbah, M.; Yuen, C. Reconfigurable intelligent surfaces for energy efficiency in wireless communication. *IEEE Trans. Wireless Commun.* **2019**, *18*, 4157–4170.

[3] Wu, Z. C.; Cheng, H. W.; Jin, C.; Yang, B. T.; Xu, C. Y.; Pei, K.; Zhang, H. B.; Yang, Z. Q.; Che, R. C. Dimensional design and core–shell engineering of nanomaterials for electromagnetic wave absorption. *Adv. Mater.* **2022**, *34*, 2107538.

[4] Longair, M. ". . . A paper. . . I hold to be great guns": A commentary on maxwell (1865) "A dynamical theory of the electromagnetic field". *Phil. Trans. Roy. Soc. A Math. , Phys. Eng. Sci.* **2015**, *373*, 20140473.

[5] Zeng, Z. H.; Jiang, F. Z.; Yue, Y.; Han, D. X.; Lin, L. C.; Zhao, S. Y.; Zhao, Y. B.; Pan, Z. Y.; Li, C. J.; Nyström, G. et al. Flexible and ultrathin waterproof cellular membranes based on high-conjunction metal-wrapped polymer nanofibers for electromagnetic interference shielding. *Adv. Mater.* **2020**, *32*, 1908496.

[6] Liu, L. Y.; Deng, H.; Tang, X. P.; Lu, Y. X.; Zhou, J. Y.; Wang, X. F.; Zhao, Y. Y.; Huang, B.; Shi, Y. G. Specific electromagnetic radiation in the wireless signal range increases wakefulness in mice. *Proc. Natl. Acad. Sci. USA* **2021**, *118*, e2105838118.

[7] Lundgren, J.; Helander, J.; Gustafsson, M.; Sjoberg, D.; Xu, B.; Colombi, D. A near-field measurement and calibration technique: Radio-frequency electromagnetic field exposure assessment of millimeter-wave 5G devices. *IEEE Antennas Propag. Mag.* **2021**, *63*, 77–88.

[8] Zhang, Y. L.; Gu, J. W. A perspective for developing polymer-based electromagnetic interference shielding composites. *Nano-Micro Lett.* **2022**, *14*, 89.

[9] Abbasi, H.; Antunes, M.; Velasco, J. I. Recent advances in carbon-based polymer nanocomposites for electromagnetic interference shielding. *Prog. Mater. Sci.* **2019**, *103*, 319–373.

[10] He, P.; Cao, M. S.; Cao, W. Q.; Yuan, J. Developing MXenes from wireless communication to electromagnetic attenuation. *Nano-Micro Lett.* **2021**, *13*, 115.

[11] Liang, C. B.; Qiu, H.; Song, P.; Shi, X. T.; Kong, J.; Gu, J. W. Ultra-light MXene aerogel/wood-derived porous carbon composites with wall-like "mortar/brick" structures for electromagnetic interference shielding. *Sci. Bull.* **2020**, *65*, 616–622.

[12] Zhang, Y. L.; Ma, Z. L.; Ruan, K. P.; Gu, J. W. Flexible $Ti_3C_2T_x$/(aramid nanofiber/PVA) composite films for superior electromagnetic interference shielding. *Research* **2022**, *2022*, 9780290.

[13] Green, M.; Chen, X. B. Recent progress of nanomaterials for microwave absorption. *J. Materiomics* **2019**, *5*, 503–541.

[14] Song, Q.; Ye, F.; Kong, L.; Shen, Q. L.; Han, L. Y.; Feng, L.; Yu, G. J.; Pan, Y. A.; Li, H. J. Graphene and MXene nanomaterials: Toward high-performance electromagnetic wave absorption in gigahertz band range. *Adv. Funct. Mater.* **2020**, *30*, 2000475.

[15] Liang, C. B.; Gu, Z. J.; Zhang, Y. L.; Ma, Z. L.; Qiu, H.; Gu, J. W. Structural design strategies of polymer matrix composites for electromagnetic interference shielding: A review. *Nano-Micro Lett.* **2021**, *13*, 181.

[16] Li, W. C.; Li, C. S.; Lin, L. H.; Wang, Y.; Zhang, J. S. All-dielectric radar absorbing array metamaterial based on silicon carbide/carbon foam material. *J. Alloys Compd.* **2019**, *781*, 883–891.

[17] Wang, J. L.; Zhou, M.; Xie, Z. C.; Hao, X. Y.; Tang, S. L.; Wang, J. W.; Zou, Z. Q.; Ji, G. B. Enhanced interfacial polarization of biomass-derived porous carbon with a low radar cross-section. *J. Colloid Interface Sci.* **2022**, *612*, 146–155.

[18] Wang, F. Y.; Cui, L. R.; Zhao, H. H.; Han, X. J.; Du, Y. C. High-efficient electromagnetic absorption and composites of carbon microspheres. *J. Appl. Phys.* **2021**, *130*, 230902.

[19] Sun, G. B.; Dong, B. X.; Cao, M. H.; Wei, B. Q.; Hu, C. W. Hierarchical dendrite-like magnetic materials of $Fe_3O_4$, $\gamma$-$Fe_2O_3$, and Fe with high performance of microwave absorption. *Chem. Mater.* **2011**, *23*, 1587–1593.

[20] Wang, T.; Han, R.; Tan, G. G.; Wei, J. Q.; Qiao, L.; Li, F. S. Reflection loss mechanism of single layer absorber for flake-shaped carbonyl-iron particle composite. *J. Appl. Phys.* **2012**, *112*, 104903.

[21] Duan, W. J.; Li, X. D.; Wang, Y.; Qiang, R.; Tian, C. H.; Wang, N.; Han, X. J.; Du, Y. C. Surface functionalization of carbonyl iron with aluminum phosphate coating toward enhanced anti-oxidative ability and microwave absorption properties. *Appl. Surf. Sci.* **2018**, *427*, 594–602.

[22] Qing, Y. C.; Min, D. D.; Zhou, Y. Y.; Luo, F.; Zhou, W. C. Graphene nanosheet- and flake carbonyl iron particle-filled epoxy-silicone composites as thin-thickness and wide-bandwidth microwave absorber. *Carbon* **2015**, *86*, 98–107.

[23] Li, Q.; Zhang, Z.; Qi, L. P.; Liao, Q. L.; Kang, Z.; Zhang, Y. Toward the application of high frequency electromagnetic wave absorption by carbon nanostructures. *Adv. Sci.* **2019**, *6*, 1801057.
[24] Wu, N. N.; Hu, Q.; Wei, R. B.; Mai, X. M.; Naik, N.; Pan, D.; Guo, Z. H.; Shi, Z. J. Review on the electromagnetic interference shielding properties of carbon based materials and their novel composites: Recent progress, challenges and prospects. *Carbon* **2021**, *176*, 88–105.
[25] Cao, M. S.; Wang, X. X.; Cao, W. Q.; Yuan, J. Ultrathin graphene: Electrical properties and highly efficient electromagnetic interference shielding. *J. Mater. Chem. C* **2015**, *3*, 6589–6599.
[26] Kumar, R.; Sahoo, S.; Joanni, E.; Singh, R. K.; Tan, W. K.; Moshkalev, S. A.; Matsuda, A.; Kar, K. K. Heteroatom doping of 2D graphene materials for electromagnetic interference shielding: A review of recent progress. *Crit. Rev. Solid State Mater. Sci.*, in press, https://doi.org/10.1080/10408436.2021.1965954.
[27] Meng, F. B.; Wang, H. G.; Huang, F.; Guo, Y. F.; Wang, Z. Y.; Hui, D.; Zhou, Z. W. Graphene-based microwave absorbing composites: A review and prospective. *Compos. Part B-Eng.* **2018**, *137*, 260–277.
[28] Wang, C.; Han, X. J.; Xu, P.; Zhang, X. L.; Du, Y. C.; Hu, S. R.; Wang, J. Y.; Wang, X. H. The electromagnetic property of chemically reduced graphene oxide and its application as microwave absorbing material. *Appl. Phys. Lett.* **2011**, *98*, 072906.
[29] Li, C.; Li, Z. H.; Qi, X. S.; Gong, X.; Chen, Y. L.; Peng, Q.; Deng, C. Y.; Jing, T.; Zhong, W. A generalizable strategy for constructing ultralight three-dimensional hierarchical network heterostructure as high-efficient microwave absorber. *J. Colloid Interface Sci.* **2022**, *605*, 13–22.
[30] González, M.; Baselga, J.; Pozuelo, J. High porosity scaffold composites of graphene and carbon nanotubes as microwave absorbing materials. *J. Mater. Chem. C* **2016**, *4*, 8575–8582.
[31] Zhao, Y. J.; Zhang, Y. N.; Yang, C. R.; Cheng, L. F. Ultralight and flexible SiC nanoparticle-decorated carbon nanofiber mats for broad-band microwave absorption. *Carbon* **2021**, *171*, 474–483.
[32] Cui, L. R.; Han, X. J.; Wang, F. Y.; Zhao, H. H.; Du, Y. C. A review on recent advances in carbon-based dielectric system for microwave absorption. *J. Mater. Sci.* **2021**, *56*, 10782–10811.
[33] Gupta, S.; Tai, N. H. Carbon materials and their composites for electromagnetic interference shielding effectiveness in X-band. *Carbon* **2019**, *152*, 159–187.
[34] Zhang, X.; Qiao, J.; Jiang, Y. Y.; Wang, F. L.; Tian, X. L.; Wang, Z.; Wu, L. L.; Liu, W.; Liu, J. R. Carbon-based MOF derivatives: Emerging efficient electromagnetic wave absorption agents. *Nano-Micro Lett.* **2021**, *13*, 135.
[35] Chen, Y. J.; Xiao, G.; Wang, T. S.; Ouyang, Q. Y.; Qi, L. H.; Ma, Y.; Gao, P.; Zhu, C. L.; Cao, M. S.; Jin, H. B. Porous $Fe_3O_4$/carbon core/shell nanorods: Synthesis and electromagnetic properties. *J. Phys. Chem. C* **2011**, *115*, 13603–13608.
[36] Wang, F. Y.; Wang, N.; Han, X. J.; Liu, D. W.; Wang, Y. H.; Cui, L. R.; Xu, P.; Du, Y. C. Core–shell FeCo@carbon nanoparticles encapsulated in polydopamine-derived carbon nanocages for efficient microwave absorption. *Carbon* **2019**, *145*, 701–711.
[37] Du, Y. C.; Liu, W. W.; Qiang, R.; Wang, Y.; Han, X. J.; Ma, J.; Xu, P. Shell thickness-dependent microwave absorption of core–shell $Fe_3O_4$@C composites. *ACS Appl. Mater. Interfaces* **2014**, *6*, 12997–13006.
[38] Meng, X.; Yang, W. W.; Han, G. H.; Yu, Y. S.; Ma, S.; Liu, W.; Zhang, Z. D. Three-dimensional foam-like $Fe_3O_4$@C core–shell nanocomposites: Controllable synthesis and wideband electromagnetic wave absorption properties. *J. Magn. Magn. Mater.* **2020**, *502*, 166518.
[39] Xu, X. F.; Shi, S. H.; Tang, Y. L.; Wang, G. Z.; Zhou, M. F.; Zhao, G. Q.; Zhou, X. C.; Lin, S. W.; Meng, F. B. Growth of NiAl-layered double hydroxide on graphene toward excellent anticorrosive microwave absorption application. *Adv. Sci.* **2021**, *8*, 2002658.
[40] Wang, G. Z.; Gao, Z.; Tang, S. W.; Chen, C. Q.; Duan, F. F.; Zhao, S. C.; Lin, S. W.; Feng, Y. H.; Zhou, L.; Qin, Y. Microwave absorption properties of carbon nanocoils coated with highly controlled magnetic materials by atomic layer deposition. *ACS Nano* **2012**, *6*, 11009–11017.
[41] Yang, K.; Cui, Y. H.; Liu, Z. H.; Liu, P.; Zhang, Q. Y.; Zhang, B. L. Design of core–shell structure NC@$MoS_2$ hierarchical nanotubes as high-performance electromagnetic wave absorber. *Chem. Eng. J.* **2021**, *426*, 131308.
[42] Zhang, Y. J.; Zhang, Y. L.; Li, Y. P.; Yao, M. H.; Miao, X. F.; Liu, C. Y.; Zhao, H. K.; Shao, Y. Y.; Xu, F. $BaTiO_3$@C core–shell nanoparticle/paraffin composites for wide-band microwave absorption. *ACS Appl. Nano Mater.* **2021**, *4*, 13176–13184.
[43] Liu, Q. H.; Cao, Q.; Bi, H.; Liang, C. Y.; Yuan, K. P.; She, W.; Yang, Y. J.; Che, R. C. CoNi@$SiO_2$@$TiO_2$ and CoNi@Air@$TiO_2$ microspheres with strong wideband microwave absorption. *Adv. Mater.* **2016**, *28*, 486–490.
[44] Li, H.; Bao, S. S.; Li, Y. M.; Huang, Y. Q.; Chen, J. Y.; Zhao, H.; Jiang, Z. Y.; Kuang, Q.; Xie, Z. X. Optimizing the electromagnetic wave absorption performances of designed $Co_3Fe_7$@C yolk–shell structures. *ACS Appl. Mater. Interfaces* **2018**, *10*, 28839–28849.
[45] Liu, X. F.; Hao, C. C.; He, L. H.; Yang, C.; Chen, Y. B.; Jiang, C. B.; Yu, R. H. Yolk–shell structured Co-C/Void/$Co_9S_8$ composites with a tunable cavity for ultrabroadband and efficient low-frequency microwave absorption. *Nano Res.* **2018**, *11*, 4169–4182.
[46] Tao, J. Q.; Zhou, J. T.; Yao, Z. J.; Jiao, Z. B.; Wei, B.; Tan, R. Y.; Li, Z. Multi-shell hollow porous carbon nanoparticles with excellent microwave absorption properties. *Carbon* **2021**, *172*, 542–555.
[47] Zhu, X. J.; Dong, Y. Y.; Pan, F.; Xiang, Z.; Liu, Z. C.; Deng, B. W.; Zhang, X.; Shi, Z.; Lu, W. Covalent organic framework-derived hollow core–shell Fe/$Fe_3O_4$@porous carbon composites with corrosion resistance for lightweight and efficient microwave absorption. *Compos. Commun.* **2021**, *25*, 100731.
[48] Tian, C. H.; Du, Y. C.; Xu, P.; Qiang, R.; Wang, Y.; Ding, D.; Xue, J. L.; Ma, J.; Zhao, H. T.; Han, X. J. Constructing uniform core–shell PPy@PANI composites with tunable shell thickness toward enhancement in microwave absorption. *ACS Appl. Mater. Interfaces* **2015**, *7*, 20090–20099.
[49] Goodenough, J. B. Summary of losses in magnetic materials. *IEEE Trans. Magn.* **2002**, *38*, 3398–3408.
[50] Yan, M.; Peng, X. L. *Fundamentals of Magnetics and Magnetic Materials*, 2nd ed.; Zhejiang University Press: Hangzhou, 2018.
[51] Liu, D. W.; Du, Y. C.; Li, Z. N.; Wang, Y. H.; Xu, P.; Zhao, H. H.; Wang, F. Y.; Li, C. L.; Han, X. J. Facile synthesis of 3D flower-like Ni microspheres with enhanced microwave absorption properties. *J. Mater. Chem. C* **2018**, *6*, 9615–9623.
[52] Wu, M. Z.; Zhang, Y. D.; Hui, S.; Xiao, T. D.; Ge, S. H.; Hines, W. A.; Budnick, J. I.; Taylor, G. W. Microwave magnetic properties of $Co_{50}/(SiO_2)_{50}$ nanoparticles. *Appl. Phys. Lett.* **2002**, *80*, 4404–4406.
[53] Wu, Y. H.; Han, M. G.; Tang, Z. K.; Deng, L. J. Eddy current effect on the microwave permeability of Fe-based nanocrystalline flakes with different sizes. *J. Appl. Phys.* **2014**, *115*, 163902.
[54] Walz, F. The role of the skin-effect in dynamic magnetic measurements. *Phys. Status Solidi A* **1992**, *134*, 509–520.
[55] Kim, S. S.; Kim, S. T.; Yoon, Y. C.; Lee, K. S. Magnetic, dielectric, and microwave absorbing properties of iron particles dispersed in rubber matrix in gigahertz frequencies. *J. Appl. Phys.* **2005**, *97*, 10F905.
[56] Seo, Y.; Ko, S.; Ha, H.; Qaiser, N.; Leem, M.; Yoo, S. J.; Jeong, J. H.; Lee, K.; Hwang, B. Stretchable carbonyl iron powder/polydimethylsiloxane composites for noise suppression in gigahertz bandwidth. *Compos. Sci. Technol.* **2022**, *218*, 109150.
[57] Zeng, M.; Zhang, X. X.; Yu, R. H.; Zhao, D. L.; Zhang, Y. H.; Wang, X. L. Improving high-frequency properties via selectable diameter of amorphous-ferroalloy particle. *Mater. Sci. Eng. B* **2014**, *185*, 21–25.
[58] Zhu, J. H.; Wei, S. Y.; Haldolaarachchige, N.; Young, D. P.; Guo, Z. H. Electromagnetic field shielding polyurethane nanocomposites reinforced with core–shell Fe-silica nanoparticles. *J. Phys. Chem. C* **2011**, *115*, 15304–15310.
[59] Stergiou, C. Magnetic, dielectric and microwave absorption properties of rare earth doped Ni-Co and Ni-Co-Zn spinel ferrites.

*J. Magn. Magn. Mater.* **2017**, *426*, 629–635.
[60] Xie, J. L.; Han, M. G.; Chen, L.; Kuang, R. X.; Deng, L. J. Microwave-absorbing properties of NiCoZn spinel ferrites. *J. Magn. Magn. Mater.* **2007**, *314*, 37–42.
[61] Aharoni, A. Exchange resonance modes in a ferromagnetic sphere. *J. Appl. Phys.* **1991**, *69*, 7762–7764.
[62] Deng, L. J.; Zhou, P. H.; Xie, J. L.; Zhang, L. Characterization and microwave resonance in nanocrystalline FeCoNi flake composite. *J. Appl. Phys.* **2007**, *101*, 103916.
[63] Zhou, C. H.; Wu, C.; Yan, M. Hierarchical FeCo@$MoS_2$ nanoflowers with strong electromagnetic wave absorption and broad bandwidth. *ACS Appl. Nano Mater.* **2018**, *1*, 5179–5187.
[64] Wen, B.; Cao, M. S.; Hou, Z. L.; Song, W. L.; Zhang, L.; Lu, M. M.; Jin, H. B.; Fang, X. Y.; Wang, W. Z.; Yuan, J. Temperature dependent microwave attenuation behavior for carbon-nanotube/silica composites. *Carbon* **2013**, *65*, 124–139.
[65] Kittel, C. *Introduction to Solid State Physics*, 8th ed.; John Wiley & Sons, Inc.: New York, 2005.
[66] Zhang, J. J.; Qi, X. S.; Gong, X.; Peng, Q.; Chen, Y. L.; Xie, R.; Zhong, W. Microstructure optimization of core@shell structured $MSe_2$/$FeSe_2$@$MoSe_2$ (M = Co, Ni) flower-like multicomponent nanocomposites towards high-efficiency microwave absorption. *J. Mater. Sci. Technol.* **2022**, *128*, 59–70.
[67] Qin, M.; Zhang, L. M.; Wu, H. J. Dielectric loss mechanism in electromagnetic wave absorbing materials. *Adv. Sci.* **2022**, *9*, 2105553.
[68] Zhao, H. H.; Xu, X. Z.; Wang, Y. H.; Fan, D. G.; Liu, D. W.; Lin, K. F.; Xu, P.; Han, X. J.; Du, Y. C. Heterogeneous interface induced the formation of hierarchically hollow carbon microcubes against electromagnetic pollution. *Small* **2020**, *16*, 2003407.
[69] Zhang, Y.; Huang, Y.; Zhang, T. F.; Chang, H. C.; Xiao, P. S.; Chen, H. H.; Huang, Z. Y.; Chen, Y. S. Broadband and tunable high-performance microwave absorption of an ultralight and highly compressible graphene foam. *Adv. Mater.* **2015**, *27*, 2049–2053.
[70] Cao, M. S.; Han, C.; Wang, X. X.; Zhang, M.; Zhang, Y. L.; Shu, J. C.; Yang, H. J.; Fang, X. Y.; Yuan, J. Graphene nanohybrids: Excellent electromagnetic properties for the absorbing and shielding of electromagnetic waves. *J. Mater. Chem. C* **2018**, *6*, 4586–4602.
[71] Wang, Y. H.; Li, X. D.; Han, X. J.; Xu, P.; Cui, L. R.; Zhao, H. H.; Liu, D. W.; Wang, F. Y.; Du, Y. C. Ternary $Mo_2C$/Co/C composites with enhanced electromagnetic waves absorption. *Chem. Eng. J.* **2020**, *387*, 124159.
[72] Cao, M. S.; Song, W. L.; Hou, Z. L.; Wen, B.; Yuan, J. The effects of temperature and frequency on the dielectric properties, electromagnetic interference shielding and microwave-absorption of short carbon fiber/silica composites. *Carbon* **2010**, *48*, 788–796.
[73] Ohlan, A.; Singh, K.; Chandra, A.; Dhawan, S. K. Microwave absorption behavior of core–shell structured poly (3,4-ethylenedioxy thiophene)-barium ferrite nanocomposites. *ACS Appl. Mater. Interfaces* **2010**, *2*, 927–933.
[74] Qin, M.; Zhang, L. M.; Zhao, X. R.; Wu, H. J. Defect induced polarization loss in multi-shelled spinel hollow spheres for electromagnetic wave absorption application. *Adv. Sci.* **2021**, *8*, 2004640.
[75] Liang, L. L.; Gu, W. H.; Wu, Y.; Zhang, B. S.; Wang, G. H.; Yang, Y.; Ji, G. B. Heterointerface engineering in electromagnetic absorbers: New insights and opportunities. *Adv. Mater.* **2022**, *34*, 2106195.
[76] Wang, G. Z.; Gao, Z.; Wan, G. P.; Lin, S. W.; Yang, P.; Qin, Y. High densities of magnetic nanoparticles supported on graphene fabricated by atomic layer deposition and their use as efficient synergistic microwave absorbers. *Nano Res.* **2014**, *7*, 704–716.
[77] Shi, X. L.; Cao, M. S.; Yuan, J.; Zhao, Q. L.; Kang, Y. Q.; Fang, X. Y.; Chen, Y. J. Nonlinear resonant and high dielectric loss behavior of CdS/α-$Fe_2O_3$ heterostructure nanocomposites. *Appl. Phys. Lett.* **2008**, *93*, 183118.
[78] Huang, W. H.; Gao, W. M.; Zuo, S. W.; Zhang, L. X.; Pei, K.; Liu, P. B.; Che, R. C.; Zhang, H. B. Hollow MoC/NC sphere for electromagnetic wave attenuation: Direct observation of interfacial polarization on nanoscale hetero-interfaces. *J. Mater. Chem. A* **2022**, *10*, 1290–1298.
[79] Wu, Z. C.; Jin, C.; Yang, Z. Q.; Che, R. C. Integrating hierarchical interfacial polarization in yeast-derived $Mo_2C$/C nanoflower/microsphere nanoarchitecture for boosting microwave absorption performance. *Carbon* **2022**, *189*, 530–538.
[80] Zhang, R. X.; Wang, L.; Xu, C. Y.; Liang, C. Y.; Liu, X. H.; Zhang, X. F.; Che, R. C. Vortex tuning magnetization configurations in porous $Fe_3O_4$ nanotube with wide microwave absorption frequency. *Nano Res.* **2022**, *15*, 6743–6750.
[81] Wang, Y.; Du, Y. C.; Qiang, R.; Tian, C. H.; Xu, P.; Han, X. J. Interfacially engineered sandwich-like RGO/carbon microspheres/RGO composite as an efficient and durable microwave absorber. *Adv. Mater. Interfaces* **2016**, *3*, 1500684.
[82] Liu, Y.; Zeng, Z. H.; Zheng, S. N.; Qiao, J.; Liu, W.; Wu, L. L.; Liu, J. R. Facile manufacturing of Ni/MnO nanoparticle embedded carbon nanocomposite fibers for electromagnetic wave absorption. *Compos. Part B-Eng.* **2022**, *235*, 109800.
[83] Samet, M.; Levchenko, V.; Boiteux, G.; Seytre, G.; Kallel, A.; Serghei, A. Electrode polarization vs. Maxwell–Wagner–Sillars interfacial polarization in dielectric spectra of materials: Characteristic frequencies and scaling laws. *J. Chem. Phys.* **2015**, *142*, 194703.
[84] Dong, X. L.; Zhang, X. F.; Huang, H.; Zuo, F. Enhanced microwave absorption in Ni/polyaniline nanocomposites by dual dielectric relaxations. *Appl. Phys. Lett.* **2008**, *92*, 013127.
[85] Zhang, P.; Han, X. J.; Kang, L. L.; Qiang, R.; Liu, W. W.; Du, Y. C. Synthesis and characterization of polyaniline nanoparticles with enhanced microwave absorption. *RSC Adv.* **2013**, *3*, 12694–12701.
[86] Xu, H. L.; Yin, X. W.; Li, M. H.; Ye, F.; Han, M. K.; Hou, Z. X.; Li, X. L.; Zhang, L. T.; Cheng, L. F. Mesoporous carbon hollow microspheres with red blood cell like morphology for efficient microwave absorption at elevated temperature. *Carbon* **2018**, *132*, 343–351.
[87] Du, L.; Du, Y. C.; Li, Y.; Wang, J. Y.; Wang, C.; Wang, X. H.; Xu, P.; Han, X. J. Surfactant-assisted solvothermal synthesis of $Ba(CoTi)_xFe_{12-2x}O_{19}$ nanoparticles and enhancement in microwave absorption properties of polyaniline. *J. Phys. Chem. C* **2010**, *114*, 19600–19606.
[88] Chen, N.; Mu, G. H.; Pan, X. F.; Gan, K. K.; Gu, M. Y. Microwave absorption properties of $SrFe_{12}O_{19}$/$ZnFe_2O_4$ composite powders. *Mater. Sci. Eng. B* **2007**, *139*, 256–260.
[89] Zheng, S. N.; Zeng, Z. H.; Qiao, J.; Liu, Y.; Liu, J. R. Facile preparation of C/MnO/Co nanocomposite fibers for high-performance microwave absorption. *Compos. Part A:Appl. Sci. Manuf.* **2022**, *155*, 106814.
[90] Kong, L. B.; Li, Z. W.; Liu, L.; Huang, R.; Abshinova, M.; Yang, Z. H.; Tang, C. B.; Tan, P. K.; Deng, C. R.; Matitsine, S. Recent progress in some composite materials and structures for specific electromagnetic applications. *Int. Mater. Rev.* **2013**, *58*, 203–259.
[91] Liu, Y.; Chen, Z.; Zhang, Y.; Feng, R.; Chen, X.; Xiong, C. X.; Dong, L. J. Broadband and lightweight microwave absorber constructed by *in situ* growth of hierarchical $CoFe_2O_4$/reduced graphene oxide porous nanocomposites. *ACS Appl. Mater. Interfaces* **2018**, *10*, 13860–13868.
[92] Zhao, H. H.; Han, X. J.; Li, Z. N.; Liu, D. W.; Wang, Y. H.; Wang, Y.; Zhou, W.; Du, Y. C. Reduced graphene oxide decorated with carbon nanopolyhedrons as an efficient and lightweight microwave absorber. *J. Colloid Interface Sci.* **2018**, *528*, 174–183.
[93] Zhang, X.; Tian, X. L.; Liu, C.; Qiao, J.; Liu, W.; Liu, J. R.; Zeng, Z. H. MnCo-MOF-74 derived porous MnO/Co/C heterogeneous nanocomposites for high-efficiency electromagnetic wave absorption. *Carbon* **2022**, *194*, 257–266.
[94] Xu, P.; Han, X. J.; Wang, C.; Zhao, H. T.; Wang, J. Y.; Wang, X. H.; Zhang, B. Synthesis of electromagnetic functionalized barium ferrite nanoparticles embedded in polypyrrole. *J. Phys. Chem. B* **2008**, *112*, 2775–2781.
[95] Lee, K. S.; Yun, Y. C.; Kim, S. W.; Kim, S. S. Microwave absorption of λ/4 wave absorbers using high permeability magnetic composites in quasimicrowave frequency band. *J. Appl. Phys.* **2008**, *103*, 07E504.
[96] Stergiou, C.; Litsardakis, G. Design of microwave absorbing

coatings with new Ni and La doped $SrCo_2$-W hexaferrites. *IEEE Trans. Magn.* **2012**, *48*, 1516–1519.

[97] Zhao, H. H.; Wang, F. Y.; Cui, L. R.; Xu, X. Z.; Han, X. J.; Du, Y. C. Composition optimization and microstructure design in MOFs-derived magnetic carbon-based microwave absorbers: A review. *Nano-Micro Lett.* **2021**, *13*, 208.

[98] Fang, J. F.; Lv, H. L.; Zhao, B.; Liu, Z. W.; Li, X. H.; Xu, C. Y.; Zhang, R. X.; Zhang, H. B.; Liu, X. H.; Zhang, X. F. et al. Selective assembly of magnetic nano-antenna for electromagnetic dissipation. *J. Mater. Chem. A* **2022**, *10*, 10909–10915.

[99] Liu, D. W.; Du, Y. C.; Xu, P.; Liu, N.; Wang, Y. H.; Zhao, H. H.; Cui, L. R.; Han, X. J. Waxberry-like hierarchical Ni@C microspheres with high-performance microwave absorption. *J. Mater. Chem. C* **2019**, *7*, 5037–5046.

[100] Ning, M. Q.; Man, Q. K.; Tan, G. G.; Lei, Z. K.; Li, J. B.; Li, R. W. Ultrathin $MoS_2$ nanosheets encapsulated in hollow carbon spheres: A case of a dielectric absorber with optimized impedance for efficient microwave absorption. *ACS Appl. Mater. Interfaces* **2020**, *12*, 20785–20796.

[101] Du, Y. C.; Liu, T.; Yu, B.; Gao, H. B.; Xu, P.; Wang, J. Y.; Wang, X. H.; Han, X. J. The electromagnetic properties and microwave absorption of mesoporous carbon. *Mater. Chem. Phys.* **2012**, *135*, 884–891.

[102] Wing, Z. N.; Wang, B.; Halloran, J. W. Permittivity of porous titanate dielectrics. *J. Am. Ceram. Soc.* **2006**, *89*, 3696–3700.

[103] Ma, Z.; Zhang, Y.; Cao, C. T.; Yuan, J.; Liu, Q. F.; Wang, J. B. Attractive microwave absorption and the impedance match effect in zinc oxide and carbonyl iron composite. *Phys. B:Condens. Matter* **2011**, *406*, 4620–4624.

[104] Liu, D. W.; Qiang, R.; Du, Y. C.; Wang, Y.; Tian, C. H.; Han, X. J. Prussian blue analogues derived magnetic FeCo alloy/carbon composites with tunable chemical composition and enhanced microwave absorption. *J. Colloid Interface Sci.* **2018**, *514*, 10–20.

[105] Yang, W. D.; Zhao, Q. Q.; Zhou, Y.; Cui, Z. L.; Liu, Y. J. Research progress of metal organic frameworks/carbon-based composites for microwave absorption. *Adv. Eng. Mater.* **2022**, *24*, 2100964.

[106] Liang, J.; Ye, F.; Cao, Y. C.; Mo, R.; Cheng, L. F.; Song, Q. Defect-engineered graphene/$Si_3N_4$ multilayer alternating core–shell nanowire membrane: A plainified hybrid for broadband electromagnetic wave absorption. *Adv. Funct. Mater.* **2022**, *32*, 2200141.

[107] Peng, H. L.; Xiong, Z. Q.; Gan, Z. H.; Liu, C. B.; Xie, Y. Microcapsule MOFs@MOFs derived porous "nut-bread" composites with broadband microwave absorption. *Compos. Part B-Eng.* **2021**, *224*, 109170.

[108] Qiao, J.; Zhang, X.; Liu, C.; Zeng, Z. H.; Yang, Y. F.; Wu, L. L.; Wang, F. L.; Wang, Z.; Liu, W.; Liu, J. R. Facile synthesis of MnS nanoparticle embedded porous carbon nanocomposite fibers for broadband electromagnetic wave absorption. *Carbon* **2022**, *191*, 525–534.

[109] Micheli, D.; Pastore, R.; Apollo, C.; Marchetti, M.; Gradoni, G.; Primiani, V. M.; Moglie, F. Broadband electromagnetic absorbers using carbon nanostructure-based composites. *IEEE Trans. Microwave Theory Techn.* **2011**, *59*, 2633–2646.

[110] Micheli, D.; Vricella, A.; Pastore, R.; Marchetti, M. Synthesis and electromagnetic characterization of frequency selective radar absorbing materials using carbon nanopowders. *Carbon* **2014**, *77*, 756–774.

[111] Wu, C.; Bi, K.; Yan, M. Scalable self-supported $FeNi_3/Mo_2C$ flexible paper for enhanced electromagnetic wave absorption evaluated via coaxial, waveguide and arch methods. *J. Mater. Chem. C* **2020**, *8*, 10204–10212.

[112] Sun, X. X.; Yang, M. L.; Yang, S.; Wang, S. S.; Yin, W. L.; Che, R. C.; Li, Y. B. Ultrabroad band microwave absorption of carbonized waxberry with hierarchical structure. *Small* **2019**, *15*, 1902974.

[113] Zhang, J. J.; Li, Z. H.; Qi, X. S.; Gong, X.; Xie, R.; Deng, C. Y.; Zhong, W.; Du, Y. W. Constructing flower-like core@shell $MoSe_2$-based nanocomposites as a novel and high-efficient microwave absorber. *Compos. Part B-Eng.* **2021**, *222*, 109067.

[114] Sotiropoulos, A.; Koulouridis, S.; Masouras, A.; Kostopoulos, V.; Anastassiu, H. T. Carbon nanotubes films in glass fiber polymer matrix forming structures with high absorption and shielding performance in X-band. *Compos. Part B-Eng.* **2021**, *217*, 108896.

[115] Wang, L.; Song, P.; Lin, C. T.; Kong, J. Gu, J. W. 3D shapeable, superior electrically conductive cellulose nanofibers/$Ti_3C_2T_x$ MXene aerogels/epoxy nanocomposites for promising EMI shielding. *Research* **2020**, *2020*, 4093732.

[116] Han, Y. X.; Ruan, K. P.; Gu, J. W. Janus (BNNS/ANF)-(AgNWs/ANF) thermal conductivity composite films with superior electromagnetic interference shielding and Joule heating performances. *Nano Res.* **2022**, *15*, 4747–4755.

[117] Jiang, J. J.; Li, D.; Geng, D. Y.; An, J.; He, J.; Liu, W.; Zhang, Z. D. Microwave absorption properties of core double-shell FeCo/C/$BaTiO_3$ nanocomposites. *Nanoscale* **2014**, *6*, 3967–3971.

[118] Liu, J. R.; Itoh, M.; Terada, M.; Horikawa, T.; Machida, K. I. Enhanced electromagnetic wave absorption properties of Fe nanowires in gigaherz range. *Appl. Phys. Lett.* **2007**, *91*, 093101.

[119] Ma, Z. L.; Xiang, X. L.; Shao, L.; Zhang, Y. L.; Gu, J. W. Multifunctional wearable silver nanowire decorated leather nanocomposites for joule heating, electromagnetic interference shielding and piezoresistive sensing. *Angew. Chem., Int. Ed.* **2022**, *61*, e202200705.

[120] Zeng, Z. H.; Wu, N.; Wei, J. J.; Yang, Y. F.; Wu, T. T.; Li, B.; Hauser, S. B.; Yang, W. D.; Liu, J. R.; Zhao, S. Y. Porous and ultra-flexible crosslinked MXene/polyimide composites for multifunctional electromagnetic interference shielding. *Nano-Micro Lett.* **2022**, *14*, 59.

[121] Wang, L.; Ma, Z. L.; Zhang, Y. L.; Qiu, H.; Ruan, K. P.; Gu, J. W. Mechanically strong and folding-endurance $Ti_3C_2T_x$ MXene/PBO nanofiber films for efficient electromagnetic interference shielding and thermal management. *Carbon Energy* **2022**, *4*, 200–210.

[122] Wang, L.; Ma, Z. L.; Zhang, Y. L.; Chen, L. X.; Cao, D. P.; Gu, J. W. Polymer-based EMI shielding composites with 3D conductive networks: A mini-review. *SusMat* **2021**, *1*, 413–431.

[123] Zhang, Y. L.; Ruan, K. P.; Gu, J. W. Flexible sandwich-structured electromagnetic interference shielding nanocomposite films with excellent thermal conductivities. *Small* **2021**, *17*, 2101951.

[124] Kong, L.; Yin, X. W.; Ye, F.; Li, Q.; Zhang, L. T.; Cheng, L. F. Electromagnetic wave absorption properties of ZnO-based materials modified with $ZnAl_2O_4$ nanograins. *J. Phys. Chem. C* **2013**, *117*, 2135–2146.

[125] Pozar, D. M. *Microwave Engineering*, 4th ed.; Wiley: Hoboken, 2012.

[126] Kong, J. A. *Electromagnetic Wave Theory*; John Wiley & Sons, Inc., 1986.

[127] Li, D.; Liao, H. Y.; Kikuchi, H.; Liu, T. Microporous Co@C nanoparticles prepared by dealloying CoAl@C precursors: Achieving strong wideband microwave absorption via controlling carbon shell thickness. *ACS Appl. Mater. Interfaces* **2017**, *9*, 44704–44714.

[128] Luo, J. H.; Zhang, K.; Cheng, M. L.; Gu, M. M.; Sun, X. K. $MoS_2$ spheres decorated on hollow porous ZnO microspheres with strong wideband microwave absorption. *Chem. Eng. J.* **2020**, *380*, 122625.

[129] Wang, P.; Liu, D. W.; Cui, L. R.; Hu, B.; Han, X. J.; Du, Y. C. A review of recent advancements in Ni-related materials used for microwave absorption. *J. Phys. D:Appl. Phys.* **2021**, *54*, 473003.

[130] Qi, X. S.; Xu, J. L.; Zhong, W.; Du, Y. W. Synthesis of high purity chain-like carbon nanospheres in ultrahigh yield, and their microwave absorption properties. *RSC Adv.* **2015**, *5*, 16010–16016.

[131] Wang, N. N.; Wu, F.; Xie, A. M.; Dai, X. Q.; Sun, M. X.; Qiu, Y. Y.; Wang, Y.; Lv, X. L.; Wang, M. Y. One-pot synthesis of biomass-derived carbonaceous spheres for excellent microwave absorption at the Ku band. *RSC Adv.* **2015**, *5*, 40531–40535.

[132] Wang, C.; Xu, T. T.; Wang, C. A. Microwave absorption properties of C/(C@CoFe) hierarchical core–shell spheres synthesized by using colloidal carbon spheres as templates. *Ceram. Int.* **2016**, *42*, 9178–9182.

[133] Li, C. P.; Ge, Y. Q.; Jiang, X. H.; Zhang, Z. M.; Yu, L. M. The rambutan-like C@$NiCo_2O_4$ composites for enhanced microwave

absorption performance. *J. Mater. Sci. :Mater. Electron.* **2019**, *30*, 3124–3136.

[134] Zhao, B.; Li, Y.; Zeng, Q. W.; Fan, B. B.; Wang, L.; Zhang, R.; Che, R. C. Growth of magnetic metals on carbon microspheres with synergetic dissipation abilities to broaden microwave absorption. *J. Mater. Sci. Technol.* **2022**, *107*, 100–110.

[135] Wang, Y.; Du, Y. C.; Guo, D.; Qiang, R.; Tian, C. H.; Xu, P.; Han, X. J. Precursor-directed synthesis of porous cobalt assemblies with tunable close-packed hexagonal and face-centered cubic phases for the effective enhancement in microwave absorption. *J. Mater. Sci.* **2017**, *52*, 4399–4411.

[136] Lian, Y. L.; Han, B. H.; Liu, D. W.; Wang, Y. H.; Zhao, H. H.; Xu, P.; Han, X. J.; Du, Y. C. Solvent-free synthesis of ultrafine tungsten carbide nanoparticles-decorated carbon nanosheets for microwave absorption. *Nano-Micro Lett.* **2020**, *12*, 153.

[137] Han, M. K.; Yin, X. W.; Ren, S.; Duan, W. Y.; Zhang, L. T.; Cheng, L. F. Core/shell structured C/ZnO nanoparticles composites for effective electromagnetic wave absorption. *RSC Adv.* **2016**, *6*, 6467–6474.

[138] Xu, J.; Liu, Z. H.; Wang, J.; Liu, P.; Ahmad, M.; Zhang, Q. Y.; Zhang, B. L. Preparation of core–shell C@$TiO_2$ composite microspheres with wrinkled morphology and its microwave absorption. *J. Colloid Interface Sci.* **2022**, *607*, 1036–1049.

[139] Yu, L. J.; Zhu, Y. F.; Fu, Y. Q. Waxberry-like carbon@polyaniline microspheres with high-performance microwave absorption. *Appl. Surf. Sci.* **2018**, *427*, 451–457.

[140] Zhang, F.; Zhang, W. D.; Zhu, W. F.; Cheng, B.; Qiu, H.; Qi, S. H. Core–shell nanostructured CS/$MoS_2$: A promising material for microwave absorption. *Appl. Surf. Sci.* **2019**, *463*, 182–189.

[141] Li, X. L.; Yin, X. W.; Song, C. Q.; Han, M. K.; Xu, H. L.; Duan, W. Y.; Cheng, L. F.; Zhang, L. T. Self-assembly core–shell graphene-bridged hollow MXenes spheres 3D foam with ultrahigh specific EM absorption performance. *Adv. Funct. Mater.* **2018**, *28*, 1803938.

[142] Li, Z. N.; Han, X. J.; Ma, Y.; Liu, D. W.; Wang, Y. H.; Xu, P.; Li, C. L.; Du, Y. C. MOFs-derived hollow Co/C microspheres with enhanced microwave absorption performance. *ACS Sustainable Chem. Eng.* **2018**, *6*, 8904–8913.

[143] Chen, G. Z.; Xu, D. W.; Chen, P.; Guo, X.; Yu, Q.; Qiu, H. F. Constructing and optimizing hollow bird-nest-patterned C@$Fe_3O_4$ composites as high-performance microwave absorbers. *J. Magn. Magn. Mater.* **2021**, *532*, 167990.

[144] Hu, P. T.; Dong, S.; Yuan, F.; Li, X. T.; Hong, C. Q. Hollow carbon microspheres modified with $NiCo_2S_4$ nanosheets as a high-performance microwave absorber. *Adv. Compos. Hybrid Mater.* **2022**, *5*, 469–480.

[145] Lv, H. L.; Ji, G. B.; Liu, W.; Zhang, H. Q.; Du, Y. W. Achieving hierarchical hollow carbon@Fe@$Fe_3O_4$ nanospheres with superior microwave absorption properties and lightweight features. *J. Mater. Chem. C* **2015**, *3*, 10232–10241.

[146] Shen, G. Z.; Ren, J. Z.; Zhao, B.; Mei, B. Q.; Wu, H. Y.; Fang, X. M.; Xu, Y. W. Magnetic hollow mesoporous carbon composites with impedance matching for highly effective microwave absorption. *J. Mater. Sci.* **2019**, *54*, 4024–4037.

[147] Wang, H. Y.; Zhang, Z. F.; Dong, C. J.; Chen, G.; Wang, Y. D.; Guan, H. T. Carbon spheres@$MnO_2$ core–shell nanocomposites with enhanced dielectric properties for electromagnetic shielding. *Sci. Rep.* **2017**, *7*, 15841.

[148] Xu, L. L.; Tao, J. Q.; Zhang, X. F.; Yao, Z. J.; Wei, B.; Yang, F.; Zhou, C. Y.; Zavabeti, A.; Zuraiqi, K.; Zhou, J. T. Hollow C@$MoS_2$ nanospheres for microwave absorption. *ACS Appl. Nano Mater.* **2021**, *4*, 11199–11209.

[149] Yang, L. J.; Lv, H. L.; Li, M.; Zhang, Y.; Liu, J. C.; Yang, Z. H. Multiple polarization effect of shell evolution on hierarchical hollow C@$MnO_2$ composites and their wideband electromagnetic wave absorption properties. *Chem. Eng. J.* **2020**, *392*, 123666.

[150] Cao, M. S.; Yang, J.; Song, W. L.; Zhang, D. Q.; Wen, B.; Jin, H. B.; Hou, Z. L.; Yuan, J. Ferroferric oxide/multiwalled carbon nanotube vs polyaniline/ferroferric oxide/multiwalled carbon nanotube multiheterostructures for highly effective microwave absorption. *ACS Appl. Mater. Interfaces* **2012**, *4*, 6949–6956.

[151] Wang, Y. C.; Wen, Z. L.; Long, L.; Li, Y.; Zhou, W. Dielectric response and microwave absorption properties of SiC whisker-coated carbon fibers. *J. Mater. Sci.:Mater. Electron.* **2019**, *30*, 15075–15083.

[152] Wu, R. B.; Yang, Z. H.; Fu, M. S.; Zhou, K. *In-situ* growth of SiC nanowire arrays on carbon fibers and their microwave absorption properties. *J. Alloys Compd.* **2016**, *687*, 833–838.

[153] Zhou, W.; Long, L.; Xiao, P.; Li, Y.; Luo, H.; Hu, W. D.; Yin, R. M. Silicon carbide Nano-fibers *in-situ* grown on carbon fibers for enhanced microwave absorption properties. *Ceram. Int.* **2017**, *43*, 5628–5634.

[154] Zhang, W. D.; Zhang, X.; Zhu, Q.; Zheng, Y.; Liotta, L. F.; Wu, H. J. High-efficiency and wide-bandwidth microwave absorbers based on $MoS_2$-coated carbon fiber. *J. Colloid Interface Sci.* **2021**, *586*, 457–468.

[155] Huan, X. H.; Wang, H. T.; Deng, W. C.; Yan, J. Q.; Xu, K.; Geng, H. B.; Guo, X. D.; Jia, X. L.; Zhou, J. S.; Yang, X. P. Integrating multi-heterointerfaces in a 1D@2D@1D hierarchical structure via autocatalytic pyrolysis for ultra-efficient microwave absorption performance. *Small* **2022**, *18*, 2105411.

[156] Tao, J. Q.; Jiao, Z. B.; Xu, L. L.; Yi, P. S.; Yao, Z. J.; Yang, F.; Zhou, C. Y.; Chen, P.; Zhou, J. T.; Li, Z. Construction of MOF-derived Co/C shell on carbon fiber surface to enhance multi-polarization effect towards efficient broadband electromagnetic wave absorption. *Carbon* **2021**, *184*, 571–582.

[157] Zhao, Z. H.; Zhou, X. J.; Kou, K. C.; Wu, H. J. PVP-assisted transformation of ZIF-67 into cobalt layered double hydroxide/carbon fiber as electromagnetic wave absorber. *Carbon* **2021**, *173*, 80–90.

[158] Dai, B. S.; Li, J. Y.; Wang, W. Z.; Liu, X. G.; Qi, Y. J.; Qi, Y. Carbon fibers with eddy current loss characteristics exhibit different microwave absorption properties in different graphitization states. *Mater. Lett.* **2020**, *281*, 128667.

[159] Zhang, Y.; Yang, Z. J.; Yu, Y.; Wen, B. Y.; Liu, Y. Y.; Qiu, M. N. Tunable electromagnetic interference shielding ability in a one-dimensional bagasse fiber/polyaniline heterostructure. *ACS Appl. Polym. Mater.* **2019**, *1*, 737–745.

[160] Tian, X.; Meng, F. B.; Meng, F. C.; Chen, X. N.; Guo, Y. F.; Wang, Y.; Zhu, W. J.; Zhou, Z. W. Synergistic enhancement of microwave absorption using hybridized polyaniline@helical CNTs with dual chirality. *ACS Appl. Mater. Interfaces* **2017**, *9*, 15711–15718.

[161] Wang, Y.; Du, Y. C.; Wu, B.; Han, B. H.; Dong, S. M.; Han, X. J.; Xu, P. Fabrication of PPy nanosphere/RGO composites via a facile self-assembly strategy for durable microwave absorption. *Polymers* **2018**, *10*, 998.

[162] Wu, T. M.; Lin, Y. W. Doped polyaniline/multi-walled carbon nanotube composites: Preparation, characterization and properties. *Polymer* **2006**, *47*, 3576–3582.

[163] Wu, T. M.; Lin, Y. W.; Liao, C. S. Preparation and characterization of polyaniline/multi-walled carbon nanotube composites. *Carbon* **2005**, *43*, 734–740.

[164] Wang, D. T.; Wang, X. C.; Zhang, X.; Yuan, H. R.; Chen, Y. J. Tunable dielectric properties of carbon nanotube@polypyrrole core–shell hybrids by the shell thickness for electromagnetic wave absorption. *Chin. Phys. Lett.* **2020**, *37*, 045201.

[165] Wang, H. G.; Meng, F. B.; Huang, F.; Jing, C. F.; Li, Y.; Wei, W.; Zhou, Z. W. Interface modulating CNTs@PANi hybrids by controlled unzipping of the walls of CNTs to achieve tunable high-performance microwave absorption. *ACS Appl. Mater. Interfaces* **2019**, *11*, 12142–12153.

[166] Cheng, J. Y.; Zhao, B.; Zheng, S. Y.; Yang, J. H.; Zhang, D. Q.; Cao, M. S. Enhanced microwave absorption performance of polyaniline-coated CNT hybrids by plasma-induced graft polymerization. *Appl. Phys. A* **2015**, *119*, 379–386.

[167] Li, X.; Yu, L. M.; Zhao, W. K.; Shi, Y. Y.; Yu, L. J.; Dong, Y. B.; Zhu, Y. F.; Fu, Y. Q.; Liu, X. D.; Fu, F. Y. Prism-shaped hollow carbon decorated with polyaniline for microwave absorption. *Chem. Eng. J.* **2020**, *379*, 122393.

[168] Wang, Y. Y.; Sun, W. J.; Lin, H.; Gao, P. P.; Gao, J. F.; Dai, K.; Yan, D. X.; Li, Z. M. Steric stabilizer-based promotion of uniform polyaniline shell for enhanced electromagnetic wave absorption of

carbon nanotube/polyaniline hybrids. *Compos. Part B-Eng.* **2020**, *199*, 108309.

[169] Kang, S.; Qiao, S. Y.; Cao, Y. T.; Hu, Z. M.; Yu, J. R.; Wang, Y.; Zhu, J. Hyper-cross-linked polymers-derived porous tubular carbon nanofibers@$TiO_2$ toward a wide-band and lightweight microwave absorbent at a low loading content. *ACS Appl. Mater. Interfaces* **2020**, *12*, 46455–46465.

[170] Lu, M. M.; Wang, X. X.; Cao, W. Q.; Yuan, J.; Cao, M. S. Carbon nanotube-CdS core–shell nanowires with tunable and high-efficiency microwave absorption at elevated temperature. *Nanotechnology* **2016**, *27*, 065702.

[171] Huang, B.; Yue, J. L.; Wei, Y. S.; Huang, X. Z.; Tang, X. Z.; Du, Z. J. Enhanced microwave absorption properties of carbon nanofibers functionalized by FeCo coatings. *Appl. Surf. Sci.* **2019**, *483*, 98–105.

[172] Zeng, S. F.; Feng, W. L.; Peng, S. Y.; Teng, Z.; Chen, C.; Zhang, H. B.; Peng, S. M. Dual-functional SiOC ceramics coating modified carbon fibers with enhanced microwave absorption performance. *RSC Adv.* **2019**, *9*, 30685–30692.

[173] Zhou, J. J.; Wang, X. Y.; Ge, K. Y.; Yang, Z. Y.; Li, H. Q.; Guo, C. F.; Wang, J. Y.; Shan, Q.; Xia, L. Core–shell structured nanocomposites formed by silicon coated carbon nanotubes with anti-oxidation and electromagnetic wave absorption. *J. Colloid Interface Sci.* **2022**, *607*, 881–889.

[174] Han, Y. H.; Yuan, J.; Zhu, Y. H.; Wang, Q. Q.; Li, L.; Cao, M. S. Implantation of $WSe_2$ nanosheets into multi-walled carbon nanotubes for enhanced microwave absorption. *J. Colloid Interface Sci.* **2022**, *609*, 746–754.

[175] Liu, L. L.; Zhang, S.; Yan, F.; Li, C. Y.; Zhu, C. L.; Zhang, X. T.; Chen, Y. J. Three-dimensional hierarchical $MoS_2$ nanosheets/ultralong N-doped carbon nanotubes as high-performance electromagnetic wave absorbing material. *ACS Appl. Mater. Interfaces* **2018**, *10*, 14108–14115.

[176] Mu, C. P.; Song, J. F.; Wang, B. C.; Zhang, C.; Xiang, J. Y.; Wen, F. S.; Liu, Z. Y. Two-dimensional materials and one-dimensional carbon nanotube composites for microwave absorption. *Nanotechnology* **2018**, *29*, 025704.

[177] Wang, R.; Yang, E. Q.; Qi, X. S.; Xie, R.; Qin, S. J.; Deng, C. Y.; Zhong, W. Constructing and optimizing core@shell structure CNTs@$MoS_2$ nanocomposites as outstanding microwave absorbers. *Appl. Surf. Sci.* **2020**, *516*, 146159.

[178] Xu, X. F.; Shi, S. H.; Wan, G. P.; Hao, C. C.; He, Z. Y.; Wang, G. Z. Uniformly coating $MnO_x$ nanoflakes onto carbon nanofibers as lightweight and wideband microwave absorbers with frequency-selective absorption. *Mater. Des.* **2019**, *183*, 108167.

[179] Ro, R.; Varadan, V. V.; Varadan, V. K. Electromagnetic activity and absorption in microwave chiral composites. *IEE Proc. H* **1992**, *139*, 441–448.

[180] Tang, N. J.; Yang, Y.; Lin, K.; Zhong, W.; Au, C.; Du, Y. W. Synthesis of plait-like carbon nanocoils in ultrahigh yield, and their microwave absorption properties. *J. Phys. Chem. C* **2008**, *112*, 10061–10067.

[181] Zhou, M. F.; Wan, G. P.; Mou, P. P.; Teng, S. J.; Lin, S. W.; Wang, G. Z. CNT@NiO/natural rubber with excellent impedance matching and low interfacial thermal resistance toward flexible and heat-conducting microwave absorption applications. J. Mater. *Chem. C* **2021**, *9*, 869–880.

[182] Zhao, S. C.; Yan, L. L.; Tian, X. D.; Liu, Y. Q.; Chen, C. Q.; Li, Y. Q.; Zhang, J. K.; Song, Y.; Qin, Y. Flexible design of gradient multilayer nanofilms coated on carbon nanofibers by atomic layer deposition for enhanced microwave absorption performance. *Nano Res.* **2018**, *11*, 530–541.

[183] Naghdi, S.; Jaleh, B.; Eslamipanah, M.; Moradi, A.; Abdollahi, M.; Einali, N.; Rhee, K. Y. Graphene family, and their hybrid structures for electromagnetic interference shielding applications: Recent trends and prospects. *J. Alloys Compd.* **2022**, *900*, 163176.

[184] Wang, C.; Murugadoss, V.; Kong, J.; He, Z. F.; Mai, X. M.; Shao, Q.; Chen, Y. J.; Guo, L.; Liu, C. T.; Angaiah, S. et al. Overview of carbon nanostructures and nanocomposites for electromagnetic wave shielding. *Carbon* **2018**, *140*, 696–733.

[185] Yu, H. L.; Wang, T. S.; Wen, B.; Lu, M. M.; Xu, Z.; Zhu, C. L.; Chen, Y. J.; Xue, X. Y.; Sun, C. W.; Cao, M. S. Graphene/polyaniline nanorod arrays: Synthesis and excellent electromagnetic absorption properties. *J. Mater. Chem.* **2012**, *22*, 21679–21685.

[186] Guo, C.; Zhang, W. D.; Wang, R. M.; Qi, S. H. Enhanced electromagnetic wave absorption by optimized impedance matching: Covalently bonded polyaniline nanorods over graphene nanoplates. *J. Mater. Sci.:Mater. Electron.* **2019**, *30*, 19426–19436.

[187] Wang, H. G.; Ren, H. S.; Jing, C. F.; Li, J. Z.; Zhou, Q.; Meng, F. B. Two birds with one stone: Graphene oxide@sulfonated polyaniline nanocomposites towards high-performance electromagnetic wave absorption and corrosion protection. *Compos. Sci. Technol.* **2021**, *204*, 108630.

[188] Ren, Y. L.; Zhu, C. L.; Qi, L. H.; Gao, H.; Chen, Y. J. Growth of γ-$Fe_2O_3$ nanosheet arrays on graphene for electromagnetic absorption applications. *RSC Adv.* **2014**, *4*, 21510–21516.

[189] Xie, A.; Sun, M. X.; Zhang, K.; Jiang, W. C.; Wu, F.; He, M. *In situ* growth of $MoS_2$ nanosheets on reduced graphene oxide (RGO) surfaces:Interfacial enhancement of absorbing performance against electromagnetic pollution. *Phys. Chem. Chem. Phys.* **2016**, *18*, 24931–24936.

[190] Zhang, H. M.; Zhu, C. L.; Chen, Y. J.; Gao, H. Growth of $Fe_3O_4$ nanorod arrays on graphene sheets for application in electromagnetic absorption fields. *ChemPhysChem* **2014**, *15*, 2261–2266.

[191] Zhao, X. N.; Nie, X. Y.; Li, Y.; Pu, Y. H.; Sun, X.; Yu, R. H.; Liu, X. F.; Shui, J. L. A layered double hydroxide-derived exchange spring magnet array grown on graphene and its application as an ultrathin electromagnetic wave absorbing material. *J. Mater. Chem. C* **2019**, *7*, 12270–12277.

[192] Sultanov, F.; Daulbayev, C.; Bakbolat, B.; Daulbayev, O. Advances of 3D graphene and its composites in the field of microwave absorption. *Adv. Colloid Interface Sci.* **2020**, *285*, 102281.

[193] Zhi, D. D.; Li, T.; Li, J. Z.; Ren, H. S.; Meng, F. B. A review of three-dimensional graphene-based aerogels: Synthesis, structure and application for microwave absorption. *Compos. Part B-Eng.* **2021**, *211*, 108642.

[194] Gu, W. H.; Tan, J. W.; Chen, J. B.; Zhang, Z.; Zhao, Y.; Yu, J. W.; Ji, G. B. Multifunctional bulk hybrid foam for infrared stealth, thermal insulation, and microwave absorption. *ACS Appl. Mater. Interfaces* **2020**, *12*, 28727–28737.

[195] Hou, Y. L.; Sheng, Z. Z.; Fu, C.; Kong, J.; Zhang, X. T. Hygroscopic holey graphene aerogel fibers enable highly efficient moisture capture, heat allocation and microwave absorption. *Nat. Commun.* **2022**, *13*, 1227.

[196] Hu, C. G.; Xue, J. L.; Dong, L. Y.; Jiang, Y.; Wang, X. P.; Qu, L. T.; Dai, L. M. Scalable preparation of multifunctional fire-retardant ultralight graphene foams. *ACS Nano* **2016**, *10*, 1325–1332.

[197] Li, Y.; Liu, X. F.; Nie, X. Y.; Yang, W. W.; Wang, Y. D.; Yu, R. H.; Shui, J. L. Multifunctional organic-inorganic hybrid aerogel for self-cleaning, heat-insulating, and highly efficient microwave absorbing material. *Adv. Funct. Mater.* **2019**, *29*, 1807624.

[198] Wang, L.; Shi, X. T.; Zhang, J. L.; Zhang, Y. L.; Gu, J. W. Lightweight and robust RGO/sugarcane derived hybrid carbon foams with outstanding EMI shielding performance. *J. Mater. Sci. Technol.* **2020**, *52*, 119–126.

[199] Li, S. S.; Tang, X. W.; Zhang, Y. W.; Lan, Q. Q.; Hu, Z. W.; Li, L.; Zhang, N.; Ma, P. M.; Dong, W. F.; Tjiu, W. et al. Corrosion-resistant graphene-based magnetic composite foams for efficient electromagnetic absorption. *ACS Appl. Mater. Interfaces* **2022**, *14*, 8297–8310.

[200] Lu, X. K.; Li, X.; Wang, Y. J.; Hu, W.; Zhu, W. J.; Zhu, D. M.; Qing, Y. C. Construction of $ZnIn_2S_4$ nanosheets/3D carbon heterostructure with Schottky contact for enhancing electromagnetic wave absorption performance. *Chem. Eng. J.* **2022**, *431*, 134078.

[201] Sharma, A.; Kumar, R.; Gupta, A.; Agrawal, P. R.; Dwivedi, N.; Mondal, D. P.; Srivastava, A. K.; Dhakate, S. R. Enhanced electromagnetic interference shielding properties of phenolic resin

derived lightweight carbon foam decorated with electrospun zinc oxide nanofibers. *Mater. Today Commun.* **2022**, *30*, 103055.

[202] Yang, X.; Duan, Y. P.; Li, S. Q.; Huang, L. X.; Pang, H. F.; Ma, B.; Wang, T. M. Constructing three-dimensional reticulated carbonyl iron/carbon foam composites to achieve temperature-stable broadband microwave absorption performance. *Carbon* **2022**, *188*, 376–384.

[203] Zhao, Y. P.; Zuo, X. Q.; Guo, Y.; Huang, H.; Zhang, H.; Wang, T.; Wen, N. X.; Chen, H.; Cong, T. Z.; Muhammad, J. et al. Structural engineering of hierarchical aerogels comprised of multi-dimensional gradient carbon nanoarchitectures for highly efficient microwave absorption. *Nano-Micro Lett.* **2021**, *13*, 144.

[204] Cheng, Y. H.; Tan, M. Y.; Hu, P.; Zhang, X. H.; Sun, B. Q.; Yan, L. W.; Zhou, S. B.; Han, W. B. Strong and thermostable SiC nanowires/graphene aerogel with enhanced hydrophobicity and electromagnetic wave absorption property. *Appl. Surf. Sci.* **2018**, *448*, 138–144.

[205] Han, M. K.; Yin, X. W.; Hou, Z. X.; Song, C. Q.; Li, X. L.; Zhang, L. T.; Cheng, L. F. Flexible and thermostable graphene/SiC nanowire foam composites with tunable electromagnetic wave absorption properties. *ACS Appl. Mater. Interfaces* **2017**, *9*, 11803–11810.

[206] Zhang, Z. L.; Wang, S.; Lv, Y. Y.; Chen, X. Q.; Wu, Z.; Zou, Y. H. $MnO_2$ nanostructures deposited on graphene foams for broadband and lightweight electromagnetic absorption. *J. Alloys Compd.* **2019**, *810*, 151744.

[207] Song, P.; Liu, B.; Liang, C. B.; Ruan, K. P.; Qiu, H.; Ma, Z. L.; Guo, Y. Q.; Gu, J. W. Lightweight, flexible cellulose-derived carbon aerogel@reduced graphene Oxide/PDMS composites with outstanding EMI shielding performances and excellent thermal conductivities. *Nano-Micro Lett.* **2021**, *13*, 91.

[208] Yang, X. T.; Fan, S. G.; Li, Y.; Guo, Y. Q.; Li, Y. G.; Ruan, K. P.; Zhang, S. M.; Zhang, J. L.; Kong, J.; Gu, J. W. Synchronously improved electromagnetic interference shielding and thermal conductivity for epoxy nanocomposites by constructing 3D copper nanowires/thermally annealed graphene aerogel framework. *Compos. Part A:Appl. Sci. Manuf.* **2020**, *128*, 105670.

[209] Ye, X. L.; Chen, Z. F.; Ai, S. F.; Hou, B.; Zhang, J. X.; Liang, X. H.; Zhou, Q. B.; Liu, H. Z.; Cui, S. Effects of SiC coating on microwave absorption of novel three-dimensional reticulated sic/porous carbon foam. *Ceram. Int.* **2019**, *45*, 8660–8668.

[210] Ye, X. L.; Chen, Z. F.; Ai, S. F.; Hou, B.; Zhang, J. X.; Liang, X. H.; Zhou, Q. B.; Liu, H. Z.; Cui, S. Porous SiC/melamine-derived carbon foam frameworks with excellent electromagnetic wave absorbing capacity. *J. Adv. Ceram.* **2019**, *8*, 479–488.

[211] Ye, X. L.; Chen, Z. F.; Zhang, J. X.; Wu, C.; Zhou, Q. B.; Ai, S. F.; Liu, H. Z.; Cui, S. Double network nested foam composites with tunable electromagnetic wave absorption performances. *Inorg. Chem. Front.* **2019**, *6*, 1579–1586.

[212] Lyu, L. F.; Zheng, S. N.; Wang, F. L.; Liu, Y.; Liu, J. R. High-performance microwave absorption of MOF-derived $Co_3O_4$@N-doped carbon anchored on carbon foam. *J. Colloid Interface Sci.* **2021**, *602*, 197–206.

[213] Wei, B.; Wang, M. Q.; Yao, Z. J.; Chen, Z. P.; Chen, P.; Tao, X. W.; Liu, Y. J.; Zhou, J. T. Bimetallic nanoarrays embedded in three-dimensional carbon foam as lightweight and efficient microwave absorbers. *Carbon* **2022**, *191*, 486–501.

[214] Yadav, K.; Bagal, R.; Parmar, S.; Patro, T. U.; Abhyankar, A. C. *In situ* coating of needle-like $NiCo_2O_4$ magnetic nanoparticles on lightweight reticulated vitreous carbon foam toward achieving improved electromagnetic wave absorption. *Ind. Eng. Chem. Res.* **2021**, *60*, 14225–14238.

[215] Zhi, D. D.; Li, T.; Qi, Z. H.; Li, J. Z.; Tian, Y. R.; Deng, W. T.; Meng, F. B. Core–shell heterogeneous graphene-based aerogel microspheres for high-performance broadband microwave absorption via resonance loss and sequential attenuation. *Chem. Eng. J.* **2022**, *433*, 134496.

[216] Che, R. C.; Peng, L. M.; Duan, X. F.; Chen, Q.; Liang, X. L. Microwave absorption enhancement and complex permittivity and permeability of Fe encapsulated within carbon nanotubes. *Adv. Mater.* **2004**, *16*, 401–405.

[217] Hu, Y.; Jiang, R. J.; Zhang, J. B.; Zhang, C. S.; Cui, G. D. Synthesis and properties of magnetic multi-walled carbon nanotubes loaded with $Fe_4N$ nanoparticles. *J. Mater. Sci. Technol.* **2018**, *34*, 886–890.

[218] Poudel, Y. R.; Li, W. Z. Synthesis, properties, and applications of carbon nanotubes filled with foreign materials: A review. *Mater. Today Phys.* **2018**, *7*, 7–34.

[219] Zhao, D. L.; Li, X.; Shen, Z. M. Preparation and electromagnetic and microwave absorbing properties of Fe-filled carbon nanotubes. *J. Alloys Compd.* **2009**, *471*, 457–460.

[220] Zhao, D. L.; Zhang, J. M.; Li, X.; Shen, Z. M. Electromagnetic and microwave absorbing properties of Co-filled carbon nanotubes. *J. Alloys Compd.* **2010**, *505*, 712–716.

[221] Lin, H. Y.; Zhu, H.; Guo, H. F.; Yu, L. F. Investigation of the microwave-absorbing properties of Fe-filled carbon nanotubes. *Mater. Lett.* **2007**, *61*, 3547–3550.

[222] Lin, H. Y.; Zhu, H.; Guo, H. F.; Yu, L. F. Microwave-absorbing properties of Co-filled carbon nanotubes. *Mater. Res. Bull.* **2008**, *43*, 2697–2702.

[223] Zhao, H. T.; Han, X. J.; Han, M. F.; Zhang, L. F.; Xu, P. Preparation and electromagnetic properties of multiwalled carbon nanotubes/Ni composites by γ-irradiation technique. *Mater. Sci. Eng. B* **2010**, *167*, 1–5.

[224] Zhang, L.; Zhu, H. Dielectric, magnetic, and microwave absorbing properties of multi-walled carbon nanotubes filled with $Sm_2O_3$ nanoparticles. *Mater. Lett.* **2009**, *63*, 272–274.

[225] Zhang, L.; Zhu, H.; Song, Y.; Zhang, Y. M.; Huang, Y. The electromagnetic characteristics and absorbing properties of multi-walled carbon nanotubes filled with $Er_2O_3$ nanoparticles as microwave absorbers. *Mater. Sci. Eng. B.* **2008**, *153*, 78–82.

[226] Zhao, D. L.; Li, X.; Shen, Z. M. Microwave absorbing property and complex permittivity and permeability of epoxy composites containing Ni-coated and Ag filled carbon nanotubes. *Compos. Sci. Technol.* **2008**, *68*, 2902–2908.

[227] Zhao, D. L.; Li, X.; Shen, Z. M. Electromagnetic and microwave absorbing properties of multi-walled carbon nanotubes filled with Ag nanowires. *Mater. Sci. Eng. B* **2008**, *150*, 105–110.

[228] Zhu, H.; Zhang, L.; Zhang, L. Z.; Song, Y.; Huang, Y.; Zhang, Y. M. Electromagnetic absorption properties of Sn-filled multi-walled carbon nanotubes synthesized by pyrolyzing. *Mater. Lett.* **2010**, *64*, 227–230.

[229] Zhou, J. H.; He, J. P.; Li, G. X.; Wang, T.; Sun, D.; Ding, X. C.; Zhao, J. Q.; Wu, S. C. Direct incorporation of magnetic constituents within ordered mesoporous carbon-silica nanocomposites for highly efficient electromagnetic wave absorbers. *J. Phys. Chem. C* **2010**, *114*, 7611–7617.

[230] Li, G. X.; Guo, Y. X.; Sun, X.; Wang, T.; Zhou, J. H.; He, J. P. Synthesis and microwave absorbing properties of FeNi alloy incorporated ordered mesoporous carbon-silica nanocomposite. *J. Phys. Chem. Solids* **2012**, *73*, 1268–1273.

[231] Mordina, B.; Kumar, R.; Tiwari, R. K.; Setua, D. K.; Sharma, A. $Fe_3O_4$ nanoparticles embedded hollow mesoporous carbon nanofibers and polydimethylsiloxane-based nanocomposites as efficient microwave absorber. *J. Phys. Chem. C* **2017**, *121*, 7810–7820.

[232] Wu, H. J.; Wang, L. D.; Wang, Y. M.; Guo, S. L.; Shen, Z. Y. Enhanced microwave performance of highly ordered mesoporous carbon coated by $Ni_2O_3$ nanoparticles. *J. Alloys Compd.* **2012**, *525*, 82–86.

[233] Wang, J. C.; Zhou, H.; Zhuang, J. D.; Liu, Q. Magnetic γ-$Fe_2O_3$, $Fe_3O_4$, and Fe nanoparticles confined within ordered mesoporous carbons as efficient microwave absorbers. *Phys. Chem. Chem. Phys.* **2015**, *17*, 3802–3812.

[234] Wang, T.; He, J. P.; Zhou, J. H.; Ding, X. C.; Zhao, J. Q.; Wu, S. C.; Guo, Y. X. Electromagnetic wave absorption and infrared camouflage of ordered mesoporous carbon-alumina nanocomposites. *Microporous Mesoporous Mater.* **2010**, *134*, 58–64.

[235] Wang, T.; He, J. P.; Zhou, J. H.; Tang, J.; Guo, Y. X.; Ding, X. C.; Wu, S. C.; Zhao, J. Q. Microwave absorption properties and infrared emissivities of ordered mesoporous C-$TiO_2$

nanocomposites with crystalline framework. *J. Solid State Chem.* **2010**, *183*, 2797–2804.
[236] Chu, W. L.; Wang, Y.; Du, Y. C.; Qiang, R.; Tian, C. H.; Han, X. J. FeCo alloy nanoparticles supported on ordered mesoporous carbon for enhanced microwave absorption. *J. Mater. Sci.* **2017**, *52*, 13636–13649.
[237] Guo, S. L.; Wang, L. D.; Wu, H. J. Facile synthesis and enhanced electromagnetic wave absorption of thorny-like Fe-Ni alloy/ordered mesoporous carbon composite. *Adv. Powder Technol.* **2015**, *26*, 1250–1255.
[238] Li, G. M.; Wang, L. C.; Li, W. X.; Xu, Y. Mesoporous Fe/C and core–shell Fe-$Fe_3C$@C composites as efficient microwave absorbents. *Microporous Mesoporous Mater.* **2015**, *211*, 97–104.
[239] Chai, L.; Wang, Y. Q.; Zhou, N. F.; Du, Y.; Zeng, X. D.; Zhou, S. Y.; He, Q. C.; Wu, G. L. *In-situ* growth of core–shell $ZnFe_2O_4$@porous hollow carbon microspheres as an efficient microwave absorber. *J. Colloid Interface Sci.* **2021**, *581*, 475–484.
[240] Cheng, Y.; Cao, J. M.; Li, Y.; Li, Z. Y.; Zhao, H. Q.; Ji, G. B.; Du, Y. W. The outside-in approach to construct $Fe_3O_4$ nanocrystals/mesoporous carbon hollow spheres core–shell hybrids toward microwave absorption. *ACS Sustainable Chem. Eng.* **2018**, *6*, 1427–1435.
[241] Ruoff, R. S.; Lorents, D. C.; Chan, B.; Malhotra, R.; Subramoney, S. Single crystal metals encapsulated in carbon nanoparticles. *Science* **1993**, *259*, 346–348.
[242] Dong, X. L.; Zhang, Z. D.; Xiao, Q. F.; Zhao, X. G.; Chuang, Y. C.; Jin, S. R.; Sun, W. M.; Li, Z. J.; Zheng, Z. X.; Yang, H. Characterization of ultrafine γ-Fe(C), α-Fe(C) and $Fe_3C$ particles synthesized by arc-discharge in methane. *J. Mater. Sci.* **1998**, *33*, 1915–1919.
[243] Zhang, X. F.; Dong, X. L.; Huang, H.; Liu, Y. Y.; Wang, W. N.; Zhu, X. G.; Lv, B.; Lei, J. P.; Lee, C. G. Microwave absorption properties of the carbon-coated nickel nanocapsules. *Appl. Phys. Lett.* **2006**, *89*, 053115.
[244] Zhang, X. F.; Dong, X. L.; Huang, H.; Lv, B.; Lei, J. P.; Choi, C. J. Microstructure and microwave absorption properties of carbon-coated iron nanocapsules. *J. Phys. D: Appl. Phys.* **2007**, *40*, 5383–5387.
[245] Zhang, X. F.; Guan, P. F.; Dong, X. L. Multidielectric polarizations in the core/shell Co/graphite nanoparticles. *Appl. Phys. Lett.* **2010**, *96*, 223111.
[246] Wu, N. D.; Liu, X. G.; Zhao, C. Y.; Cui, C. Y.; Xia, A. L. Effects of particle size on the magnetic and microwave absorption properties of carbon-coated nickel nanocapsules. *J. Alloys Compd.* **2016**, *656*, 628–634.
[247] Wang, H.; Guo, H. H.; Dai, Y. Y.; Geng, D. Y.; Han, Z.; Li, D.; Yang, T.; Ma, S.; Liu, W.; Zhang, Z. D. Optimal electromagnetic-wave absorption by enhanced dipole polarization in Ni/C nanocapsules. *Appl. Phys. Lett.* **2012**, *101*, 083116.
[248] Du, Y. C.; Wang, J. Y.; Cui, C. K.; Liu, X. R.; Wang, X. H.; Han, X. J. Pure carbon microwave absorbers from anion-exchange resin pyrolysis. *Synth. Met.* **2010**, *160*, 2191–2196.
[249] Du, Y. C. Advances in carbon-based microwave absorbing materials. *Materials* **2022**, *15*, 1359.
[250] Liu, T.; Xie, X. B.; Pang, Y.; Kobayashi, S. Co/C nanoparticles with low graphitization degree: A high performance microwave-absorbing material. *J. Mater. Chem. C* **2016**, *4*, 1727–1735.
[251] Li, Y. X.; Liu, X. F.; Liu, R. G.; Pang, X. Y.; Zhang, Y. H.; Qin, G. W.; Zhang, X. F. Improved microwave absorption properties by atomic-scale substitutions. *Carbon* **2018**, *139*, 181–188.
[252] Li, Y. X.; Liu, R. G.; Pang, X. Y.; Zhao, X. N.; Zhang, Y. H.; Qin, G. W.; Zhang, X. F. Fe@C nanocapsules with substitutional sulfur heteroatoms in graphitic shells for improving microwave absorption at gigahertz frequencies. *Carbon* **2018**, *126*, 372–381.
[253] Liu, R. G.; Li, Y. X.; Yu, J. Y.; Zhang, X. F. Fe@graphite nanocapsules with atomic-scale substitutional oxygen in graphitic shells for improving gigahertz dielectric losses and microwave absorption properties. *J. Alloys Compd.* **2019**, *792*, 291–296.
[254] Yu, Z. X.; Zhang, N.; Yao, Z. P.; Han, X. J.; Jiang, Z. H. Synthesis of hierarchical dendritic micro-nano structure $Co_xFe_{1-x}$ alloy with tunable electromagnetic absorption performance. *J. Mater. Chem. A* **2013**, *1*, 12462–12470.
[255] Duan, Y. P.; Zhang, Y. H.; Wang, T. M.; Gu, S. C.; Li, X.; Lv, X. J. Evolution study of microstructure and electromagnetic behaviors of Fe-Co-Ni alloy with mechanical alloying. *Mater. Sci. Eng. B* **2014**, *185*, 86–93.
[256] Liu, X. G.; Ou, Z. Q.; Geng, D. Y.; Han, Z.; Jiang, J. J.; Liu, W.; Zhang, Z. D. Influence of a graphite shell on the thermal and electromagnetic characteristics of FeNi nanoparticles. *Carbon* **2010**, *48*, 891–897.
[257] Qu, X. H.; Zhou, Y. L.; Li, X. Y.; Javid, M.; Huang, F. R.; Zhang, X. F.; Dong, X. L.; Zhang, Z. D. Nitrogen-doped graphene layer-encapsulated NiFe bimetallic nanoparticles synthesized by an arc discharge method for a highly efficient microwave absorber. *Inorg. Chem. Front.* **2020**, *7*, 1148–1160.
[258] Wang, H.; Dai, Y. Y.; Gong, W. J.; Geng, D. Y.; Ma, S.; Li, D.; Liu, W.; Zhang, Z. D. Broadband microwave absorption of CoNi@C nanocapsules enhanced by dual dielectric relaxation and multiple magnetic resonances. *Appl. Phys. Lett.* **2013**, *102*, 223113.
[259] Xie, Z. G.; Geng, D. Y.; Liu, X. G.; Ma, S.; Zhang, Z. D. Magnetic and microwave-absorption properties of graphite-coated (Fe, Ni) nanocapsules. *J. Mater. Sci. Technol.* **2011**, *27*, 607–614.
[260] Han, Z.; Li, D.; Wang, H.; Liu, X. G.; Li, J.; Geng, D. Y.; Zhang, Z. D. Broadband electromagnetic-wave absorption by FeCo/C nanocapsules. *Appl. Phys. Lett.* **2009**, *95*, 023114.
[261] Lei, Z. X.; Li, S. Z.; Zhang, A. Q.; Song, Y. H.; He, N.; Li, M. Z.; Geng, D. Y.; Liu, W.; Ma, S.; Zhang, Z. D. Electromagnetic wave absorption superalloy/graphite magnetic nanocapsules applied in wide temperature range. *Compos. Part B-Eng.* **2022**, *234*, 109692.
[262] Han, D. D.; Or, S. W.; Dong, X. R.; Liu, B. $FeSn_2$/defective onion-like carbon core–shell structured nanocapsules for high-frequency microwave absorption. *J. Alloys Compd.* **2017**, *695*, 2605–2611.
[263] Hua, A.; Pan, D. S.; Li, Y.; Luan, J.; Wang, Y.; He, J.; Geng, D. Y.; Liu, W.; Ma, S.; Zhang, Z. D. $Fe_3Si$-core/amorphous-C-shell nanocapsules with enhanced microwave absorption. *J. Magn. Magn. Mater.* **2019**, *471*, 561–567.
[264] Zhang, X. F.; Rao, Y.; Guo, J. J.; Qin, G. W. Multiple-phase carbon-coated $FeSn_2$/Sn nanocomposites for high-frequency microwave absorption. *Carbon* **2016**, *96*, 972–979.
[265] Liu, X. G.; Ou, Z. Q.; Geng, D. Y.; Han, Z.; Wang, H.; Li, B.; Brück, E.; Zhang, Z. D. Enhanced absorption bandwidth in carbon-coated supermalloy FeNiMo nanocapsules for a thin absorb thickness. *J. Alloys Compd.* **2010**, *506*, 826–830.
[266] Li, Y. X.; Liao, Y. J.; Ji, L. Z.; Hu, C. L.; Zhang, Z. H.; Zhang, Z. Y.; Zhao, R. Z.; Rong, H. W.; Qin, G. W.; Zhang, X. F. Quinary high-entropy-alloy@graphite nanocapsules with tunable interfacial impedance matching for optimizing microwave absorption. *Small* **2022**, *18*, 2107265.
[267] Javid, M.; Qu, X. H.; Zhao, Y. P.; Huang, F. R.; Farid, A.; Zhang, H.; Shah, A.; Sammed, K. A.; Duan, Y. P.; Zhang, Z. D. et al. Synthesis of hexagonal-shaped $Cr_3C_2$@C nanoplatelets and role of their intrinsic properties towards microwave absorption. *Mater. Lett.* **2021**, *288*, 129329.
[268] Rong, H. W.; Zhang, Z. Q.; Li, Y. X.; Zhang, X. F.; Li, L. W. Significant magnetocaloric and microwave absorption performances in ultrafine $ErC_2$@C core–shell structural nanocomposites. *Compos. Commun.* **2019**, *12*, 123–127.
[269] Wang, Z. H.; Han, Z.; Geng, D. Y.; Zhang, Z. D. Synthesis, characterization and microwave absorption of carbon-coated Sn nanorods. *Chem. Phys. Lett.* **2010**, *489*, 187–190.
[270] Zhou, Y. L.; Wang, N.; Qu, X. H.; Huang, F. R.; Duan, Y. P.; Zhang, X. F.; Dong, X. L.; Zhang, Z. D. Arc-discharge synthesis of nitrogen-doped C embedded TiCN nanocubes with tunable dielectric/magnetic properties for electromagnetic absorbing applications. *Nanoscale* **2019**, *11*, 19994–20005.
[271] Cui, C. K.; Du, Y. C.; Li, T. H.; Zheng, X. Y.; Wang, X. H.; Han, X. J.; Xu, P. Synthesis of electromagnetic functionalized $Fe_3O_4$ microspheres/polyaniline composites by two-step oxidative polymerization. *J. Phys. Chem. B* **2012**, *116*, 9523–9531.
[272] Li, C. P.; Chen, G. B.; Jiang, W. T.; Jiang, X. H.; Yan, X. F. High-

performance electromagnetic wave absorption of FeNi/N, S-codoped carbon composites in 2–40 GHz. *Carbon* **2021**, *174*, 201–213.
[273] Wu, T.; Liu, Y.; Zeng, X.; Cui, T. T.; Zhao, Y. T.; Li, Y. N.; Tong, G. X. Facile hydrothermal synthesis of $Fe_3O_4$/C core–shell nanorings for efficient low-frequency microwave absorption. *ACS Appl. Mater. Interfaces* **2016**, *8*, 7370–7380.
[274] Ding, D.; Wang, Y.; Li, X. D.; Qiang, R.; Xu, P.; Chu, W. L.; Han, X. J.; Du, Y. C. Rational design of core–shell Co@C microspheres for high-performance microwave absorption. *Carbon* **2017**, *111*, 722–732.
[275] Chen, X. L.; Wang, Y.; Liu, H. L.; Jin, S.; Wu, G. L. Interconnected magnetic carbon@$Ni_xCo_{1-x}Fe_2O_4$ nanospheres with core–shell structure: An efficient and thin electromagnetic wave absorber. *J. Colloid Interface Sci.* **2022**, *606*, 526–536.
[276] Dai, W. Y.; Chen, F.; Luo, H.; Xiong, Y.; Wang, X.; Cheng, Y. Z.; Gong, R. Z. Synthesis of yolk–shell structured carbonyl iron@void@nitrogen doped carbon for enhanced microwave absorption performance. *J. Alloys Compd.* **2020**, *812*, 152083.
[277] Shen, X.; Yang, S. H.; Yin, P. G.; Li, C. Q.; Ye, J. R.; Wang, G. S. Enhancement in microwave absorption properties by adjusting the sintering conditions and carbon shell thickness of Ni@C submicrospheres. *CrystEngComm* **2022**, *24*, 765–774.
[278] Wang, B. L.; Chen, H. Y.; Wang, S.; Shi, Y.; Liu, X. D.; Fu, Y. G.; Liu, T. Construction of core–shell structured $Co_7Fe_3$@C nanocapsules with strong wideband microwave absorption at ultra-thin thickness. *Carbon* **2021**, *184*, 223–231.
[279] Guan, Z. J.; Jiang, J. T.; Chen, N.; Gong, Y. X.; Zhen, L. Carbon-coated CoFe-$CoFe_2O_4$ composite particles with high and dual-band electromagnetic wave absorbing properties. *Nanotechnology* **2018**, *29*, 305604.
[280] Cui, L. R.; Tian, C. H.; Tang, L. L.; Han, X. J.; Wang, Y. H.; Liu, D. W.; Xu, P.; Li, C. L.; Du, Y. C. Space-confined synthesis of core–shell $BaTiO_3$@carbon microspheres as a high-performance binary dielectric system for microwave absorption. *ACS Appl. Mater. Interfaces* **2019**, *11*, 31182–31190.
[281] Liang, C. Y.; Wang, Z. J. Controllable fabricating dielectric-dielectric SiC@C core–shell nanowires for high-performance electromagnetic wave attenuation. *ACS Appl. Mater. Interfaces* **2017**, *9*, 40690–40696.
[282] Xu, D. M.; Yang, Y. F.; Lyu, L.; Ouyang, A. C.; Liu, W.; Wang, Z.; Wu, L. L.; Yang, F.; Liu, J. R.; Wang, F. L. One-dimensional MnO@N-doped carbon nanotubes as robust dielectric loss electromagnetic wave absorbers. *Chem. Eng. J.* **2021**, *410*, 128295.
[283] Yan, L. L.; Zhang, M.; Zhao, S. C.; Sun, T. J.; Zhang, B.; Cao, M. S.; Qin, Y. Wire-in-tube ZnO@carbon by molecular layer deposition: Accurately tunable electromagnetic parameters and remarkable microwave absorption. *Chem. Eng. J.* **2020**, *382*, 122860.
[284] Dong, S.; Zhang, W. Z.; Zhang, X. H.; Hu, P.; Han, J. C. Designable synthesis of core–shell SiCw@C heterostructures with thickness-dependent electromagnetic wave absorption between the whole X-band and Ku-band. *Chem. Eng. J.* **2018**, *354*, 767–776.
[285] Lv, H. L.; Yang, Z. H.; Xu, H. B.; Wang, L. Y.; Wu, R. B. An electrical switch-driven flexible electromagnetic absorber. *Adv. Funct. Mater.* **2020**, *30*, 1907251.
[286] Lv, H. L.; Yang, Z. H.; Wang, P. L.; Ji, G. B.; Song, J. Z.; Zheng, L. R.; Zeng, H. B.; Xu, Z. J. A voltage-boosting strategy enabling a low-frequency, flexible electromagnetic wave absorption device. *Adv. Mater.* **2018**, *30*, 1706343.
[287] Liu, X. F.; Cui, X. R.; Chen, Y. X.; Zhang, X. J.; Yu, R. H.; Wang, G. S.; Ma, H. Modulation of electromagnetic wave absorption by carbon shell thickness in carbon encapsulated magnetite nanospindles-poly(vinylidene fluoride) composites. *Carbon* **2015**, *95*, 870–878.
[288] Liu, Y.; Fu, Y. W.; Liu, L.; Li, W.; Guan, J. G.; Tong, G. X. Low-cost carbothermal reduction preparation of monodisperse $Fe_3O_4$/C core–shell nanosheets for improved microwave absorption. *ACS Appl. Mater. Interfaces* **2018**, *10*, 16511–16520.
[289] Wang, X.; Pan, F.; Xiang, Z.; Zeng, Q. W.; Pei, K.; Che, R. C.; Lu, W. Magnetic vortex core–shell $Fe_3O_4$@C nanorings with enhanced microwave absorption performance. *Carbon* **2020**, *157*, 130–139.
[290] Cui, X. Q.; Liang, X. H.; Chen, J. B.; Gu, W. H.; Ji, G. B.; Du, Y. W. Customized unique core–shell $Fe_2N$@N-doped carbon with tunable void space for microwave response. *Carbon* **2020**, *156*, 49–57.
[291] Gao, S. T.; Zhang, Y. C.; Xing, H. L.; Li, H. X. Controlled reduction synthesis of yolk–shell magnetic@void@C for electromagnetic wave absorption. *Chem. Eng. J.* **2020**, *387*, 124149.
[292] Li, B.; Liu, M. J.; Zhong, W. X.; Xu, J.; Zhang, X.; Zhang, X. L.; Zhang, X. T.; Chen, Y. J. Partially contacted $Ni_xS_y$@N, S-codoped carbon yolk–shelled structures for efficient microwave absorption. *Carbon* **2021**, *182*, 276–286.
[293] Ma, W. J.; He, P.; Wang, T. Y.; Xu, J.; Liu, X. Y.; Zhuang, Q. X.; Cui, Z. K.; Lin, S. L. Microwave absorption of carbonization temperature-dependent uniform yolk–shell H-$Fe_3O_4$@C microspheres. *Chem. Eng. J.* **2021**, *420*, 129875.
[294] Park, J. H.; Lee, S.; Ro, J. V.; Suh, S. J. Yolk–shell Fe-$Fe_3O_4$@C nanoparticles with excellent reflection loss and wide bandwidth as electromagnetic wave absorbers in the high-frequency band. *Appl. Surf. Sci.* **2022**, *573*, 151469.
[295] Wang, B. L.; Fu, Y. G.; Li, J.; Liu, T. Yolk–shelled Co@$SiO_2$@mesoporous carbon microspheres: Construction of multiple heterogeneous interfaces for wide-bandwidth microwave absorption. *J. Colloid Interface Sci.* **2022**, *607*, 1540–1550.
[296] Wang, K.; Wan, G. P.; Wang, G. L.; He, Z. Y.; Shi, S. H.; Wu, L. H.; Wang, G. Z. The construction of carbon-coated $Fe_3O_4$ yolk–shell nanocomposites based on volume shrinkage from the release of oxygen anions for wide-band electromagnetic wave absorption. *J. Colloid Interface Sci.* **2018**, *511*, 307–317.
[297] Han, M. K.; Yin, X. W.; Kong, L.; Li, M.; Duan, W. Y.; Zhang, L. T.; Cheng, L. F. Graphene-wrapped ZnO hollow spheres with enhanced electromagnetic wave absorption properties. *J. Mater. Chem. A* **2014**, *2*, 16403–16409.
[298] Huang, Y.; Xing, W. J.; Fan, J. L.; Dai, J. X.; Liu, Q.; Hu, F.; Xu, G. L. Preparation and microwave absorption properties of the hollow $ZnFe_2O_4$@C composites with core–shell structure. *J. Magn. Magn. Mater.* **2020**, *502*, 166543.
[299] Xu, L. L.; Tao, J. Q.; Zhang, X. F.; Yao, Z. J.; Zavabeti, A.; Zhou, J. T. Co@N-doped double-shell hollow carbon via self-templating-polymerization strategy for microwave absorption. *Carbon* **2022**, *188*, 34–44.
[300] Wang, F. Y.; Liu, Y. L.; Zhao, H. H.; Cui, L. R.; Gai, L. X.; Han, X. J.; Du, Y. C. Controllable seeding of nitrogen-doped carbon nanotubes on three-dimensional Co/C foam for enhanced dielectric loss and microwave absorption characteristics. *Chem. Eng. J.* **2022**, *450*, 138160.
[301] Cui, L. R.; Wang, Y. H.; Han, X. J.; Xu, P.; Wang, F. Y.; Liu, D. W.; Zhao, H. H.; Du, Y. C. Phenolic resin reinforcement: A new strategy for hollow NiCo@C microboxes against electromagnetic pollution. *Carbon* **2021**, *174*, 673–682.
[302] Müller, C.; Leonhardt, A.; Kutz, M. C.; Büchner, B.; Reuther H. Growth aspects of iron-filled carbon nanotubes obtained by catalytic chemical vapor deposition of ferrocene. *J. Phys. Chem. C* **2009**, *113*, 2736–2740.
[303] Lv, R. T.; Kang, F. Y.; Cai, D. Y.; Wang, C.; Gu, J. L.; Wang, K. L.; Wu, D. H. Long continuous FeNi nanowires inside carbon nanotubes: Synthesis, property and application. *J. Phys. Chem. Solids* **2008**, *69*, 1213–1217.
[304] Lv, R. T.; Kang, F. Y.; Gu, J. L.; Gui, X. C.; Wei, J. Q.; Wang, K. L.; Wu, D. H. Carbon nanotubes filled with ferromagnetic alloy nanowires: Lightweight and wide-band microwave absorber. *Appl. Phys. Lett.* **2008**, *93*, 223105.
[305] Su, Q. M.; Li, J.; Zhong, G.; Du, G. H.; Xu, B. S. *In situ* synthesis of iron/nickel sulfide nanostructures-filled carbon nanotubes and their electromagnetic and microwave-absorbing properties. *J. Phys. Chem. C* **2011**, *115*, 1838–1842.
[306] Zhu, H.; Lin, H. Y.; Guo, H. F.; Yu, L. F. Microwave absorbing property of Fe-filled carbon nanotubes synthesized by a practical route. *Mater. Sci. Eng. B* **2007**, *138*, 101–104.
[307] Xu, Z.; Du, Y. C.; Liu, D. W.; Wang, Y. H.; Ma, W. J.; Wang, Y.;

Xu, P.; Han, X. J. Pea-like Fe/$Fe_3C$ nanoparticles embedded in nitrogen-doped carbon nanotubes with tunable dielectric/magnetic loss and efficient electromagnetic absorption. *ACS Appl. Mater. Interfaces* **2019**, *11*, 4268–4277.

[308] Liu, X. Y.; Zhang, X.; Shen, Y.; Yan, F.; Chen, Y. J. Fabrication of Fe/$Fe_3C$-nanoparticles encapsulated nitrogen-doped carbon nanotubes with thin wall thickness as high-efficiency electromagnetic wave absorbing materials. *J. Alloys Compd.* **2022**, *898*, 162833.

[309] Zeng, B.; Zhang, P.; Li, H. J.; Peng, Y. H.; Qin, L. L.; Qu, Z. W.; Qiu, L. L.; Gao, X. H.; Huang, S. X.; Deng, L. W. Flammulina velutipes-like Co@NCNTs enhancing the electromagnetic wave absorption performance. *Results Phys.* **2021**, *29*, 104751.

[310] Zhang, Y.; Huang, Y. A.; Liang, X. H.; Yang, Y.; Zhang, R. L.; Huang, R. S. Preparation and microwave absorption of nitrogen-doped carbon nanotubes with iron particles. *IEEE Trans. Magn.* **2018**, *54*, 2300606.

[311] Zhu, X. Y.; Qiu, H. F.; Chen, P.; Liu, J. L.; Chen, G. Z. Environmentally friendly synthesis of velutipes-shaped Ni@CNTs composites as efficient thin microwave absorbers. *J. Electron. Mater.* **2020**, *49*, 5368–5378.

[312] Sun, Y. P.; Liu, X. G.; Feng, C.; Fan, J. C.; Lv, Y. H.; Wang, Y. R.; Li, C. T. A facile synthesis of $FeNi_3$@C nanowires for electromagnetic wave absorber. *J. Alloys Compd.* **2014**, *586*, 688–692.

[313] Wu, G. L.; Cheng, Y. H.; Ren, Y. Y.; Wang, Y. Q.; Wang, Z. D.; Wu, H. J. Synthesis and characterization of γ-$Fe_2O_3$@C nanorod-carbon sphere composite and its application as microwave absorbing material. *J. Alloys Compd.* **2015**, *652*, 346–350.

[314] Wang, Y. H.; Han, X. J.; Xu, P.; Liu, D. W.; Cui, L. R.; Zhao, H. H.; Du, Y. C. Synthesis of pomegranate-like $Mo_2C$@C nanospheres for highly efficient microwave absorption. *Chem. Eng. J.* **2019**, *372*, 312–320.

[315] Liu, L.; He, P. G.; Zhou, K. C.; Chen, T. F. Microwave absorption properties of helical carbon nanofibers-coated carbon fibers. *AIP Adv.* **2013**, *3*, 082112.

[316] Singh, S. K.; Akhtar, M. J.; Kar, K. K. Hierarchical carbon nanotube-coated carbon fiber: Ultra lightweight, thin, and highly efficient microwave absorber. *ACS Appl. Mater. Interfaces* **2018**, *10*, 24816–24828.

[317] Zhang, X. X.; Wang, J.; Su, X. G.; Huo, S. Q. Facile synthesis of reduced graphene oxide-wrapped CNFs with controllable chemical reduction degree for enhanced microwave absorption performance. *J. Colloid Interface Sci.* **2019**, *553*, 402–408.

[318] Zhao, H. H.; Xu, X. Z.; Fan, D. G.; Xu, P.; Wang, F. Y.; Cui, L. R.; Han, X. J.; Du, Y. C. Anchoring porous carbon nanoparticles on carbon nanotubes as a high-performance composite with a unique core–sheath structure for electromagnetic pollution precaution. *J. Mater. Chem. A* **2021**, *9*, 22489–22500.

[319] Tian, C. H.; Du, Y. C.; Cui, C. S.; Deng, Z. L.; Xue, J. L.; Xu, P.; Qiang, R.; Wang, Y.; Han, X. J. Synthesis and microwave absorption enhancement of yolk–shell $Fe_3O_4$@C microspheres. *J. Mater. Sci.* **2017**, *52*, 6349–6361.

[320] Tian, C. H.; Du, Y. C.; Xu, H. Y.; Xue, J. L.; Chu, W. L.; Qiang, R.; Han, X. J.; Xu, P. Differential shrinkage induced formation of yolk–shell carbon microspheres toward enhanced microwave absorption. *Appl. Phys. Lett.* **2017**, *111*, 133103.

[321] Qiang, R.; Du, Y. C.; Wang, Y.; Wang, N.; Tian, C. H.; Ma, J.; Xu, P.; Han, X. J. Rational design of yolk–shell C@C microspheres for the effective enhancement in microwave absorption. *Carbon* **2016**, *98*, 599–606.

[322] Wang, Y. C.; Zhou, W.; Zeng, G. L.; Chen, H.; Luo, H.; Fan, X. M.; Li, Y. Rational design of multi-shell hollow carbon submicrospheres for high-performance microwave absorbers. *Carbon* **2021**, *175*, 233–242.

[323] Sun, H.; Che, R. C.; You, X.; Jiang, Y. S.; Yang, Z. B.; Deng, J.; Qiu, L. B.; Peng, H. S. Cross-stacking aligned carbon-nanotube films to tune microwave absorption frequencies and increase absorption intensities. *Adv. Mater.* **2014**, *26*, 8120–8125.

[324] Yuan, K. P.; Che, R. C.; Cao, Q.; Sun, Z. K.; Yue, Q.; Deng, Y. H. Designed fabrication and characterization of three-dimensionally ordered arrays of core–shell magnetic mesoporous carbon microspheres. *ACS Appl. Mater. Interfaces* **2015**, *7*, 5312–5319.

[325] Song, Y.; Yin, F. X.; Zhang, C. W.; Guo, W. B.; Han, L. Y.; Yuan, Y. Three-dimensional ordered mesoporous carbon spheres modified with ultrafine zinc oxide nanoparticles for enhanced microwave absorption properties. *Nano-Micro Lett.* **2021**, *13*, 76.

[326] Zhang, C. W.; Peng, Y.; Song, Y.; Li, J. J.; Yin, F. X.; Yuan, Y. Periodic three-dimensional nitrogen-doped mesoporous carbon spheres embedded with Co/$Co_3O_4$ nanoparticles toward microwave absorption. *ACS Appl. Mater. Interfaces* **2020**, *12*, 24102–24111.

[327] Lü, Y. Y.; Wang, Y. T.; Li, H. L.; Lin, Y.; Jiang, Z. Y.; Xie, Z. X.; Kuang, Q.; Zheng, L. S. MOF-derived porous Co/C nanocomposites with excellent electromagnetic wave absorption properties. ACS Appl. Mater. *Interfaces* **2015**, *7*, 13604–13611.

[328] Yan, J.; Huang, Y.; Yan, Y. H.; Ding, L.; Liu, P. B. High-performance electromagnetic wave absorbers based on two kinds of nickel-based MOF-derived Ni@C microspheres. *ACS Appl. Mater. Interfaces* **2019**, *11*, 40781–40792.

[329] Yang, Z. H.; Lv, H. L.; Wu, R. B. Rational construction of graphene oxide with MOF-derived porous NiFe@C nanocubes for high-performance microwave attenuation. *Nano Res.* **2016**, *9*, 3671–3682.

[330] Qiu, Y.; Lin, Y.; Yang, H. B.; Wang, L.; Wang, M. Q.; Wen, B. Hollow Ni/C microspheres derived from Ni-metal organic framework for electromagnetic wave absorption. *Chem. Eng. J.* **2020**, *383*, 123207.

[331] Wang, L.; Huang, M. Q.; Yu, X. F.; You, W. B.; Zhang, J.; Liu, X. H.; Wang, M.; Che, R. C. MOF-derived $Ni_{1-x}Co_x$@carbon with tunable nano-microstructure as lightweight and highly efficient electromagnetic wave absorber. *Nano-Micro Lett.* **2020**, *12*, 150.

[332] Quan, B.; Liang, X. H.; Zhang, X.; Xu, G. Y.; Ji, G. B.; Du, Y. W. Functionalized carbon nanofibers enabling stable and flexible absorbers with effective microwave response at low thickness. *ACS Appl. Mater. Interfaces* **2018**, *10*, 41535–41543.

[333] Ding, J. W.; Song, K.; Gong, C. C.; Wang, C. X.; Guo, Y.; Shi, C. S.; He, F. Design of conical hollow ZnS arrays vertically grown on carbon fibers for lightweight and broadband flexible absorbers. *J. Colloid Interface Sci.* **2022**, *607*, 1287–1299.

[334] Li, X.; Wang, L.; You, W. B.; Xing, L. S.; Yang, L. T.; Yu, X. F.; Zhang, J.; Li, Y. S.; Che, R. C. Enhanced polarization from flexible hierarchical $MnO_2$ arrays on cotton cloth with excellent microwave absorption. *Nanoscale* **2019**, *11*, 13269–13281.

[335] Liu, P. B. ; Zhu, C. Y. ; Gao, S. ; Guan, C. ; Huang, Y. ; He, W. J. N-doped porous carbon nanoplates embedded with $CoS_2$ vertically anchored on carbon cloths for flexible and ultrahigh microwave absorption. *Carbon* **2020**, *163*, 348–359.

[336] Wang, L.; Li, X.; Li, Q. Q.; Yu, X. F.; Zhao, Y. H.; Zhang, J.; Wang, M.; Che, R. C. Oriented polarization tuning broadband absorption from flexible hierarchical ZnO arrays vertically supported on carbon cloth. *Small* **2019**, *15*, 1900900.

[337] Cui, C.; Guo, R. H.; Ren, E. H.; Xiao, H. Y.; Zhou, M.; Lai, X. X.; Qin, Q.; Jiang, S. X.; Qin, W. F. MXene-based rGO/$Nb_2CT_x$/$Fe_3O_4$ composite for high absorption of electromagnetic wave. *Chem. Eng. J.* **2021**, *405*, 126626.

[338] Wang, J. Q.; Cui, Y. H.; Wu, F.; Shah, T.; Ahmad, M.; Zhang, A. B.; Zhang, Q. Y.; Zhang, B. L. Core–shell structured Fe/$Fe_3O_4$@TCNFs@$TiO_2$ magnetic hybrid nanofibers: Preparation and electromagnetic parameters regulation for enhanced microwave absorption. *Carbon* **2020**, *165*, 275–285.

[339] Liu, Y.; Jia, Z. R.; Zhan, Q. Q.; Dong, Y. H.; Xu, Q. M.; Wu, G. L. Magnetic manganese-based composites with multiple loss mechanisms towards broadband absorption. *Nat. Catal.* **2022**, *15*, 5590–5600.

[340] Shi, X. F.; You, W. B.; Zhao, Y. H.; Li, X.; Shao, Z. Z.; Che, R. C. Multi-scale magnetic coupling of Fe@$SiO_2$@C-Ni yolk@triple-shell microspheres for broadband microwave absorption. *Nanoscale* **2019**, *11*, 17270–17276.

[341] Chen, X. L.; Jia, Z. R.; Feng, A. L.; Wang, B. B.; Tong, X. H.; Zhang, C. H.; Wu, G. L. Hierarchical $Fe_3O_4$@carbon@$MnO_2$

hybrid for electromagnetic wave absorber. *J. Colloid Interface Sci.* **2019**, *553*, 465–474.

[342] Liu, Y.; Jia, Z. R.; Zhan, Q. Q.; Dong, Y. H.; Xu, Q. M.; Wu, G. L. Magnetic manganese-based composites with multiple loss mechanisms towards broadband absorption. *Nano Res.* **2022**, *15*, 5590–5600.

[343] Ning, M. Q.; Lei, Z. K.; Tan, G. G.; Man, Q. K.; Li, J. B.; Li, R. W. Dumbbell-like $Fe_3O_4$@N-doped carbon@2H/1T-$MoS_2$ with tailored magnetic and dielectric loss for efficient microwave absorbing. *ACS Appl. Mater. Interfaces* **2021**, *13*, 47061–47071.

[344] Tong, Z. Y.; Liao, Z. J.; Liu, Y. Y.; Ma, M. L.; Bi, Y. X.; Huang, W. B.; Ma, Y.; Qiao, M. T.; Wu, G. L. Hierarchical $Fe_3O_4$/Fe@C@$MoS_2$ core–shell nanofibers for efficient microwave absorption. *Carbon* **2021**, *179*, 646–654.

[345] Wang, L.; Yu, X. F.; Li, X.; Zhang, J.; Wang, M.; Che, R. C. MOF-derived yolk–shell Ni@C@ZnO Schottky contact structure for enhanced microwave absorption. *Chem. Eng. J.* **2020**, *383*, 123099.

[346] Wang, S. S.; Zhu, H. H.; Jiao, Q. Z.; Jiao, X. G.; Feng, C. H.; Li, H. S.; Shi, D. X.; Wu, Q.; Zhao, Y. Controllable synthesis of multi-shelled $SiO_2$@C@$NiCo_2O_4$ yolk–shell composites for enhancing microwave absorbing properties. *New J. Chem.* **2021**, *45*, 20928–20936.

[347] Xu, C.; Wu, F.; Duan, L. Q.; Xiong, Z. M.; Xia, Y. L.; Yang, Z. Q.; Sun, M. X.; Xie, A. M. Dual-interfacial polarization enhancement to design tunable microwave absorption nanofibers of SiC@C@PPy. *ACS Appl. Electron. Mater.* **2020**, *2*, 1505–1513.

[348] Yang, Z. H.; Li, M.; Zhang, Y.; Yang, L. J.; Liu, J. C.; Wang, Y. H.; He, Q. J. Constructing uniform $Fe_3O_4$@C@$MnO_2$ microspheres with yolk–shell interior toward enhancement in microwave absorption. *J. Alloys Compd.* **2020**, *817*, 152795.

[349] You, W. B.; Bi, H.; She, W.; Zhang, Y.; Che, R. C. Dipolar-distribution cavity γ-$Fe_2O_3$@C@α-$MnO_2$ nanospindle with broadened microwave absorption bandwidth by chemically etching. *Small* **2017**, *13*, 1602779.

[350] Han, X. P.; Huang, Y.; Gao, S.; Zhang, G. Z.; Li, T. H.; Liu, P. B. A hierarchical carbon fiber@MXene@ZnO core-sheath synergistic microstructure for efficient microwave absorption and photothermal conversion. *Carbon* **2021**, *183*, 872–883.

[351] Lv, H. L.; Ji, G. B.; Zhang, H. Q.; Du, Y. W. Facile synthesis of a CNT@Fe@$SiO_2$ ternary composite with enhanced microwave absorption performance. *RSC Adv.* **2015**, *5*, 76836–76843.

[352] Wang, J. Q.; Liu, L.; Jiao, S. L.; Ma, K. J.; Lv, J.; Yang, J. J. Hierarchical carbon fiber@MXene@$MoS_2$ core–sheath synergistic microstructure for tunable and efficient microwave absorption. *Adv. Funct. Mater.* **2020**, *30*, 2002595.

[353] Huang, M. Q.; Wang, L.; Liu, Q.; You, W. B.; Che, R. C. Interface compatibility engineering of Multi-shell Fe@C@$TiO_2$@$MoS_2$ heterojunction expanded microwave absorption bandwidth. *Chem. Eng. J.* **2022**, *429*, 132191.

[354] Liu, D. W.; Du, Y. C.; Xu, P.; Wang, F. Y.; Wang, Y. H.; Cui, L. R.; Zhao, H. H.; Han, X. J. Rationally designed hierarchical N-doped carbon nanotubes wrapping waxberry-like Ni@C microspheres for efficient microwave absorption. *J. Mater. Chem. A* **2021**, *9*, 5086–5096.

[355] Qiu, Y.; Yang, H. B.; Ma, L.; Lin, Y.; Zong, H. W.; Wen, B.; Bai, X. Y.; Wang, M. Q. *In situ*-derived carbon nanotube-decorated nitrogen-doped carbon-coated nickel hybrids from MOF/melamine for efficient electromagnetic wave absorption. *J. Colloid Interface Sci.* **2021**, *581*, 783–793.

[356] Xu, C. Y.; Wang, L.; Li, X.; Qian, X.; Wu, Z. C.; You, W. B.; Pei, K.; Qin, G.; Zeng, Q. W.; Yang, Z. Q. et al. Hierarchical magnetic network constructed by CoFe nanoparticles suspended within "tubes on rods" matrix toward enhanced microwave absorption. *Nano-Micro Lett.* **2021**, *13*, 47.